R-09-33

Mechanical and thermo-mechanical analyses of the tapered plug for plugging of deposition tunnels

A feasibility study

Billy Fälth, Clay Technology AB

Patrik Gatter, Vattenfall Power Consultant AB

September 2009

Svensk Kärnbränslehantering AB
Swedish Nuclear Fuel
and Waste Management Co

Box 250, SE-101 24 Stockholm
Phone +46 8 459 84 00

ISSN 1402-3091
SKB Rapport R-09-33

Mechanical and thermo-mechanical analyses of the tapered plug for plugging of deposition tunnels

A feasibility study

Billy Fälth, Clay Technology AB

Patrik Gatter, Vattenfall Power Consultant AB

September 2009

Summary

This report presents results from a study that was carried out in order to examine the applicability of the tapered plug concept for plugging of deposition tunnels in the deep repository for spent nuclear fuel. The report presents results from mechanical and thermo-mechanical models of the tapered plug. The models were analyzed with *3DEC*. The models included a portion of a deposition tunnel and its intersection with a main tunnel. In the deposition tunnel, a tapered concrete plug was installed. The plug was subjected to the combined load from the swelling backfill material and from pore pressure inside the deposition tunnel. The thermo-mechanical effects due to the heat generation in the spent fuel were also included in the analyses. Generic material parameter values for the concrete were used. The following items were studied:

- Stresses and displacements in the plug.
- Shear stresses and shear displacements in the rock-concrete interface.
- Stress additions in the rock due to the loads.

The sensitivity of the results to changes of constitutive models, to changes of the plug geometry and to pore water pressure in the rock-concrete interface was examined.

The results indicate that the displacements in the plug will be within reasonable ranges but the stresses may locally be high enough that they exceed acceptable levels. However, they can be reduced by choice of advantageous plug geometry and by having a good rock-concrete bond. The results also show that the stress additions in the rock due to the thermal load may yield stresses that locally exceed the spalling strength of the rock. At most locations, however, the rock stresses will amount at lower levels. It was concluded that, with choice of an appropriate design, the tapered plug seems to be an applicable concept for plugging of deposition tunnels. It was also concluded that further studies of the tapered plug concept should use material properties parameter values for low-pH concrete. Further, they should also include a closer examination of the rock-concrete interaction, a better model for the thermal load and a study of the effects of having rock fractures in the region around the plug.

Sammanfattning

Denna rapport presenterar resultat från en studie som genomfördes i syfte att undersöka om en svagt konformad plugg kan användas för förslutning av deponeringstunnlar i slutförvaret för använt kärnbränsle. Rapporten presenterar resultat från mekaniska och termo-mekaniska modeller av den svagt konformade pluggen. Modellerna analyserades med hjälp av *3DEC*. Modellerna inkluderade en del av en deponeringstunnel och dess skärning med en huvudtunnel. I deponeringstunneln installerades en svagt konformad betongplugg. Pluggen utsattes för den kombinerade lasten från det svällande tunnelåterfyllnadsmaterialet och från porvattentryck i deponeringstunneln. De termo-mekaniska effekterna på grund av värmegenereringen i det använda kärnbränslet inkluderades också i analyserna. Generiska parametervärden för betongmaterialet användes. Följande studerades:

- Spänningar och rörelser i pluggen.
- Skjuvspänningar och skjuvrörelser i berg-betonggränssnittet.
- Spänningstillskott i berget på grund av lasterna.

Resultatens känslighet för ändringar av konstitutiva modeller, för ändringar av pluggens geometri samt för porvattentryck i berg-betonggränssnittet undersöktes.

Resultaten indikerar att rörelserna i pluggen kommer att vara inom rimliga gränser men att spänningarna lokalt kan bli högre än acceptabelt. Dessa kan emellertid reduceras genom att en fördelaktig plug-geometri väljs och genom att en god vidhäftning mellan berg och betong erhålls. Resultaten visar också att spänningstillskotten i berget på grund av den termiska lasten kan ge spänningar som lokalt överstiger bergets spjälkningshållfasthet. Till en övervägande del kommer spänningarna emellertid att vara lägre. Det konstaterades att, med en lämplig design, användandet av en svagt konformad plugg verkar vara en gångbar metod för att försluta deponeringstunnlar. Det konstaterades också att vidare studier av den svagt konformade pluggen bör använda parametervärden för låg-pH-betong. Vidare bör de också inkludera en närmare studie av berg-betongkontakten, en bättre modell för den termiska lasten samt en studie av effekterna av att ha bergsprickor i området kring pluggen.

Contents

1 Introduction

1.1 Background

SKB applies the KBS-3 repository concept for deposition of spent nuclear fuel. The concept is based on horizontal tunnels at 400–700 m depth in crystalline rock. The spent fuel is deposited in copper canisters which are placed in vertical deposition holes in the tunnel floor. The deposition tunnels will be backfilled with a clay-based backfill material. During the operational time of the repository (about 100 years) the main tunnels, to which the deposition tunnels are connected, will be open (Figure 1-1). It is important for the long-term safety that the backfill properties are kept intact during the operational phase. Thus, in order to keep the backfill in place and to seal off the deposition tunnels hydraulically, a plug will be installed in each deposition tunnel close to the tunnel intersection immediately after the completion of the deposition tunnel backfill.

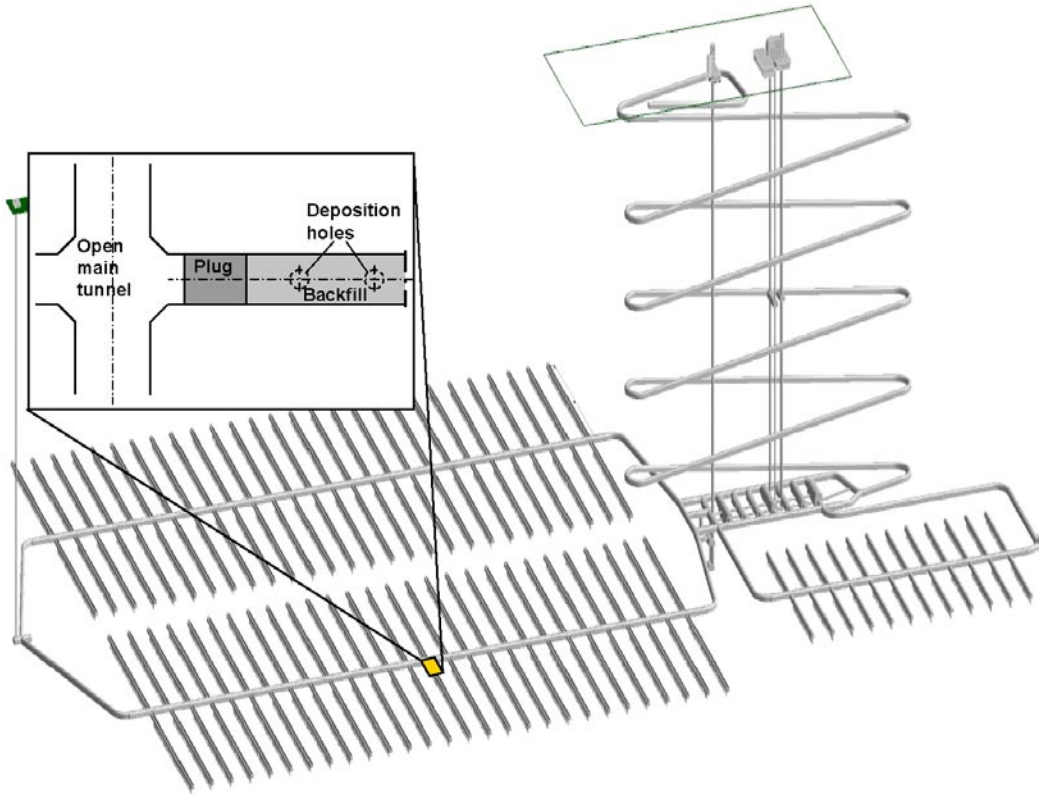

Figure 1-1. *Schematic figure of a general repository layout. The close-up shows a principle sketch of a horizontal section of the deposition tunnel-main tunnel intersection with a plug installed.*

There are a number of function requirements that the plug system must fulfill. Some of them are listed here:

- The plug shall withstand the combined pressure from the swelling backfill and from the ground water inside the deposition tunnel. The clay in the backfill will swell as it takes up water from the host rock and the maximum swelling pressure is predicted to be 2 MPa. The undisturbed hydrostatic pore water pressure in the repository will amount at 4–5 MPa depending on the chosen deposition depth. In this study, the water pressure is assumed to amount at 4 MPa at a maximum. Thus, the plug shall be designed to withstand a total mechanical pressure of 2 + 4 = 6 MPa. The water pressure assumption can be regarded as conservative since it does not account for the drainage caused by the excavations during the operational phase. The displacements and stresses in the plug shall be within acceptable ranges.
- The plug has to be tight enough to prevent backfill material from being eroded and transported out from the deposition tunnel.
- The plug shall be constructed in low-pH concrete. The basic requirement is that leachates from the concrete must have a pH $\leq$ 11.
- The plug shall have a life length of 100 years which is the estimated operational time of the repository. Hence, after closure of the repository the plug will not have any long-term safety function.

In addition to the requirements listed above, there are requirements regarding constructability and environmental requirements on the production and installation methods /SKB 2008a/. These have no direct importance for the present study and are not listed here.

There are alternative designs considered for the plug. The main alternative presently applied in the KBS-3V concept is to use a reinforced arc shape design (Figure 1-2, left). Full-scale tests of this concept has been made in both the reference projects Prototype repository and Backfill and plug test /Gunnarsson et al. 2001/. When this concept is used, the installation of the plug is complicated due to the recess in the rock at the support of the plug. If reinforcement has to be used, the plug construction will be yet more complicated. For these reasons SKB considers an alternative plug concept without the need for any recess or reinforcement. The alternative concept is a so called tapered plug (covering one or two rounds along the tunnel) (Figure 1-2, right). This type of plug is kept in place due to the cone-shaped tunnel perimeter (as a result of drill and blast tunneling technique) and the friction against the walls.

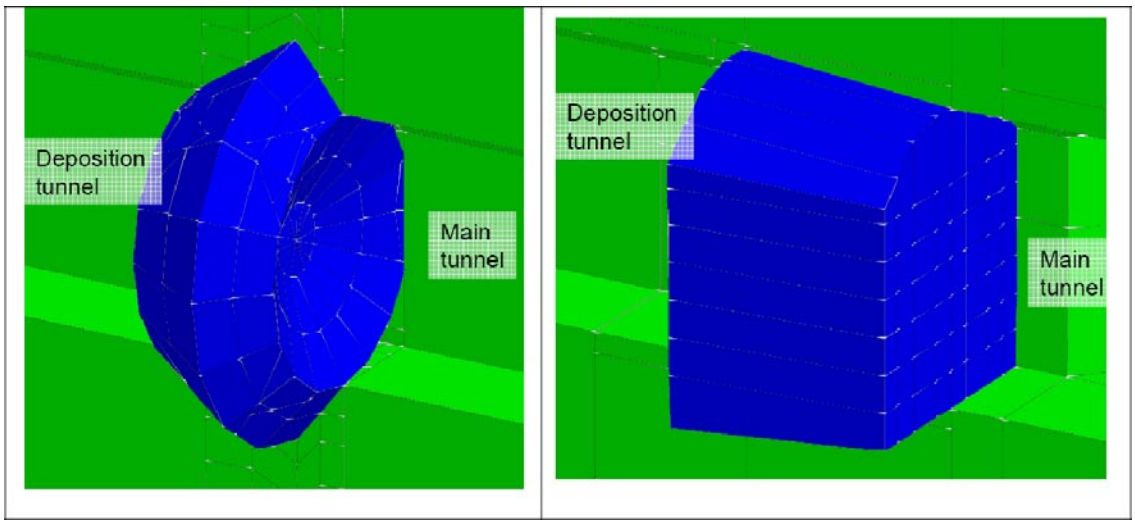

Figure 1-2. *Left: Reinforced arc-shaped plug concept. Right: Tapered plug concept.*

The swelling pressure from the clay-based backfill material combined with high pore water pressure inside the deposition tunnel may result in high loads on the plug. In addition, the spent fuel produces heat which will introduce thermal stresses in the rock and in the plug. In order to assess the applicability of the tapered plug concept for plugging of deposition tunnels, the mechanical stability of this type of plug has to be studied. Since the plug is kept in place by its cone-shape and by the friction in the rock-concrete interface, it is of particular interest to examine the interface behavior.

1.2 Scope of the report

This report is as a feasibility study where the applicability of the tapered plug concept for plugging of deposition tunnels is assessed. The report presents results from mechanical and thermo-mechanical models of the tapered plug. For the mechanical properties of the concrete, generic values were used and the results were compared with acceptance criteria based on BBK 04 /Boverket 2004/. The plug shall be constructed in low-pH concrete, and in parallel with this study, CBI Betonginstitutet AB has developed a concept for low-pH concrete /Vogt et al. 2008/. However, at the time when the calculations were carried out, the full set of material parameter values for low-pH concrete were not available. The results from the work at CBI should be taken into account in further studies of the tapered plug concept.

As a background to the modeling approach, Chapter 2 provides a brief description of a proposed concept for the tapered plug. During the course of the work, some modeling assumptions have stayed unchanged while others have been revised. In order to document this process, the modeling assumptions are described and discussed in Chapter 3. In Chapter 4 the modeling approach is described and in Chapter 5, the results are presented. In Chapter 6, the results are concluded and discussed. There is also given a proposal of items for further studies.

1.3 Objectives

In order to assess the applicability of the tapered plug concept for plugging of deposition tunnels during the operational phase, numerical calculations were performed by use of *3DEC*. A concrete plug in a deposition tunnel was subjected to both mechanical loads (pressure in backfill) and thermal loads. The objective was to calculate

- Stresses and deformations in the plug.
- Shear stresses and shear displacements in the rock-concrete interface.
- Stress additions in the rock due to the loads.

The sensitivity of the results to the following quantities was studied

- Concrete material model.
- Assumptions regarding rock-concrete interface behavior.
- Plug length.
- Look-out angle.
- Pore water pressure in rock-concrete interface.

The analysis holds for the time span when the concrete has gained its full strength until closure of the repository: 90 days after construction – 100 years. Before day 90, the plug is assumed be unloaded. The behavior of the plug before it has gained its full strength is not considered in this report.

2 Outline of the tapered plug concept

This chapter provides a brief description of how a plug system for closure of deposition tunnels can be constructed. The description is based on a description in /SKB 2008a/. A schematic sketch of a tentative design for the tapered plug system is shown in Figure 2-1. In the figure the concrete plug covers one round along the deposition tunnel. In addition to the actual concrete plug, there are a several supporting components with different functionalities:

- Water leaking from the backfill is collected in a filter material made of crushed rock. In order to control the water pressure that is applied on the plug before it has gained its full strength, the water can be drained out from the deposition tunnel through drainage pipes in the plug. The valves on these pipes will be closed when the concrete has matured.
- A seal of bentonite blocks is installed in front of the concrete plug in order to not apply an unfavorable water pressure in the interface between the rock and the concrete. The intention is to prevent water leaking from the backfill to find its way through fractures passing the concrete plug. However, there is a possibility that the water pressure gradient over the plug system not will be taken by the bentonite blocks alone. High water pressures that are built up in front of the bentonite will be spread in the surrounding rock and may eventually reach the space between the bentonite and concrete plug. Besides of reducing water pressures applied at the concrete plug, the bentonite will also contribute to an enhanced self-sealing capability of small cracks in the concrete plug.
- There will be a layer of concrete beams on each side of the bentonite seal for construction reasons.
- Grouting pipes will be installed at the interface between the rock and the concrete plug. The interface will be grouted when the concrete has matured. The concrete plug will also contain pipes for cooling and evacuation of air during concreting.

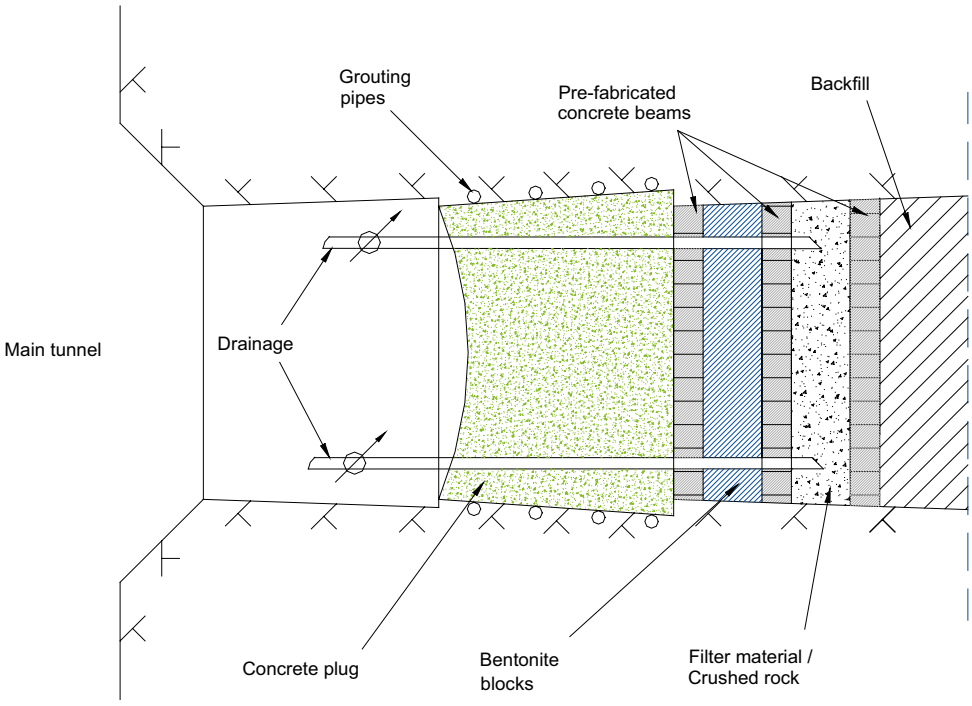

Figure 2-1. *Schematic sketch of a tentative design for a plug system with a tapered concrete plug covering one round along the deposition tunnel /SKB 2008a/. In front of the concrete plug there are bentonite blocks for hydraulic sealing and a filter where water leaking from the backfill is collected.*

3 Modeling assumptions

In this chapter the assumptions, which formed the basis for the modeling work, are presented and discussed. Some assumptions have been unchanged during the project whereas others have been revised during the course of the work. The chapter is divided into three sections which correspond to three categories of assumptions:

1. Loads.
2. Demands on the plug.
3. Plug properties.

3.1 Loads

3.1.1 Total pressure in the backfilled tunnel

The total pressure inside the backfilled deposition tunnel was assumed to be 6 MPa. This is the sum of the estimated swelling pressure in the backfill of 2 MPa and a pore water pressure of 4 MPa. The swelling pressure can be assumed to be fully developed 3–4 years after plug construction. The intention is to install drainage facilities which give the opportunity to control the water pressure in front of the plug. Thus, the water pressure can be assumed to be fully developed after that the concrete has developed sufficient strength and stiffness (cf. Chapter 2 above). It should be noted that assuming the water pressure to be 4 MPa most likely is conservative (cf. Section 1.1).

3.1.2 Water pressure in the rock-concrete interface

As shown in Chapter 2, the intention is to install a bentonite plug in front of the concrete plug. The function of the bentonite is to provide a seal that reduces the water pressure on the concrete plug. At the time of model set up it was not known to what extent the bentonite will reduce the water pressure on the concrete plug. Thus, two separate load cases were analyzed. In one case it was assumed that there will be no water pressures applied directly at the concrete plug. In another load case, the effect of a high water pressure was applied in the interface between the rock and the concrete plug (note that no hydraulic calculations were done). This latter case represents a situation that may arise if the bentonite plug loses its sealing function or if water-bearing rock fractures completely short-circuit the bentonite plug. The water pressure reduces the effective stress in the interface and thus reduces the interface shear strength. The pressure was assumed to be fully developed at the plug front and to taper off linearly to zero at the plug end (toward the open tunnel). This is probably a conservative assumption:

- The assumption implies that there is a leakage of water over the entire plug envelope surface. A leakage is most likely to take place along channels.
- A leakage would probably cause water pressure decrease inside the tunnel but in the model, the pressure was held constant. A high water supply rate from the deposition tunnel is needed to maintain the full pressure.

3.1.3 Lithostatic pressure

The possibility of time dependent strains in the rock was considered during the course of the work. The concern was that creep in the rock could introduce high stresses in the plug which eventually could result in damage. However, regularly measurements made in the final repository for radioactive operational waste (SFR) at Forsmark show small time dependent rock displacements. The measured average displacements around the SFR silo have been of the order of 0.2 mm during the first 20 years after construction. The displacements show a decreasing trend /Bodén and Lundin 2007/. Based on this, it was concluded that such effects did not have to be considered in the modeling here.

3.1.4 Thermal load from spent fuel

The decaying spent fuel will generate heat. This will induce thermal stresses in the rock mass and in the plug. The thermal expansion of concrete is higher than for granitic rock. Thus, the thermo-mechanical effects of the heat load were included in the modeling. As of yet, the exact repository layout is not known. As a basis for the thermal calculations, a generic layout was applied.

3.1.5 Grouting of the perimeter of the plug

For a low-pH concrete it will take about 90 days to reach its design strength. The shrinkage in the concrete during this period will results in a slot between rock and concrete. In order to achieve a good bond between rock and concrete, the plug will be cooled and the interface will be grouted. The temperature recover will then introduce pre-stress in the plug. This pre-stress is assumed to compensate for the further shrinkage that will take place during a long period of time. The pre-stress was not considered in the present work.

3.1.6 Earthquakes

The Baltic Shield area is a low-seismic area with few seismic events exceeding $M_L = 4$ /Slunga 1991/ and the likelihood of large event is very low. According to a very conservative estimate, a large earthquake might induce accelerations of the tunnel backfill that correspond to a 1 MPa pressure on the concrete plug. Due to the low probability of large earthquakes during the operational time, the effects earthquakes were not included in the analysis.

3.2 Demands on the plug

3.2.1 Operational time

The operational time for the plug is assumed to be equal to the operational time for the repository, i.e. about 100 years. There are no long-term demands on the plug, i.e. after closure of the repository there are no demands on the plug in terms of mechanical stability or hydraulic sealing capability.

3.2.2 Maximum stresses accepted

Load combinations

According to the code BBK 04 /Boverket 2004/, the plug shall be analyzed in three limit states:

1. Ultimate Limit State – fundamental combination.
2. Ultimate Limit State – accidental combination.
3. Serviceability Limit State – rare combination.

Requirements in the Ultimate Limit State are to not exceed characteristics values with applied partial coefficients relating to the strength properties of concrete. The requirements in the Ultimate Limit State are depending on the safety class of the structure. The plug is defined as a Safety Class 3 construction, which means that a collapse of the structure will result in very serious consequences.

Requirements in the Serviceability Limit State apply primarily to deformations and cracking of the structure.

There are different load factors for the different service states. The present analysis is simplified to only use the load combination in the Serviceability Limit State i.e. only use the load factor 1.0 of all loads. This load combination will, in the evaluation process, be valid for all states.

Compressive strength in conjunktion with load other than fatigue load

The characteristic values of the compressive strength, f_{cck}, are given in Table 3-1. In the ultimate limit state, the design value, f_{ccd}, of the compressive strength shall be determined from the expression

$$f_{ccd} = \frac{f_{cck}}{\eta\gamma_m\gamma_n} \quad (1)$$

where $\eta\gamma_m$ = 1.5 and γ_n=1.2 for Safety Class 3. (In design with respect to accidental load and progressive collapse, $\eta\gamma_m$ = 1.2 and γ_n = 1.0).

In the serviceability state, the value $f_{ccd} = f_{cck}$ may be used.

Tensile strength in conjunktion with load other than fatigue load

The characteristic values of the tensile strength, f_{ctk}, for ordinary aggregate are given in Table 3-2 for strength class C 28/35–C 60/75. In the ultimate limit state, the design value, f_{ctd}, of the tensile strength shall be determined in analogy with Eq. 1 with $\eta\gamma_m$ = 1.5 and γ_n =1.2 for Safety Class 3. (In design with respect to accidental load and progressive collapse, $\eta\gamma_m$ = 1.2 and γ_n = 1.0).

In the serviceability state, the value $f_{ctd} = f_{ctk}$ may be used.

Table 3-1. Characteristic values of the compressive strength, f_{cck}, of concrete. From Regulations for concrete structures BBK 04 /Boverket 2004/.

Strength class	f_{cck} (MPa)	Strength class	f_{cck} (MPa)
C 12/15	11.5	C 40/50	38.0
C 16/20	15.5	C 45/55	43.0
C 20/25	19.0	C 50/60	47.5
C 25/30	24.0	C 54/65	51.5
C 28/35	27.0	C 55/67	52.0
C 30/37	29.0	C 58/70	55.0
C 32/40	30.5	C 60/75	57.0
C 35/45	33.5		

Table 3-2. Characteristic values of the tensile strength, f_{ctk}, of concrete. From Regulations for concrete structures BBK 04 /Boverket 2004/.

Strength class	f_{ctk}[1] (MPa)	Strength class	f_{ctk}[1] (MPa)
C 28/35	1.80	C 55/67	2.85
C 30/37	1.90	C 58/70	2.90
C 32/40	2.00	C 60/75	2.95
C 35/45	2.10		

[1] Long term effects considered.

Acceptance criteria for the plug

Based on the first tests of the low-pH concrete /Vogt et al. 2008/, it can be assumed that the concrete complies with the strength class C 55/67 after approximately 90 days from start of hardening. According to Table 3-1 and Table 3-2, this gives a characteristic compression strength, f_{cck}, of 52.0 MPa and characteristic tensile strength, f_{ctk}, of 2.85 MPa. Based on this and on the load combination considerations above, the acceptance criteria for the concrete will be:

- Acceptance criteria in the ultimate limit state:
  $\sigma_{cc} < 52.0 / 1.5 / 1.2 = 29$ MPa
  $\sigma_{ct} < 2.85 / 1.5 / 1.2 = 1.6$ MPa
- Acceptance criteria in the serviceability state:
  $\sigma_{cc} < 52.0$ MPa or
  $\sigma_{cc} < 0.6 \cdot 52.0 = 31.0$ MPa*
  ($\sigma_{ct} < 2.85$ MPa), this value shall only be used when checking deformations and cracking of the concrete.

According to this, the largest acceptable compressive and tensile stresses in the plug are about 30 MPa and 1.5 MPa, respectively.

3.2.3 Maximum deformations accepted

As of yet, there are no specifications of the maximum accepted displacement of the plug. However, a rough estimate of such a limit may be made according to the following. Displacements of the plug front (the end facing the backfilled tunnel) may yield density reductions in the bentonite blocks placed inside the plug. A reduction of the bentonite density will increase its hydraulic conductivity, and if the density becomes too low, the sealing function of the bentonite blocks may be jeopardized. Assume that the thickness of the blocks is 500 mm, that they are designed to have a saturated density of 2,000 kg/m^3 and that the minimum density allowed is 1,950 kg/m^3. Then, the maximum allowed volumetric strain will be 1–1,950/2,000 = 0.025, which corresponds to an average displacement of the plug front of 0.025 · 500 mm = 12.5 mm. Based on this simple calculation, the maximum allowed average displacement of the plug front may be set to 10 mm.

3.3 Plug properties

3.3.1 Mechanical properties

It was assumed that the plug will be constructed without any reinforcement and thus will have a relatively low tensile load bearing capability. This was considered when the effects of tensile stresses were studied. The basic assumption was that the concrete is linear elastic but in one model, a limited tensile strength was applied.

At the time when the calculations were initiated, no parameter values were available for low-pH concrete. Hence, it was assumed that the material characteristics of low-pH concrete are similar to that of ordinary concrete. In the first models studied the value of Young's modulus was set to a generic value. This first assumption was revised when creep in the concrete was considered. According to /Boverket 2004/, a K50 concrete with the thickness $t > 0.3$ m and an age of 1,000 days operating in RH 100% should have a creep factor of 1.4. This gives a Young's modulus of about 24 GPa. The Poisson's ratio was set to the generic value 0.2.

* According to BBK 04, there are limitations of the compressive stresses in concrete due to long-term loads, $f_{ccd} = 0.6 \cdot f_{cck}$ /Boverket 2004/.

3.3.2 Rock-concrete interaction

The tapered plug is held in place by its cone-shape and by the friction between the rock and the concrete. Thus, the behavior (stiffness and strength) of the rock-concrete interface is important for the performance of the plug. The exact behavior is dependent on factors such as the detailed geometry of the rock surface and the stiffness and strength of rock and concrete. A detailed study of how these factors influence the interface behavior was beyond the scope of this study. Instead, two previously established models that relate the interface shear strength σ_s to the interface effective normal stress $\sigma_{n,eff}$ were tested:

- Mohr-Coulomb law: $\sigma_s = c + \sigma_{n,eff} \tan(\varphi)$, where c is cohesion and φ is friction angle.
- Law for concrete-concrete interaction according to /CEB 1993/: $\sigma_s = 0.4 f_{ccd}^{2/3} \sigma_{n,eff}^{1/3}$, where f_{ccd} is the design value of the concrete compressive strength.

The Mohr-Coulomb law was considered to be more conservative since it gives lower shear strength for normal stresses up to about 10 MPa (for the values of f_{ccd}, c and φ applied here).

3.3.3 Plug geometry

A rule of thumb used when tunnel plugs are constructed in conjunction with for instance water power dams is that the plug length L is set according to

$$L = a \cdot H \tag{2}$$

where a is a factor set to be in the range 0.04–0.08 and H is the pressure gradient over the plug (water head). The main reason for applying a length according to Eq. 2 is to reduce the leakage of the plug and not for structural reasons. Applying this rule of thumb and assuming a total gradient of 6 MPa (600 m water head) would give a plug length of 24–48 m. A plug of that length would require too much space, take too much time to construct and be too expensive for the repository application. If this type of plug should come in question, it has to be much shorter. As a first modeling assumption, the plug length was set to 8 m (2 rounds). As the work progressed, the plug length was decreased to 4 m (one round) in order to save space and costs for the construction.

It was assumed that the deposition tunnel will be constructed using two different techniques. The upper parts of the tunnel will be excavated by drill and blast technique whereas the bottom bench (≈ 1 m) will be excavated by wire sawing (field-tests of this method will be carried out as a part of SKB's RD&D programme /SKB 2007/). This will provide a flat tunnel floor with a minimized EDZ (Excavation Damaged Zone). Thus, the first assumption made regarding the plug geometry was that the walls and the roof give the upper parts of the plug a conic shape whereas the floor was kept flat. When the plug was shortened from 8 m to 4 m, the floor was also given an inclination in order to give the plug better load bearing capability.

There are uncertainties about which look-out angle that will be used when excavating the tunnel. In order to study the sensitivity of stresses and displacements in the plug to the look-out angle, two angles were tried: 2° and 4°. When the tunnel is constructed there may be more overbreak on one side of the plug which will give a non-symmetric plug geometry. This possibility has not been accounted for in the present study but should be considered if further studies of this plug concept are carried out.

The dimensions of the deposition tunnel were set to 4.4 m (width) and 5 m (height). It shall be noted that these dimensions are smaller compared to what was specified for instance in /SKB 2006a/. There is an intention to keep the tunnel cross section area as small as possible and the specified tunnel dimensions were subject to revision at the time of the model set up.

4 Modeling approach

4.1 General

This chapter presents the modeling approach. The first section is a presentation of the code that was used. In the following three sections, the geometric outlines of the model, material properties, initial conditions and boundary conditions are described.

4.2 Description of *3DEC*

The models were analyzed with *3DEC* (3 Dimensional Distinct Element Code), version 3.0 /Itasca 2003/. *3DEC* is a three-dimensional numerical program based on the distinct element method for discontinuum modeling. *3DEC* simulates the response of discontinuous media (such as jointed rock mass) subjected to either static or dynamic loading. The discontinuous medium is represented by an assemblage of discrete blocks. The discontinuities are treated as boundary conditions between the blocks; large displacements along discontinuities and rotations of blocks are allowed. Individual blocks behave either as rigid or deformable material. Deformable blocks are subdivided into a mesh of finite difference elements, and each element responds according to a prescribed linear or non-linear stress-strain law. The relative motion of the discontinuities is also governed by linear or non-linear force-displacement relations for movement both in the normal and shear directions. *3DEC* is based on a "Lagrangian" calculation scheme that is well-suited to model the large movement and deformations of a blocky system /Itasca 2003/.

Implemented in *3DEC*, there is a thermal logic that provides the possibility to calculate thermal stresses based on heat contributions from heat sources arbitrarily located in the 3D-space. The thermal logic is based on analytical solutions and no heat transport calculations are made. This logic was used here to calculate thermal stresses due to the heat produced by the decaying spent fuel.

3DEC also contains a built-in programming language called *FISH* (short for *FLAC*ish; *FISH* was originally developed for the finite difference continuum code *FLAC* /Itasca 2005/). With *FISH* it is possible to extend *3DEC's* usefulness by the definition of own functions and variables /Itasca 2003/. *FISH* was used here for the implementation of a model for rock-concrete interaction.

4.3 Model description

4.3.1 Geometric outlines

The geometric outlines of the *3DEC* model are presented in this section. A model overview is shown in Figure 4-1. The model included a portion of the host rock around the intersection between a deposition tunnel and a main tunnel. After tunnel excavation, the deposition tunnel was filled with backfill material and the concrete plug was installed close to the intersection with the main tunnel. The main tunnel was kept open. Note that parts of the model are hidden in the figure. The orthogonally oriented planes are construction planes which were used to define the geometry and to facilitate the discretization of the continuum.

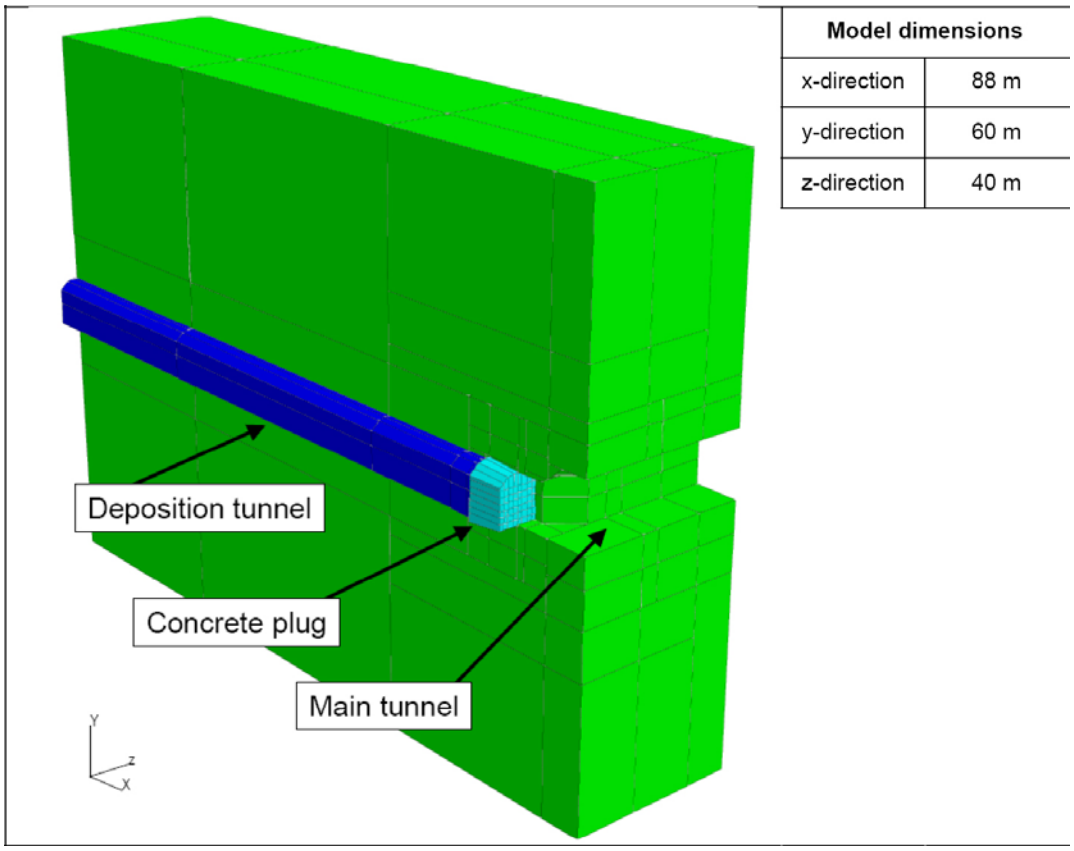

Model dimensions	
x-direction	88 m
y-direction	60 m
z-direction	40 m

Figure 4-1. *Geometric outlines of the model. The orthogonally oriented planes are construction planes which were used to define the geometry and to facilitate the discretization of the continuum. Parts of the model are hidden in the figure.*

The dimensions of the model were 88 m in the deposition tunnel direction, 40 m across the deposition tunnel and 60 m in the vertical direction. The deposition tunnel distance was assumed to be 40 m. Thus the vertical boundaries parallel to the deposition tunnel were located halfway to the neighboring deposition tunnels and hence could be regarded as symmetry boundaries (Figure 4-2). By making the assumption that two deposition tunnels run into the main tunnel opposite to each other (as indicated by the wire-framed part of the figure), the vertical boundary along the main tunnel center can also be regarded as a symmetry boundary. In Figure 4-2, the chamfered corners at the tunnel intersection also are shown. The chamfer length was 3 m and the angle was 45°. The plug end was located 1 m from the chamfer.

Figure 4-3 shows vertical sections of the deposition tunnel and of the main tunnel. The tunnel dimensions are indicated in the figure. The dimensions of the main tunnel (width 10 m and height 7 m) were set in accordance with the specifications in /SKB 2006a/. The dimensions of the deposition tunnel were set to 4.4 m (width) and 5 m (height). It shall be noted that both the dimensions of the deposition tunnel are smaller compared to what was specified in /SKB 2006a/. There is an intention to keep the tunnel cross section area as small as possible and the specified tunnel dimensions were subject to revision at the time of the model set up.

Two values of the plug length L were tested: 8 m (two rounds) and 4 m (one round) (Figure 4-4, left). The smallest part of each round had the same dimensions as the remaining parts of the deposition tunnel (Figure 4-3, left and Figure 4-4, right). The envelope surfaces of the plug were inclined with respect to the tunnel direction, i.e. the geometry of a drill-and-blast-excavated tunnel was explicitly modeled at the particular tunnel section where the plug was located (in two cases the floor was flat, cf. Table 4-3 below). Two look-out angles were tested: $\alpha = 2°$ and 4°. In the remaining parts of the deposition tunnel and in the main tunnel, such inclinations (necessary for construction) were omitted in the modeling.

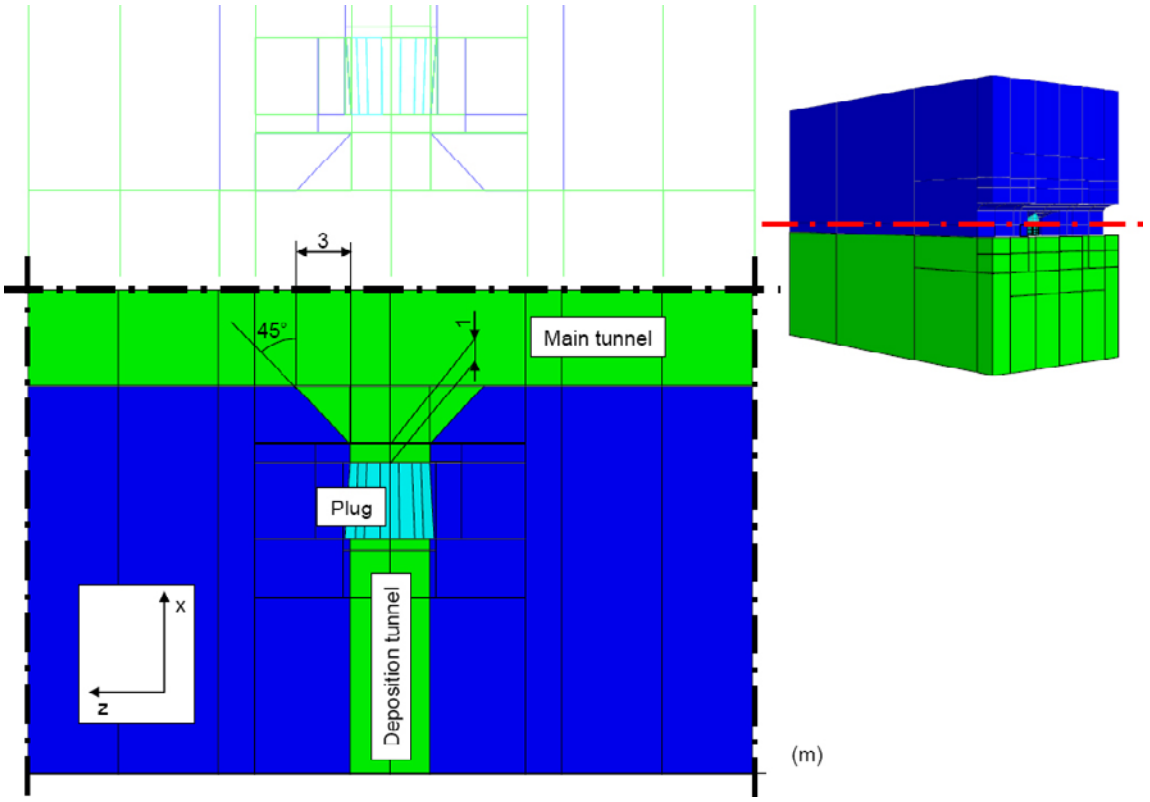

Figure 4-2. *Horizontal section through deposition tunnel center showing the geometry of the tunnel intersection. The dashed and dotted lines indicate boundaries that can be regarded as symmetry boundaries. The wire framed part of the picture was not a part of the model. It just indicates the assumption that two deposition tunnels run into the main tunnel opposite to each other. The orthogonally oriented planes are construction planes which were used to define the geometry and to facilitate the discretization of the continuum.*

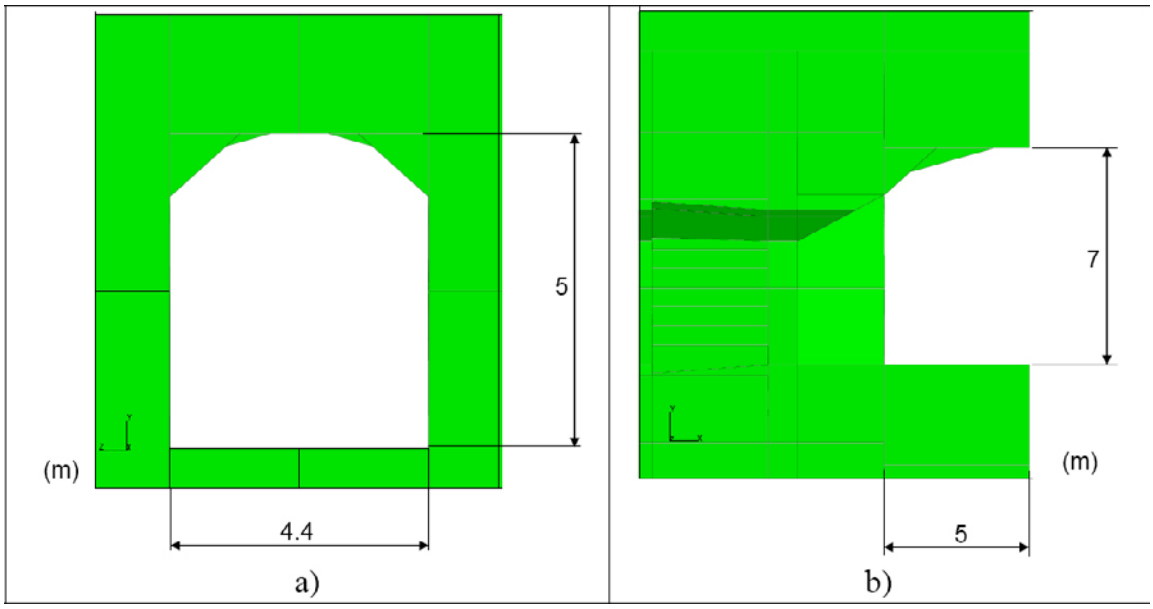

Figure 4-3. *Vertical sections showing the dimensions of a) the deposition tunnel and of b) the main tunnel. The orthogonally oriented planes are construction planes which were used to define the geometry and to facilitate the discretization of the continuum.*

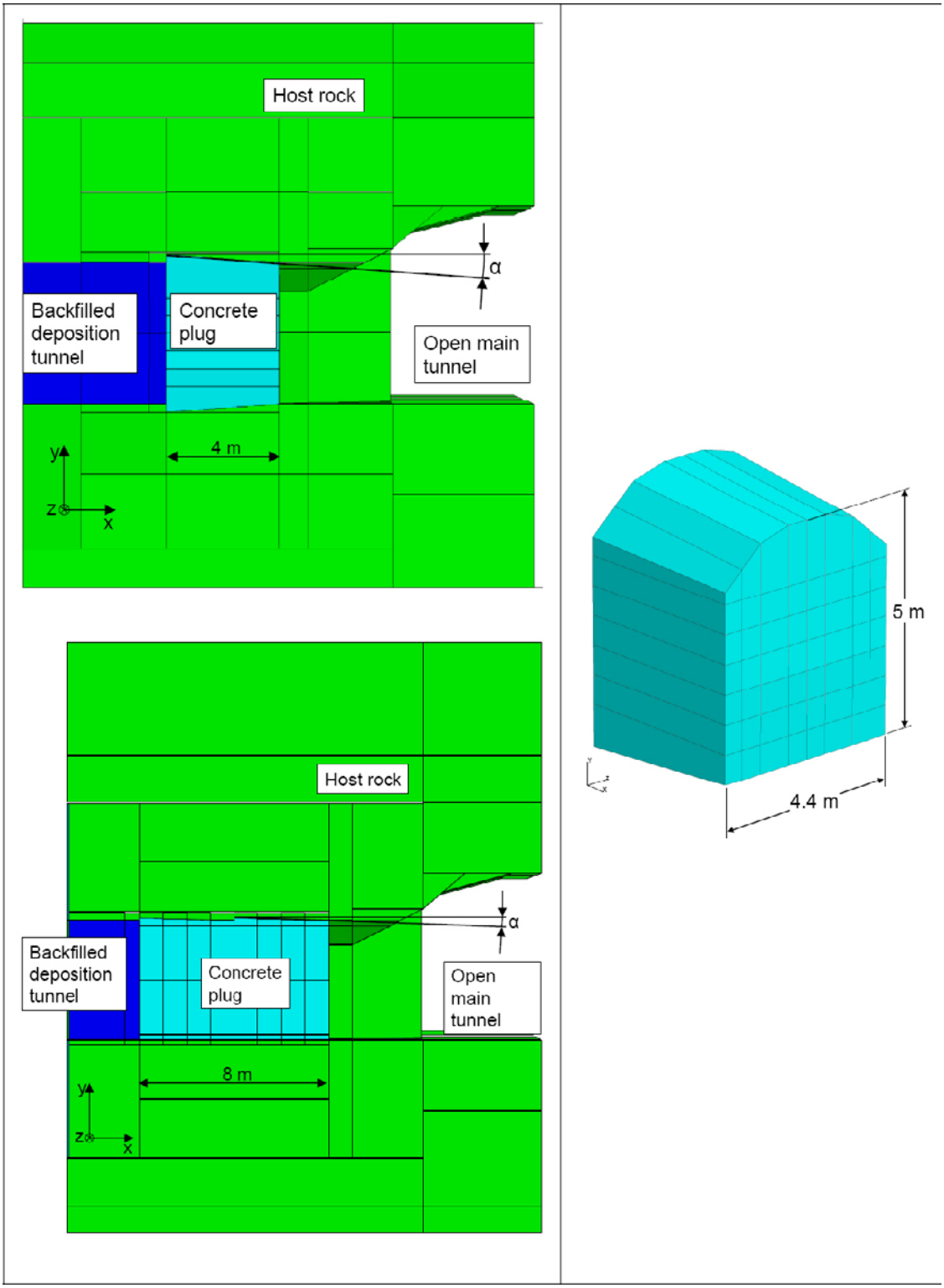

Figure 4-4. *Geometry of plug. Left: Vertical section along the deposition tunnel axis showing the plug and tunnel intersection for both cases with plug length 4 m and 8 m, respectively. Right: Plug dimensions at the end facing the open main tunnel. The orthogonally oriented planes are construction planes which were used to define the geometry and to facilitate the discretization of the continuum.*

In Figure 4-5, the finite difference mesh is shown. The type of finite difference element differs between the model variants (8 m and 4 m). In the 4 m model, elements which provide so called mixed discretization /Itasca 2003/ were used. This was done since the influence of using a non-linear constitutive model for the concrete was tested in one variant of this model. The mixed discretization element gives a much more accurate plastic solution compared to the tetrahedral element which was used in the 8 m model. When applying a linear elastic material model, the different element types give similar results.

4.3.2 Material properties and constitutive laws

Continuum properties

The basic assumption was that all continua were linear elastic with parameter values according to Table 4-1. The values of Young's modulus and Poisson's ratio of the rock were in agreement with site investigations data for the Forsmark site /Glamheden et al. 2007/. The mechanical properties of the backfill material have no importance for the results since the stress (pressure) in this material was a load condition that was controlled during the calculations. In one model variant, the concrete was given a limited tensile strength of 2 MPa. The analytic solution that is used by *3DEC* for thermal calculations implies that all materials have the same thermal properties.

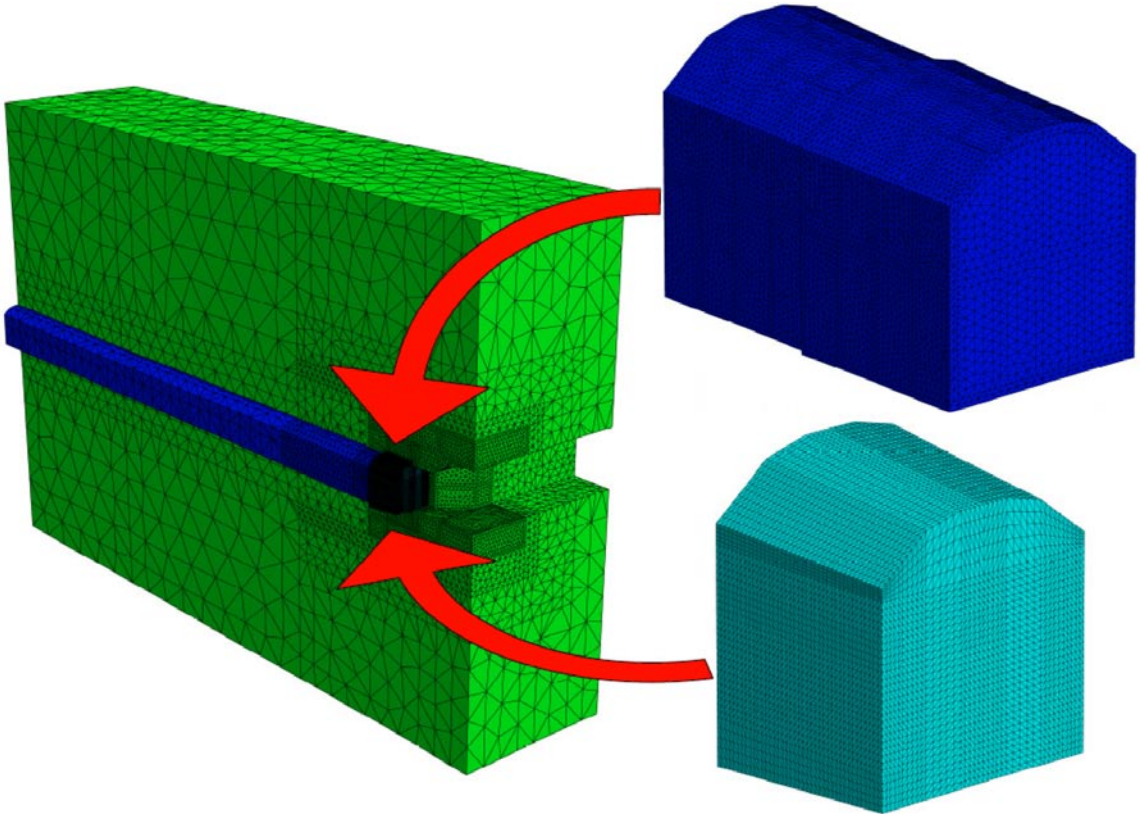

Figure 4-5. *The finite difference mesh of the model. The discretization of the plug is shown in the close-up to the right. Note that parts of the rock are hidden in the figure.*

Table 4-1. Continuum properties.

Material	E (MPa)	υ	Tensile strength (MPa)	Density (kg/m³)	Thermal expansion coefficient (K^{-1})	Heat conductivity (W/(m·K))	Thermal diffusivity (m^2/s)
Rock	70,000	0.25	–	2,700	$6 \cdot 10^{-6}$	3.6	$1.67 \cdot 10^{-6}$
Concrete	24,000	0.20	2*	2,200	$1 \cdot 10^{-5}$		
Backfill	18	0.31	–	2,000			

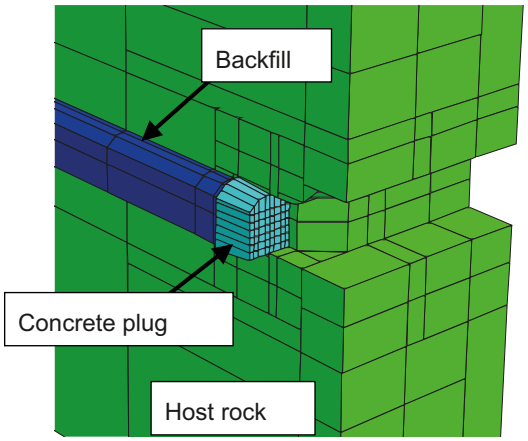

* Set in one model.

Rock-concrete interface properties

The interface logic in *3DEC* is based on force-displacement laws both in the shear and in the normal directions. The force-displacement laws are applied at "sub contacts" in the interface. The number of "sub contacts" in an interface is proportional to the number of finite difference zones adjacent to the face /Itasca 2003/. Thus, a finer discretization of the continua close to the interface gives a finer discretization of the interface.

At the rock-concrete interface surfaces (Figure 4-6), linear force-displacement laws were applied in the elastic range. The normal stiffness was arbitrarily set to K_n = 100 GPa/m and the shear stiffness to K_s = 42 GPa/m. The ratio K_s/ K_n is 0.42 which is equal to the shear modulus to Young's modulus ratio, *G/E*, for the concrete.

Two different laws for the relation between the interface effective normal stress $\sigma_{n,\,\mathrm{eff}}$ and shear strength σ_s were tested:

Mohr-Coulomb criterion (base case assumption).

$$\sigma_s = c + \sigma_{n,eff} \cdot \tan\varphi \qquad (3)$$

where c is cohesion and φ is friction angle. The law was implemented such that failure of joint in shear or tension resulted in zero cohesion, c, following failure.

Law according to CEB-FIP MODEL CODE 1990 /CEB 1993/.

$$\sigma_s = 0.4 \cdot f_{ccd}^{2/3} \cdot \sigma_{n,eff}^{1/3} \qquad (4)$$

where f_{ccd} is the design value of the concrete compressive strength. Here, f_{ccd} was set to 32 MPa, which was regarded to be a relevant generic value. It was set at an early state of the modeling work before data for low-pH concrete were available. Even if it is not exact the same as the value used as acceptance criterion (cf. Section 3.2.2), the difference is small and considered of minor importance for the conclusions of this study.

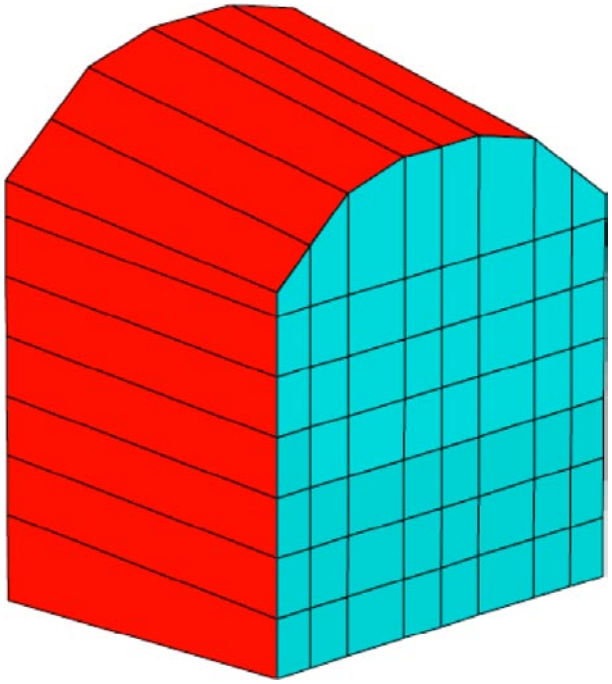

Figure 4-6. *The plug with the plug-rock interface surfaces indicated with red (4 m case).*

Even if no hydraulic calculations are performed, the effect on the interface shear strength of a pore water pressure can be considered. The effect of the pore water pressure was accounted for according to the law of effective stress, i.e.

$$\sigma_{n,eff} = \sigma_{n,tot} - \sigma_w \quad (5)$$

where

$\sigma_{n,\,eff}$ is the effective normal stress

$\sigma_{n,\,tot}$ is the total normal stress

σ_w is the pore water pressure

The laws in Eqs. 3 and 4 are compared in Figure 4-7. In the Figure, the friction angle, φ, in the Mohr-Coulomb law was set to 45° and the cohesion, c, to zero. The FIP model stress-strength law (Eq. 4) was implemented in *3DEC* by use of the built-in programming language *FISH*. The solid blue curve shows how the FIP model was represented by *3DEC*. The steps in the curve are due to a limitation in the code; the shear strength can not be varied continuously. Instead, it was varied in steps. This has a minor importance for the results.

4.3.3 Initial conditions, boundary conditions and loads

In situ stress

The main purpose of the model was to calculate stresses and displacements in the plug and in the rock due to the pressure build up inside the closed deposition tunnel. However, the model was also used to make an estimate of the rock stresses due to the combination of the loads and the in situ stresses. Thus, in situ stresses were included in the model. These are presented in Table 4-2. The stress magnitudes were in accordance with the stress model in the Forsmark site descriptive model (SDM) version 1.2 /SKB 2005/ applied at 400 m depth. Later reporting proposes that the stress levels at this depth may be somewhat lower /see e.g. SKB 2008b/. The major principal stress was set to be aligned with the deposition tunnel and the intermediate principal stress was set to be perpendicular to the deposition tunnel.

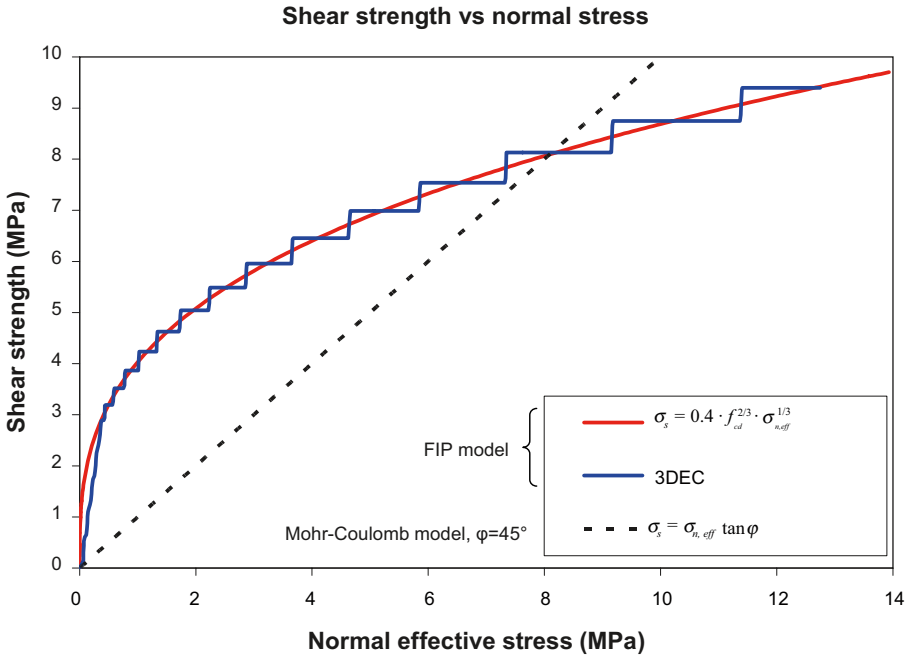

Figure 4-7. Normal effective stress-shear strength relations. The step-wise changes of the strength in the 3DEC response are due to a limitation in the code.

Table 4-2. In situ stresses.

Component	Stress (MPa)	Comment
$S_{xx} = S_1$	43	Along deposition tunnel
$S_{yy} = S_3$	11	Vertical
$S_{zz} = S_2$	29	Across the deposition tunnel
$S_{xy} = S_{xz} = S_{yz}$	0	

Boundary conditions

The boundary conditions are illustrated in Figure 4-8. All vertical boundaries and the bottom boundary were locked for displacements in their normal directions (roller boundaries). At the top boundary, a constant stress of 11 MPa was applied. When the effect of the heating from the decaying spent fuel was applied in the model, the expansion of the rock mass outside the model was not taken into account. This gives some overestimation of the thermal stresses and is thus conservative. According to thermo-mechanical near-field analyses by /Fälth and Hökmark 2006/, the use of fixed boundaries, similar to those used here, gave an overestimation of the thermal stresses in the rock close to a canister of about 7% after 100 years. Before that, the overestimation was smaller. The overestimation made in the present study is of the same magnitude.

Pressure inside deposition tunnel

The total pressure of 6 MPa (swelling pressure from the clay-based backfill material (2 MPa) + pore water pressure (4 MPa)) inside the deposition tunnel was applied as a hydrostatic stress field in the backfill material. Thus, both the plug and the rock around the tunnel were subjected to the stress.

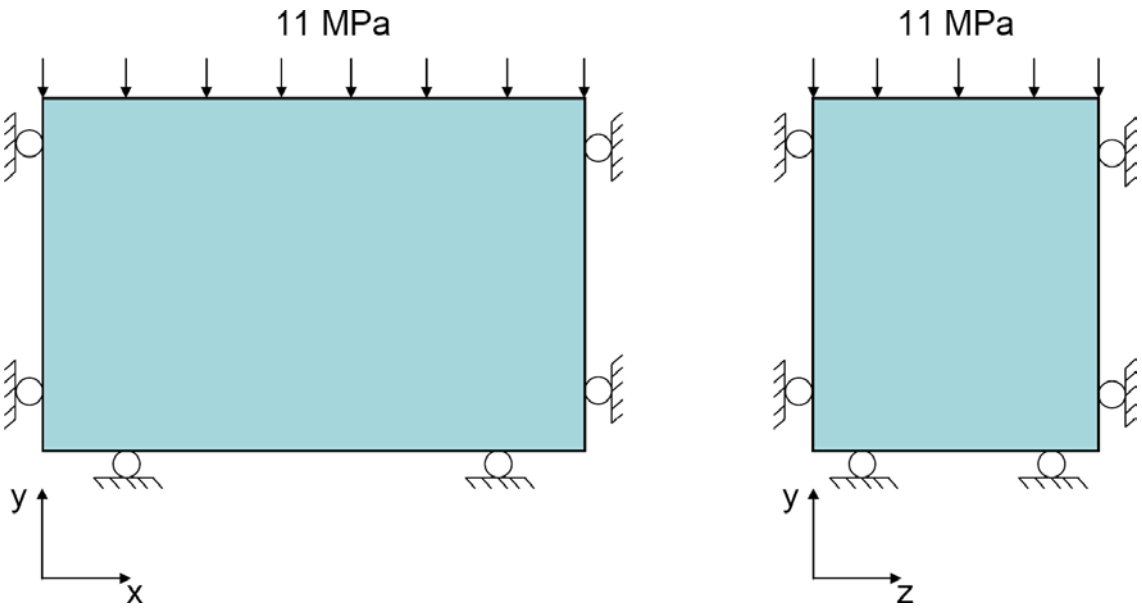

Figure 4-8. *Boundary conditions. All vertical boundaries and the bottom boundary were locked for displacements in their normal directions (roller boundaries). At the top boundary, a constant stress of 11 MPa was applied.*

Pore pressure

As a load case, the effect of a pore pressure in the concrete-rock interface (Figure 4-6) was considered. Thus, it was assumed that there was a leakage of water from the deposition tunnel into the open main tunnel and that the leakage was taking place along the rock-concrete interface. The assumed distribution of pore pressure along the plug is shown in Figure 4-9. The pressure was assumed to amount at 4 MPa inside the tunnel and decrease linearly to zero at the plug end. It shall be pointed out that no hydraulic calculations were done. The pore pressure was held constant and influenced the mechanical calculation by decreasing the effective normal stress at each sub contact location (cf. Section 4.3.2).

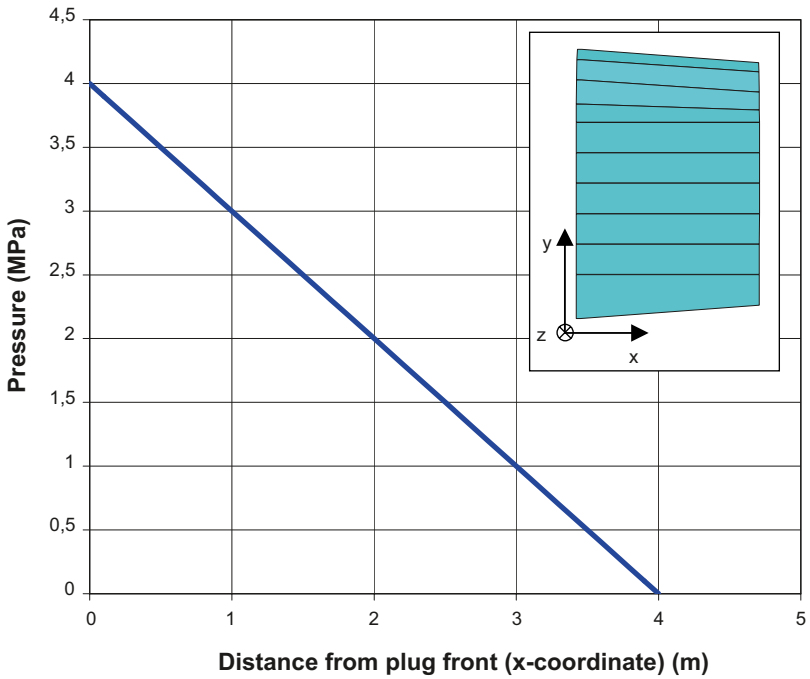

Figure 4-9. *Distribution of pore pressure along the plug. The pressure was assumed to decrease linearly along the plug.*

Heat load

The thermo-mechanical effects on the plug of the heat generated by the deposited spent fuel were considered. The thermal logic in *3DEC* is based on analytic solutions and no heat flow calculations are done. Linear heat conduction is assumed which means that the principle of superposition can be used. The temperatures in the model are calculated as sums of the contributions of heat sources that can be arbitrary located in the 3D-space. For this project, a generic repository layout with five deposition areas was assumed (Figure 4-10). Each deposition area consisted of 29 × 41 = 1,189 canisters (heat sources). The canister spacing was set to 6 m and the deposition tunnel spacing to 40 m. The canister centers were assumed to be located 5 m below the tunnel floor. The model origin was located at the plug front, i.e. the plug was assumed to be located close to the center of the repository. The distance between the plug front and the closest canister center was assumed to be 6 m. The analytic solution does not account for any openings. This gives a slight over estimation of the temperatures and is thus conservative. The thermo-mechanical properties are presented in Table 4-1 above. The heat transport properties are assumed to be the same for all materials. The initial temperature has no importance for the thermo-mechanical calculations since the thermal stresses are calculated based on temperature increments. The initial temperature was set to zero.

The canisters were assumed to have the heating power $P(0)$ = 1,700 W each at the time of deposition /SKB 2006b/. Here, the power decay is expressed as:

$$P(t) = P(0)\sum_{i=1}^{7} a_i \exp(-t / t_i) \qquad (6)$$

where t is time. The values of t_i and a_i are listed in Figure 4-11 along with a graph showing the normalized power as a function of time. The decay function coefficients were obtained by interpolating between values for 30-year-old and 40-year-old fuel /Hökmark and Fälth 2003/. It was assumed that all canisters were deposited simultaneously at t = 0.

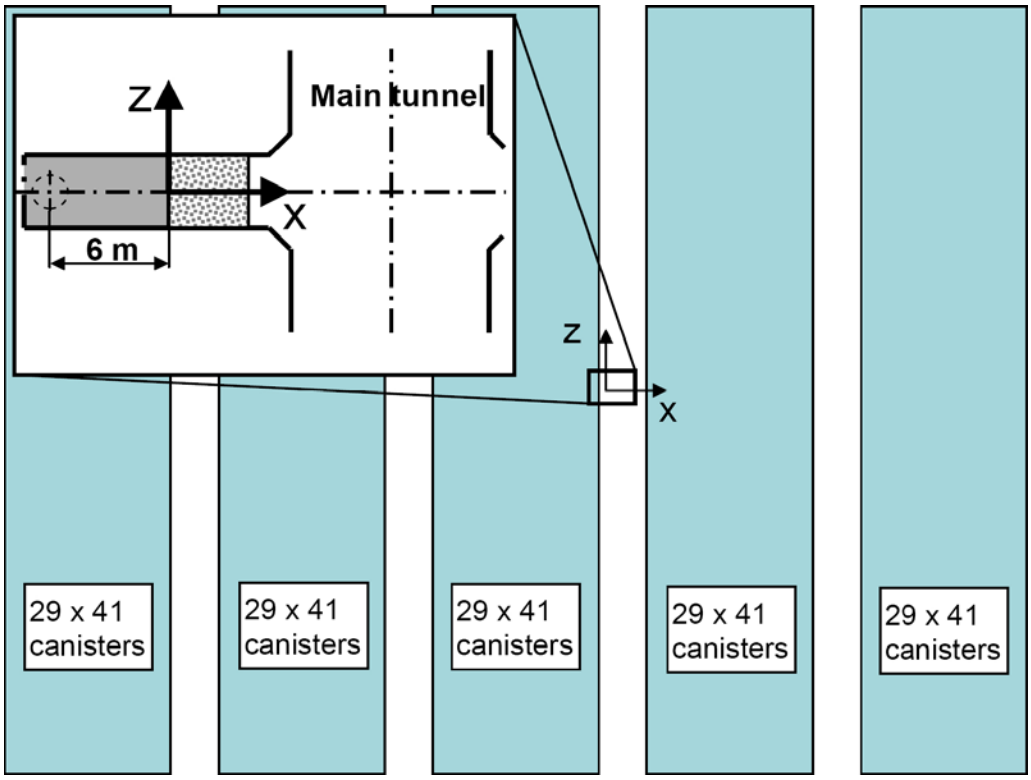

Figure 4-10. *Outline of the generic repository layout used for thermal calculations. The 3DEC model was located at the origin, i.e. close to the center of the repository.*

i	t_i (years)	a_i
1	20	0.060
2	50	0.705
3	200	-0.055
4	500	0.250
5	2000	0.025
6	5000	-0.009
7	20000	0.024

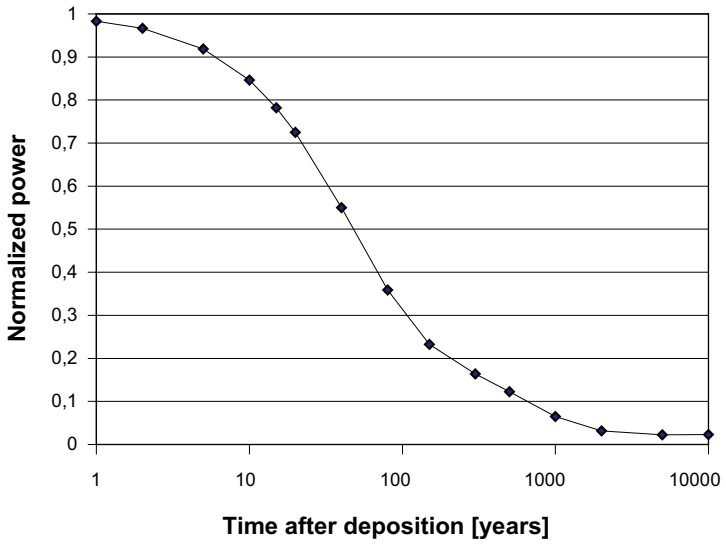

Figure 4-11. *Decay function for the spent fuel.*

4.3.4 Calculation sequence

The calculation comprised of the following steps (Figure 4-12):

1. Application of in situ stresses and establishment of initial equilibrium.
2. Excavation of main tunnel.
3. Excavation of deposition tunnel.
4. Installation of backfill material and of plug. A 6 MPa stress was applied in the backfill material to simulate the total effect of swelling pressure and a pore water pressure inside the tunnel.
5. Thermo-mechanical calculation to examine effects of heat from the spent fuel.
6. The effect of pore water pressure in the plug-rock interface was applied (accidental case).

At each calculation step, mechanical equilibrium was achieved and the current state was saved. Step 5 and 6 were not analyzed in sequence but as separate load cases. It shall also be noted that even if step 5 always was applied after step 4, this is not necessarily the load sequence in reality. If the water supply rate to the deposition tunnel is low, the plug may be subjected to thermal loads before any significant pressure has developed inside the deposition tunnel.

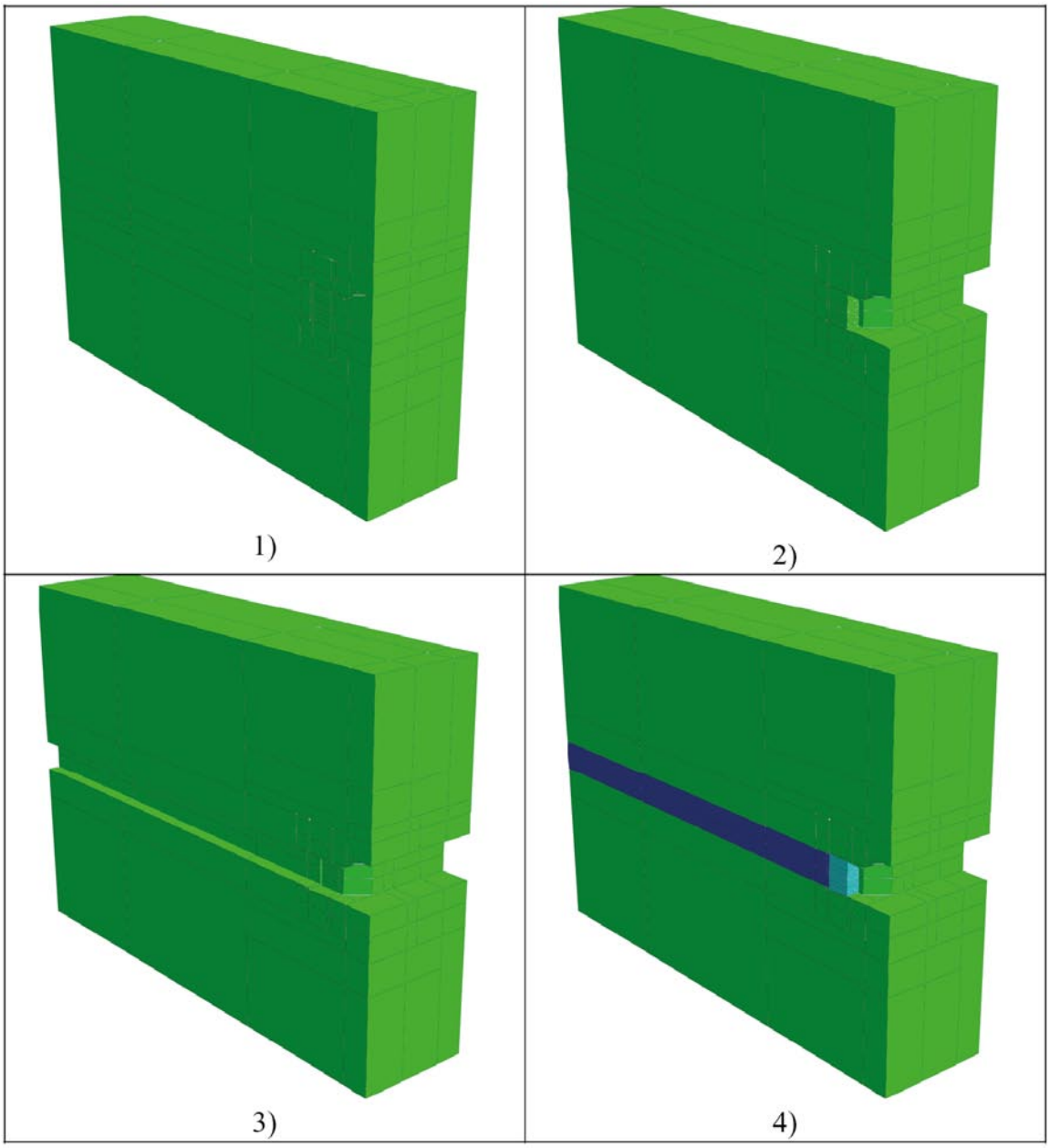

Figure 4-12. *Illustration of the calculation sequence: 1) Establishment of initial equilibrium. 2) Excavation of main tunnel. 3) Excavation of deposition tunnel. 4) Installation of backfill and plug. Pressure was applied in the backfill. Note that half of the model is hidden in the figure.*

4.4 Model map

Eight models have been analyzed. They are presented in Table 4-3. Two plug lengths (4 and 8 m) and two look-out angles (2° and 4°) have been studied. In the 8 m model, the floor was assumed to be flat (c.f. Section 3.3.3). In order to study the influence of plug length only, one of the 4 m models was also given a flat floor.

When using an elastic material model, tensile stresses were developed at some locations. Thus, in order to see what importance a limited tensile strength in the concrete has for the stress redistributions and displacements, a limited concrete tensile strength was set in one model.

Two different types of rock-concrete interface constitutive laws were tried: Mohr-Coulomb model and FIP model (c.f. Section 4.3.2). For the Mohr-Coulomb model, the sensitivity to the friction angle was examined. The case with 50° friction angle and cohesion 2 MPa can be regarded as a bounding case where the best possible bonding has been achieved in the interface. According to /Johansson 2005/, a 35° friction angle seem to be a relevant value for the interaction between sawed rock surfaces. In the rock/concrete interface there will be undulations and asperities which will contribute to the total shear strength of the interface. Thus, 35° can be regarded as a conservative value (at least in terms of shear deformations) which may be applicable if a bad bonding has been achieved in the interface. In order to be conservative, the model with friction angle 35° was regarded as a base case in this study.

The models are described with the naming convention A_B_C–D_E, where the first three slots regard the plug geometry and the last two slots regard material properties:

- The first slot A denotes the plug length {4M, 8M} corresponding to 4 m and 8 m length, respectively.
- The second slot B denotes the look-out angle {2D, 4D} corresponding to 2° and 4°, respectively.
- The third slot C denotes floor geometry {FL, INCL} corresponding to flat and inclined floor, respectively.
- The fourth slot D denotes concrete material model {EL, PL} corresponding to elastic material and plastic material with 2 MPa tensile strength, respectively.
- The fifth slot E denotes interface model {MOφ, FIP} corresponding to Mohr-Coulomb (φ – friction angle) and model from CEB-FIP Model Code 90, respectively.

Table 4-3. Models that have been analyzed.

Model name	Plug length (m)	Look-out angle (degrees)	Concrete material model	Interface model	Comment
4M_2D_FL–EL_MO45	4	2	Elastic	Mohr-Coulomb φ = 45°, c = 0	Flat floor
4M_2D_INCL–EL_FIP	4	2	Elastic	FIP	
4M_4D_ INCL–EL_FIP	4	4	Elastic	FIP	
4M_4D_ INCL–PL_FIP	4	4	Tensile strength 2 MPa	FIP	
4M_4D_ INCL–EL_MO35	4	4	Elastic	Mohr-Coulomb φ = 35°, c = 0	Base case
4M_4D_ INCL–EL_MO45	4	4	Elastic	Mohr-Coulomb φ = 45°, c = 0	
4M_4D_ INCL–EL_MO50	4	4	Elastic	Mohr-Coulomb φ = 50°, c = 2 MPa	
8M_2D_ FL–EL_MO45	8	2	Elastic	Mohr-Coulomb φ = 45°, c = 0	Flat floor

5 Results

The results from the simulations are presented in this chapter. For the plug, four types of results are presented:

- Principal stresses in the plug.
- Displacements in the plug.
- Shear stresses in the rock-concrete interface.
- Shear displacements in the rock-concrete interface.

The chapter is divided into four main sections. The first section contains the results from the 4M_4D_INCL–EL_MO35 model, which is regarded as a base case. In the next section, the sensitivity to the application of different constitutive models and to a high pore water pressure in the rock-concrete interface is examined. The third section examines the effect of changing the plug geometry, i.e. look-out angle and plug length. In the fourth and last section, rock stress results are presented.

5.1 Base case results

The results presented in this section are from the 4M_4D_ INCL–EL_MO35 model, which is regarded as a base case. The results are divided into three sections. The first section presents the temperature increase in the plug due to the heat from the spent fuel. The second section presents principal stresses and displacements in the plug. The third section presents interface shear stresses and shear displacements. Results are presented for the following load stages:

- Application of 6 MPa pressure in the backfill.
- Application of 6 MPa pressure in the backfill with the addition of the thermo-mechanical effects 5, 10, 50 and 100 years after deposition of the spent fuel.

5.1.1 Temperature increase in the plug

Figure 5-1 is a diagram that shows the temperature increase histories for two points in the plug. The points are located along the tunnel axis at the plug front and at the plug end, respectively. In Figure 5-2, contour plots of the temperature increase after 5 years and 100 years are shown for a vertical section along the tunnel axis. The following can be observed:

- The maximum temperature increase is found after 100 years and is about 24°C. The exact temperature increase varies depending on the location in the plug.
- The heating of the plug is non-even. There is a temperature gradient in the horizontal direction due to the open main tunnel with no heat sources at the end side of the plug. There is also temperature gradient in the vertical direction due to the location of the canisters below the tunnel floor (Figure 5-2).
- The gradients are largest at the beginning of the heating and become reduced after longer times (Figure 5-1). After 5 years, the maximum gradient is about 3.7°C (Figure 5-2, top) and after 100 years it is about 1.7°C (Figure 5-2, bottom).

It shall be noted here that when the model was set up, the details of the repository layout were not known. Thus, the temperature calculations were based on a generic repository layout. Changes in the layout may also change the maximum temperature in the plug. One layout detail that is important for the temperature evolution is the distance between the nearest canister and the plug front. Here it was arbitrarily set to be equal to one canister distance, i.e. 6 m. An increase of this distance would result in a decrease of the temperatures.

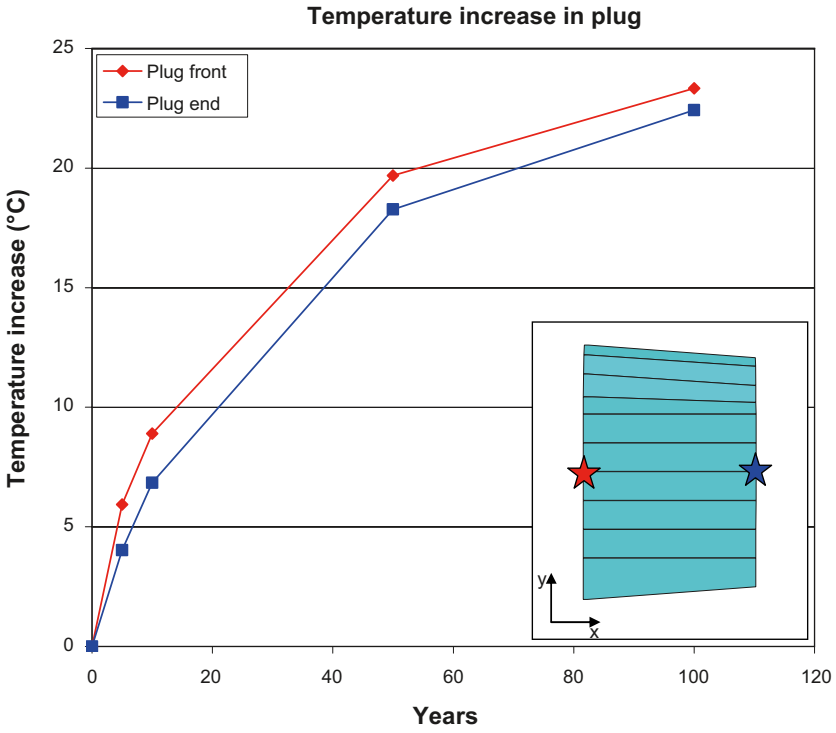

Figure 5-1. *Temperature increase histories in plug.*

5.1.2 Stresses and displacements in the plug

This section presents the continuum stresses in the plug. First a set of diagrams showing stresses along three scan-lines are presented. After that, principal stress vector plots are shown. The scan-lines are indicated in Figure 5-3. Scan-line A goes along the tunnel axis, line B along the roof-wall edge and line C goes along the wall-floor edge. The stresses along these scan-lines are shown in Figure 5-4 through Figure 5-6. The x-axes in the diagrams indicate the distance from the plug front that faces the backfilled deposition tunnel. The principal stress vector plots are shown in Figure 5-7 through Figure 5-10. In all diagrams and plots, compressive stresses are negative. The following can be observed:

- The stresses along the wall-floor and wall-roof edges are in general higher than in the center of the plug. The edges causes stress concentrations at these locations (Figure 5-4 – Figure 5-6). The highest stresses are found at the end of the plug close to the walls and the floor. Without heating, the maximum compressive stress amounts locally at about 50 MPa (Figure 5-9). However, the average stress along the edges at the plug end amounts at about 20 MPa.
- The thermal load gives significant increase of the compressive stresses. After 100 years of heating the maximum stress is locally increased to about 70 MPa. However, the average stress along the edges at the plug end amounts at about 30 MPa (Figure 5-9).
- The maximum tensile stress amount at 2 MPa at 6 MPa load. The thermal load tends to reduce the tensile stresses around the tunnel axis at the end of the plug (Figure 5-4) and increase it along the edges where they amount at about 4 MPa at a maximum after 100 years (Figure 5-10).
- The thermal stresses cause stress redistributions and rotation of the stress tensors (Figure 5-7 and Figure 5-8). The directions of the stress tensors clearly indicate how a major part of the roof looses shear stress. This effect can also be observed on the interface shear stresses in the roof presented in the next section. In Figure 5-7 and Figure 5-8 it can also be observed how the compressive stresses are increasing more in the lower parts than in the upper part of the plug. This is a result of the arced roof and of the friction against the walls. The vertical expansion of the plug is limited by the friction forces against the walls, which increase due to the horizontal expansion. Due to the arced roof, the horizontal expansion of the upper parts results in stress concentrations along scan-line B (Figure 5-5, left and Figure 5-9).

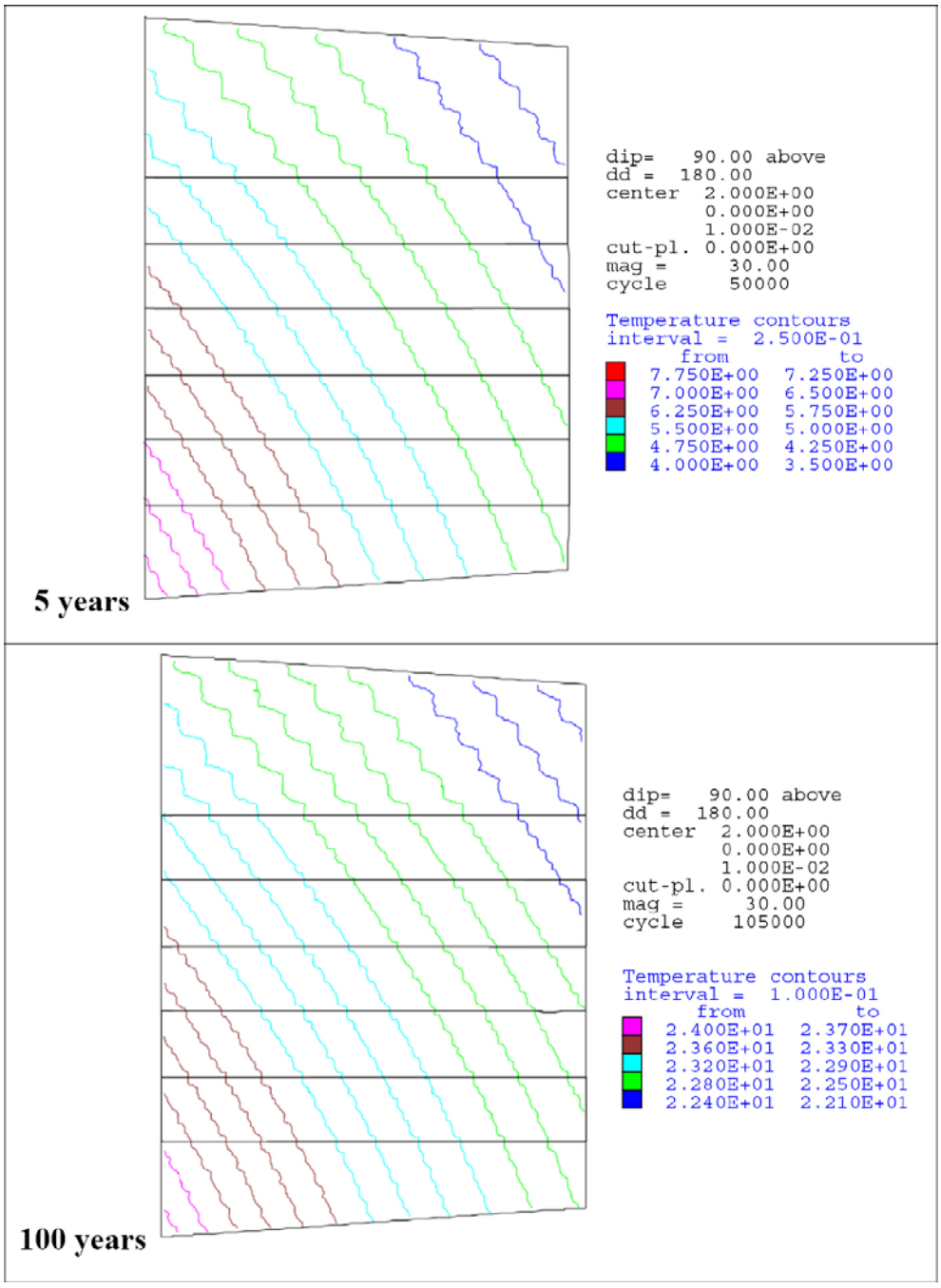

Figure 5-2. *Temperature increase in a vertical section along the tunnel axis after (top) 5 years and after (bottom) 100 years of heating.*

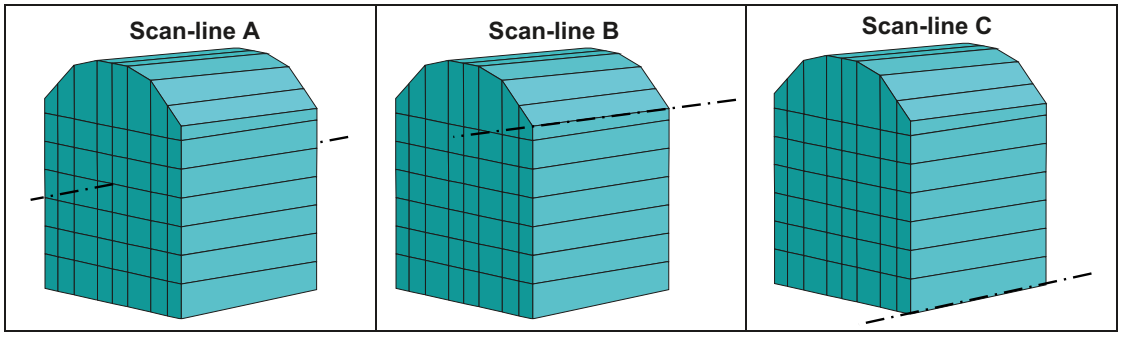

Figure 5-3. *Scan-lines for evaluation of stresses.*

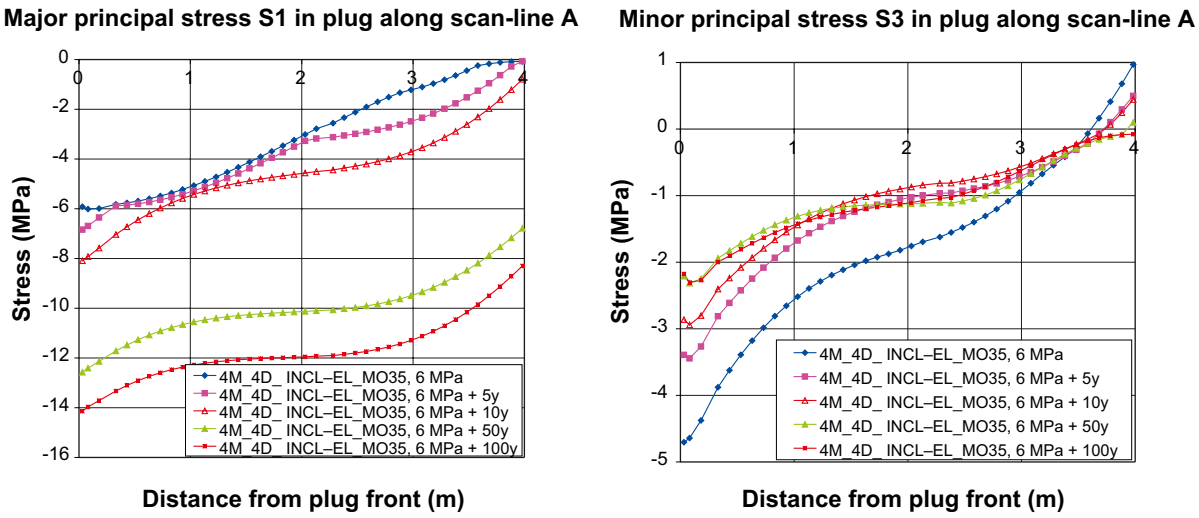

Figure 5-4. *Major (left) and minor (right) principal stresses along scan-line A (cf. Figure 5-3) at different load stages. Compressive stresses are negative. The plug front faces the backfilled deposition tunnel.*

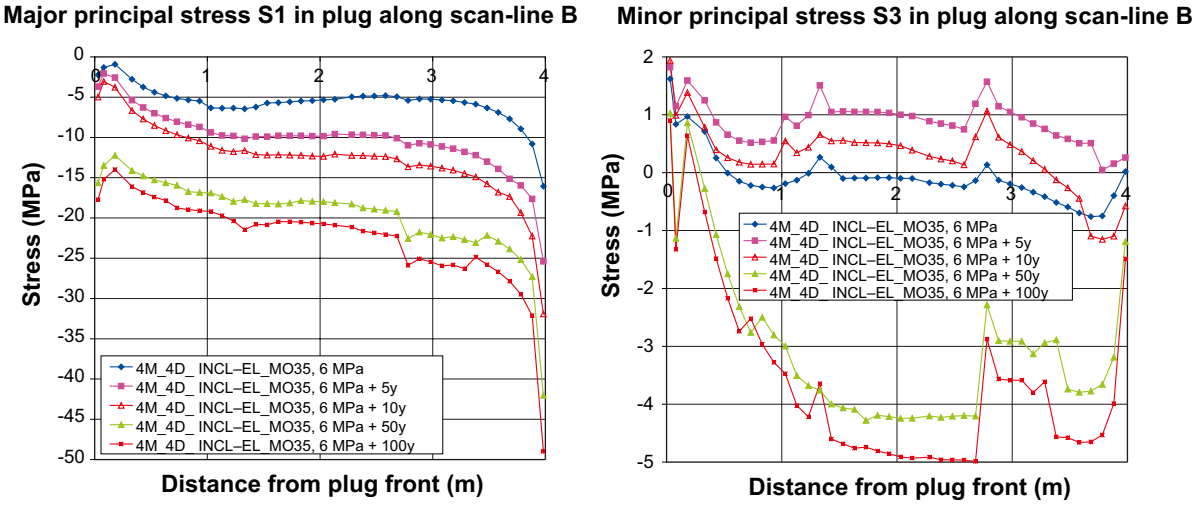

Figure 5-5. *Major (left) and minor (right) principal stresses along scan-line B (cf. Figure 5-3) at different load stages. Compressive stresses are negative. The plug front faces the backfilled deposition tunnel.*

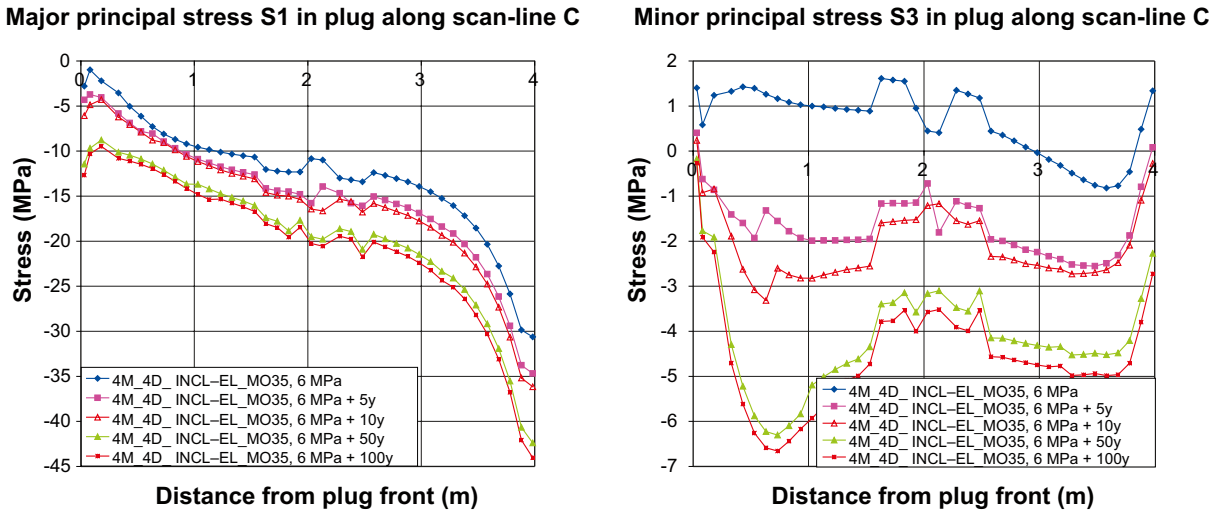

Figure 5-6. *Major (left) and minor (right) principal stresses along scan-line C (cf. Figure 5-3) at different load stages. Compressive stresses are negative. The plug front faces the backfilled deposition tunnel.*

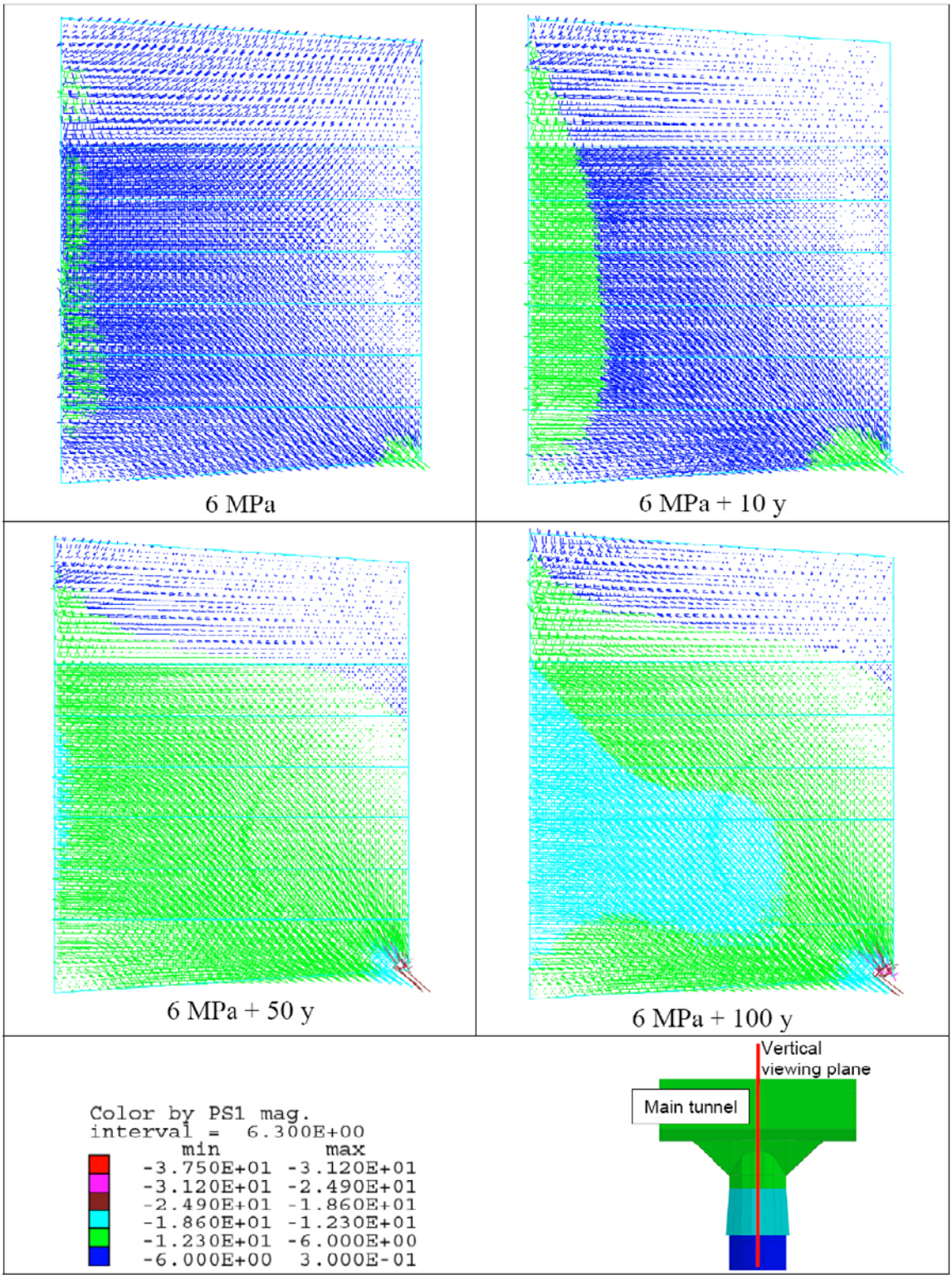

Figure 5-7. *Principal stress vector plots in vertical section through plug along tunnel axis (lower right). Results from four load stages are shown. The tensor symbols scale with the projection of the principal stresses onto the viewing plane and are colored according to the major principal stress.*

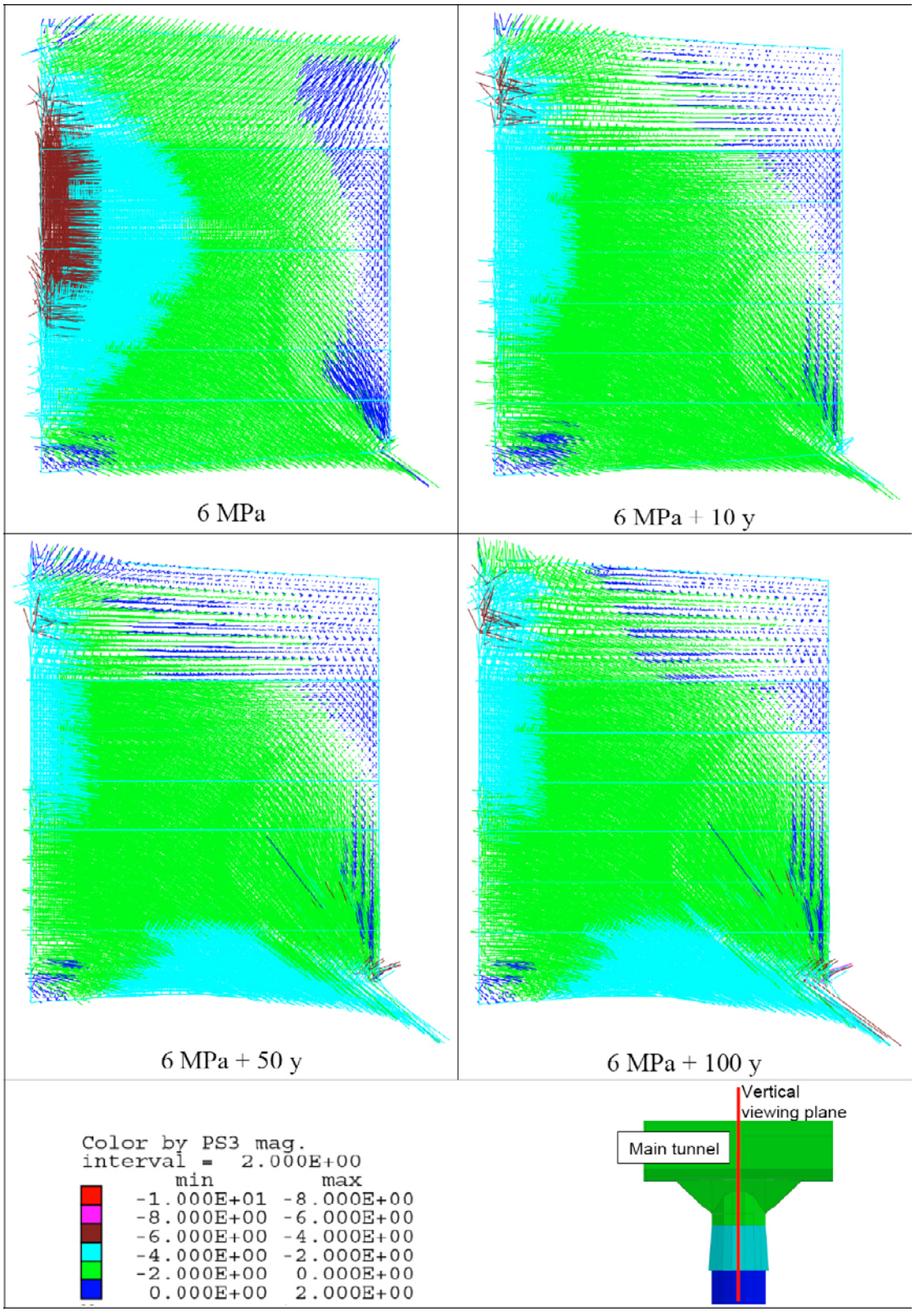

Figure 5-8. *Principal stress vector plots in vertical section through plug along tunnel axis (lower right). Results from four load stages are shown. The tensor symbols scale with the projection of the principal stresses onto the viewing plane and are colored according to the minor principal stress.*

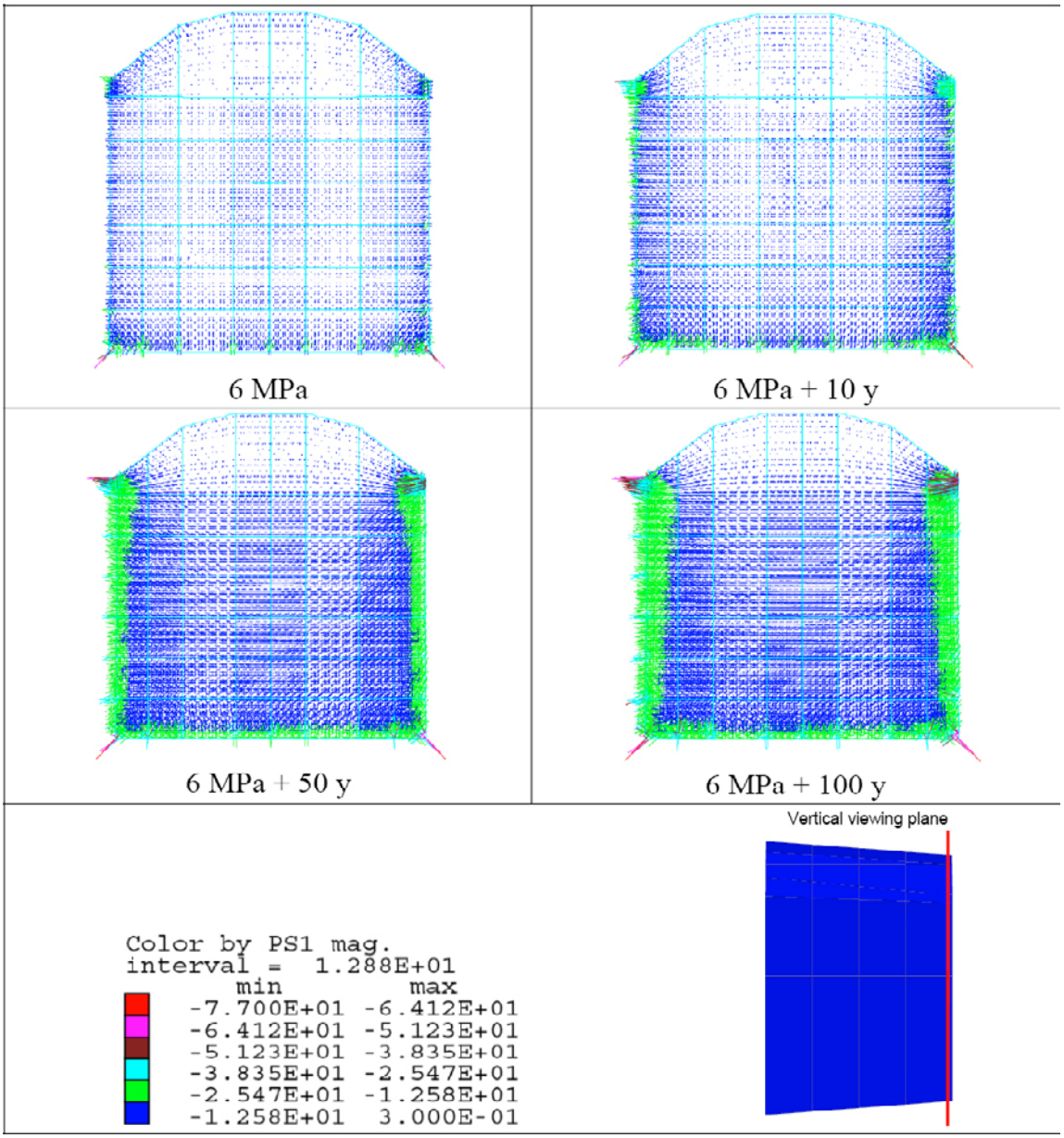

Figure 5-9. *Principal stress vector plots in vertical section perpendicular to the tunnel axis close to the plug end (lower right). Results from four load stages are shown. The tensor symbols scale with the projection of the principal stresses onto the viewing plane and are colored according to the major principal stress.*

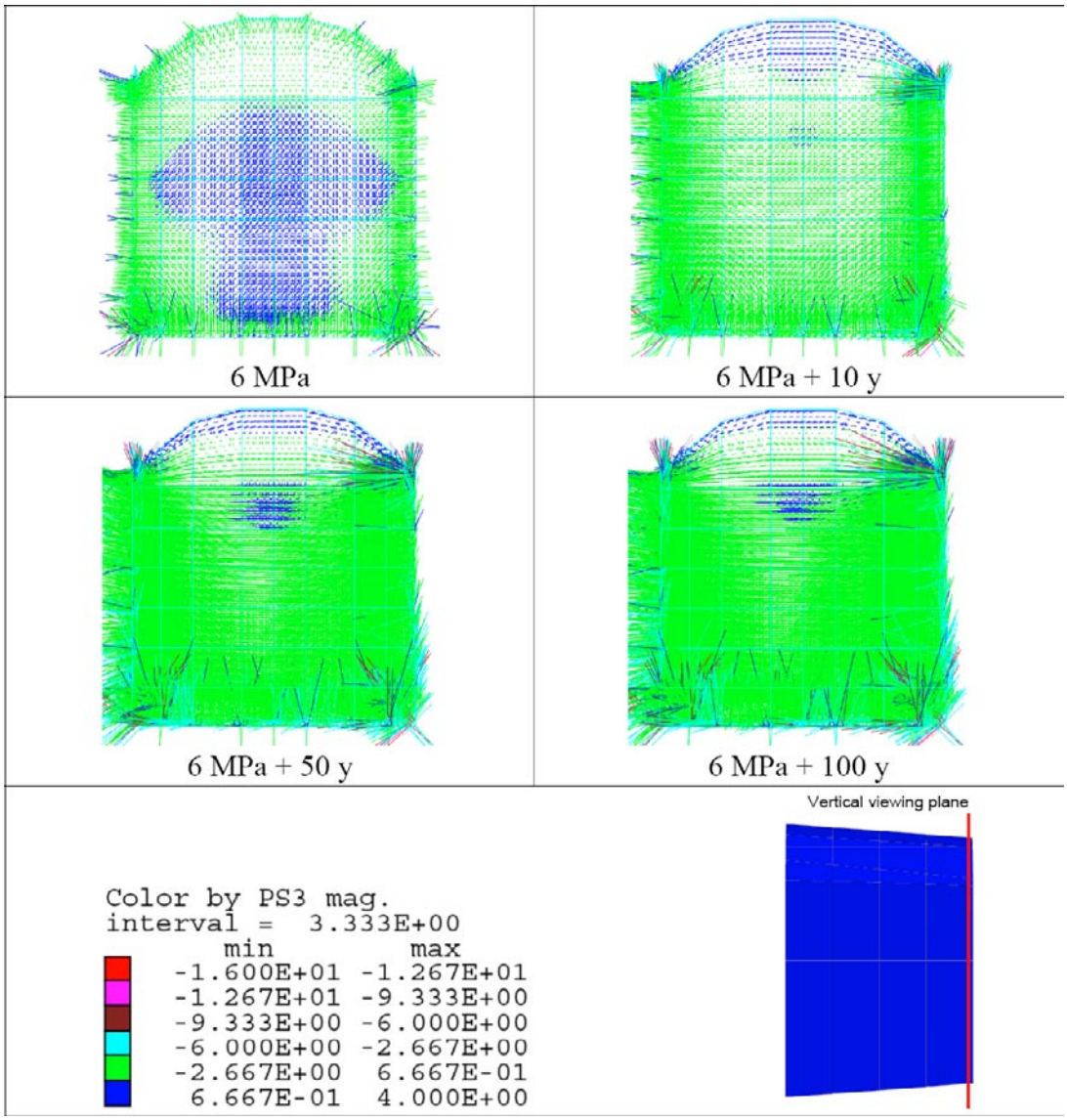

Figure 5-10. *Principal stress vector plots in vertical section perpendicular to the tunnel axis close to the plug end (lower right). Results from four load stages are shown. The tensor symbols scale with the projection of the principal stresses onto the viewing plane and are colored according to the minor principal stress.*

Figure 5-11 shows a vector plot of displacements in the plug at 6 MPa load in a vertical section along the tunnel axis. The maximum displacement is found at the plug front and amounts at about 4 mm. At the plug end, the displacement is about 3.5 mm. The displacements are well below the 10 mm criterion suggested in Section 3.2.2. In Figure 5-12, a displacement vector plot captured 100 years after installation is shown. The maximum displacement is about 10 mm. The plot shows how the thermal expansion of the rock translates the plug upwards and towards the main tunnel. Both the plug and the rock move due to the heat load. Thus, the displacements due to the heating can not directly be compared with any criterion for maximum allowed plug displacement. The upward component of the movement is due to that the heat generating canisters are located below the tunnel floor (cf. Section 4.3.3). In order to differentiate the translation of the plug from its internal deformations, the displacement evolution in the horizontal direction at the plug front and at the plug end were plotted. This is shown in Figure 5-13. At 6 MPa load, the displacement at the front is about 0.5 mm larger than at the end, i.e. the plug has been compressed in the axial direction (cf. Figure 5-11). When the thermal load is applied, the plug becomes longer again due to the thermal expansion and after 10 years it has recovered to its original length. As the heating progresses and the temperature increases further, the plug length is also increased further. The maximum elongation after 100 years is about 1 mm.

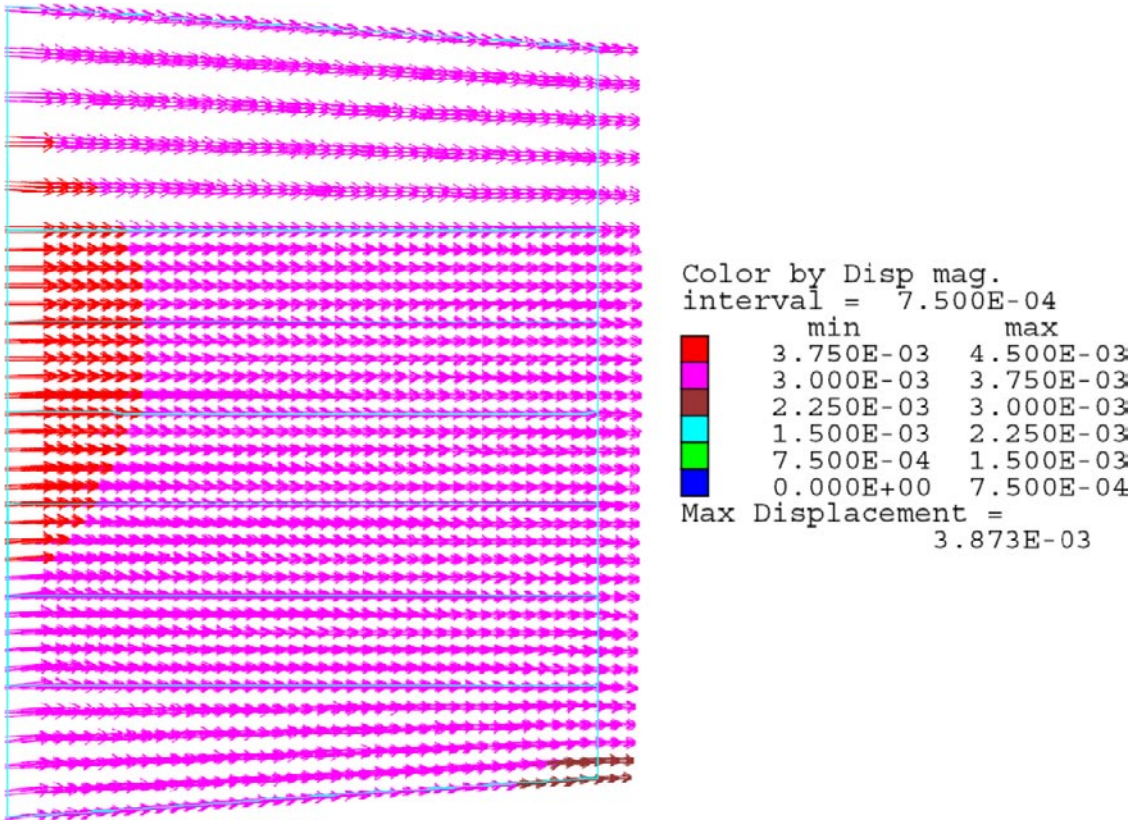

Figure 5-11. *Displacements in the plug at 6 MPa load.*

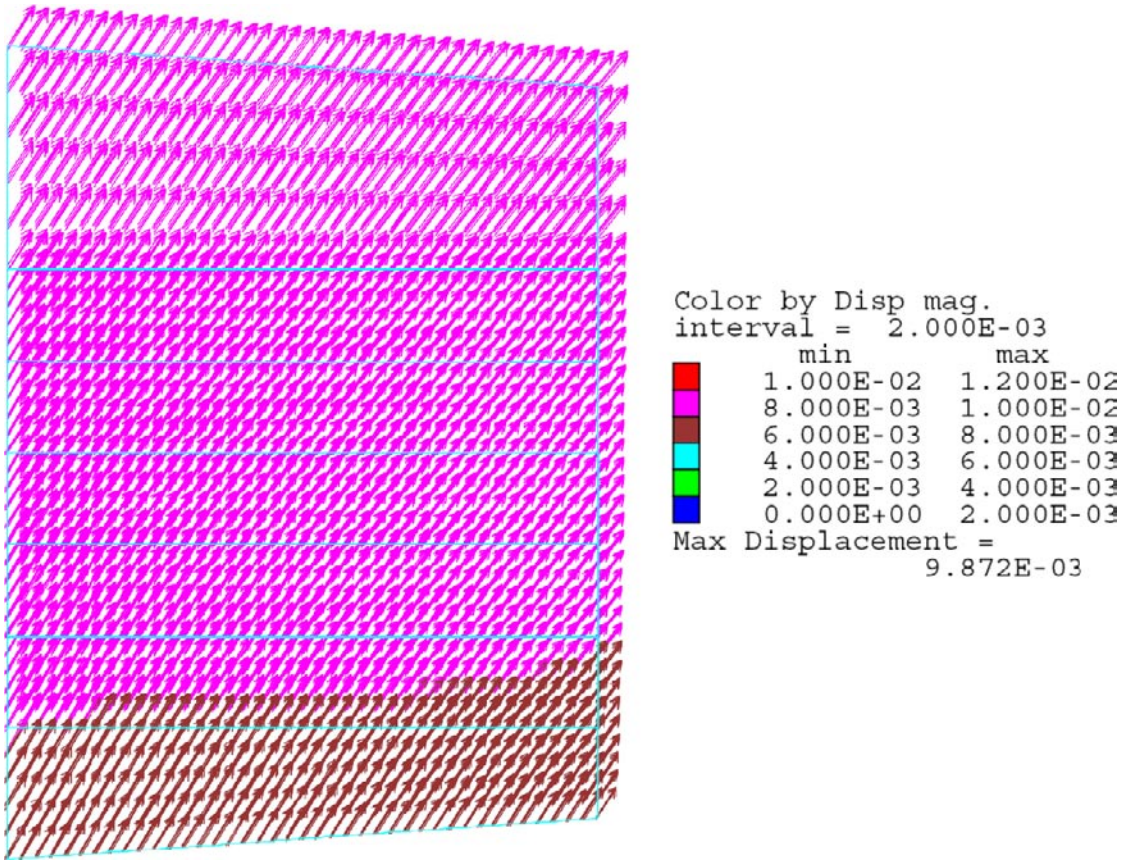

Figure 5-12. *Displacements in the plug at 6 MPa load with the addition of thermal load 100 years after deposition.*

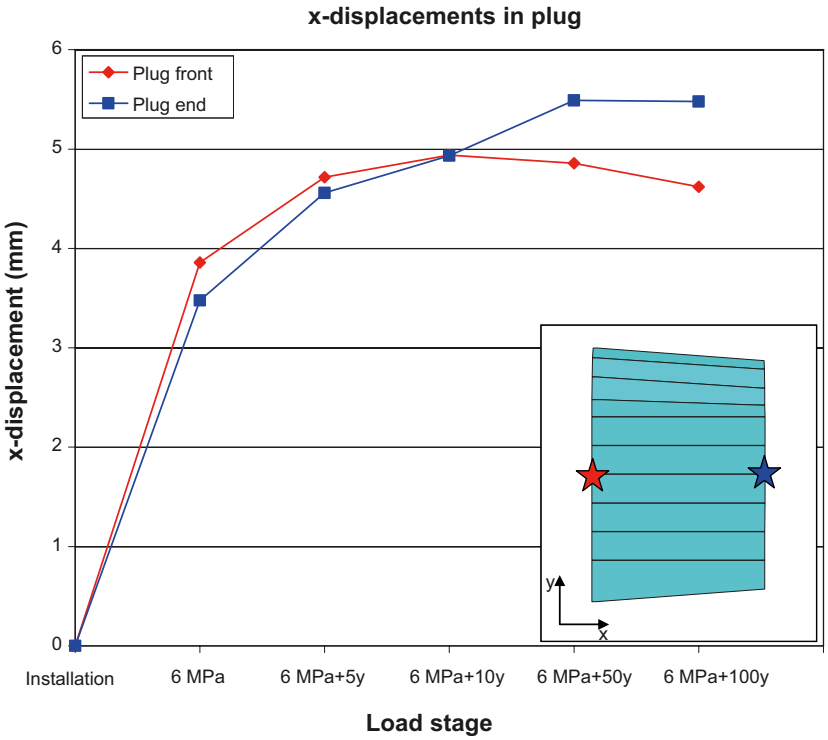

Figure 5-13. *X-displacement evolution at the plug front and at the plug end (at the tunnel axis). The location of the history points are indicated in the inset.*

5.1.2 Rock-concrete interface shear stresses and shear displacements

The shear stresses in the rock-concrete interface were evaluated along three scan-lines along the tunnel floor, the tunnel wall and the tunnel roof, respectively (Figure 5-14). The shear stress results along the scan-lines are shown in Figure 5-15 through Figure 5-17. The x-axes in the diagrams indicate the distance from the plug front that faces the backfilled deposition tunnel. Figure 5-18 shows a contour plot of interface shear stresses at 6 MPa load and after 50 years of heating. The following can be observed:

- At the first load step with the 6 MPa load applied, the shear stresses are close to zero at the plug front and have their maximum at the end of the plug. The maximum stress amounts at 10–15 MPa.
- As the thermal load is applied, stress redistributions take place. At the floor and at the walls, the shear stress is increased at most locations. This increase is accompanied by a loss of shear stress in the roof along about half of the plug length (after 5 years). After longer times of heating, the distance with zero shear stress in the roof is longer. The redistribution of shear loads between floor, walls and roof is in line with the stress results presented in Section 5.1.2 above.

In Figure 5-19, interface shear displacement contour plots from four load stages are shown. At the load stage with 6 MPa load only, the maximum shear displacement is about 3.4 mm and is found in the roof close to the plug front. This is about 0.6 mm less than the displacement at the middle of the plug front shown in Figure 5-13. The heating causes an increase of the maximum shear displacement. The increase is particularly pronounced in to the roof. After 100 years of heating, the maximum shear displacement is about 5 mm and is found in the roof near the plug end. The fact that the increase is more pronounced in the roof is in line with the shear stress results presented above; the heating causes significant decrease of the shear stresses in the roof.

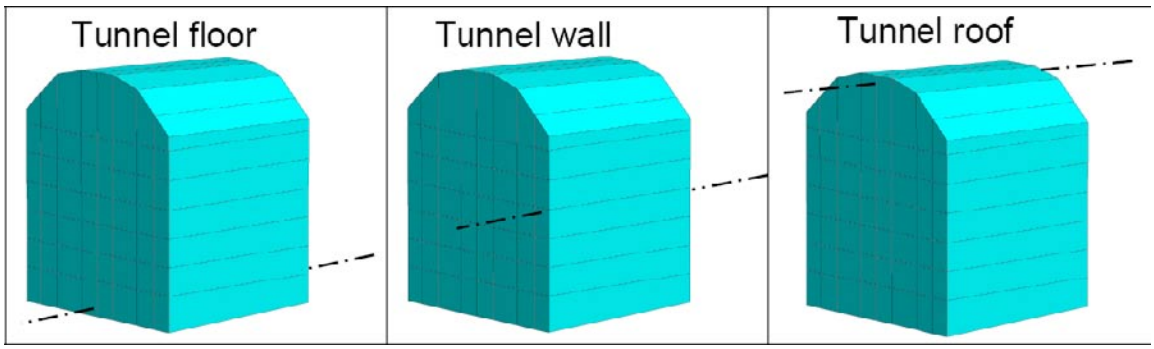

Figure 5-14. *Scan-lines for evaluation of interface shear stresses.*

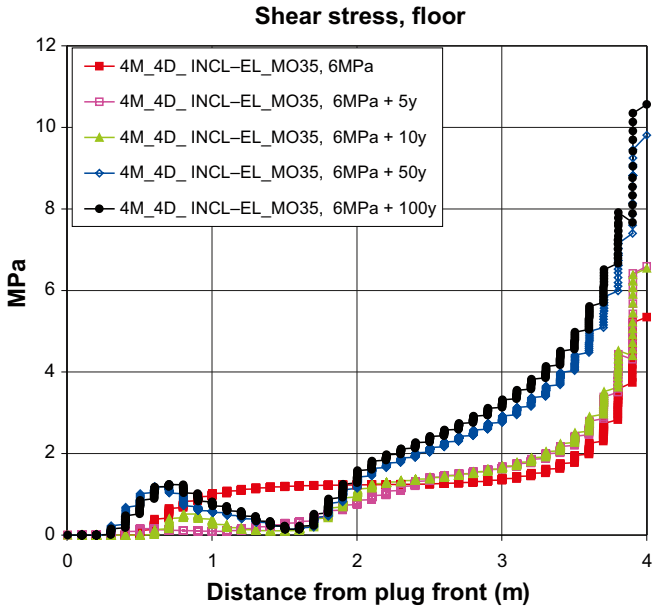

Figure 5-15. *Shear stress in rock-concrete interface along the floor scan-line (cf. Figure 5-14) at different loading stages.*

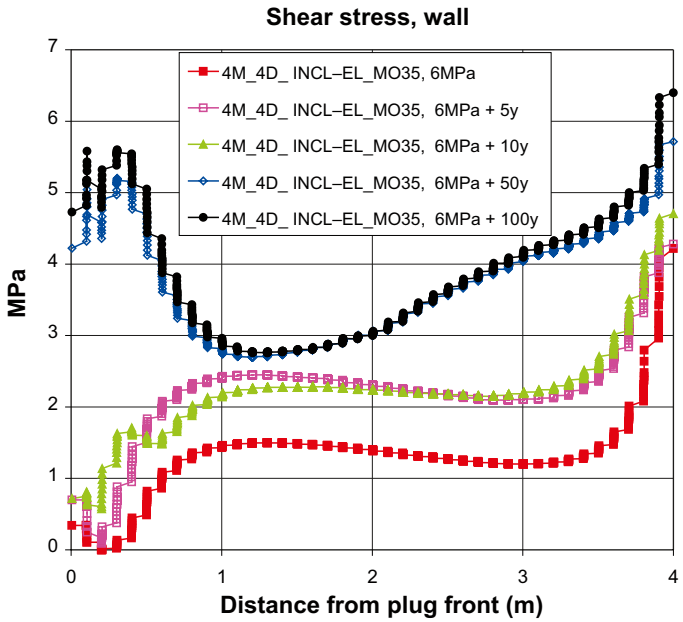

Figure 5-16. *Shear stress in rock-concrete interface along the wall scan-line (cf. Figure 5-14) at different loading stages.*

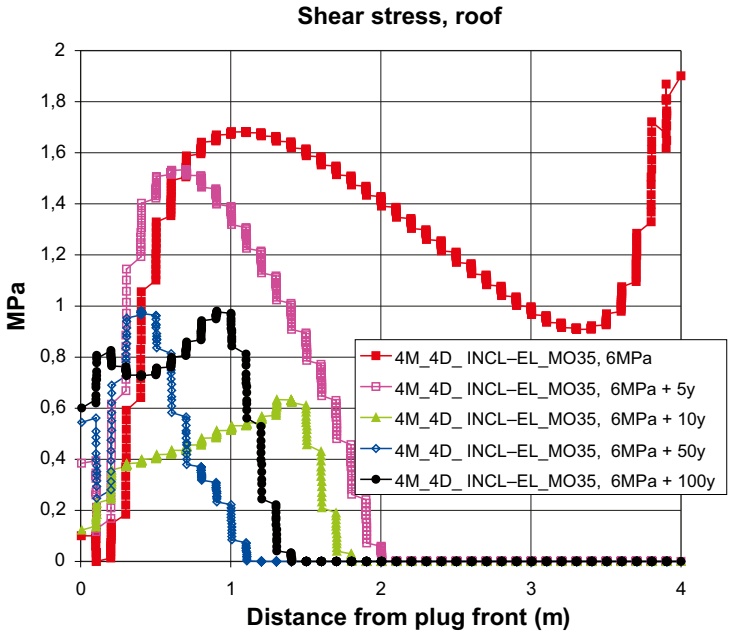

Figure 5-17. *Shear stress in rock-concrete interface along the roof scan-line (cf. Figure 5-14) at different loading stages.*

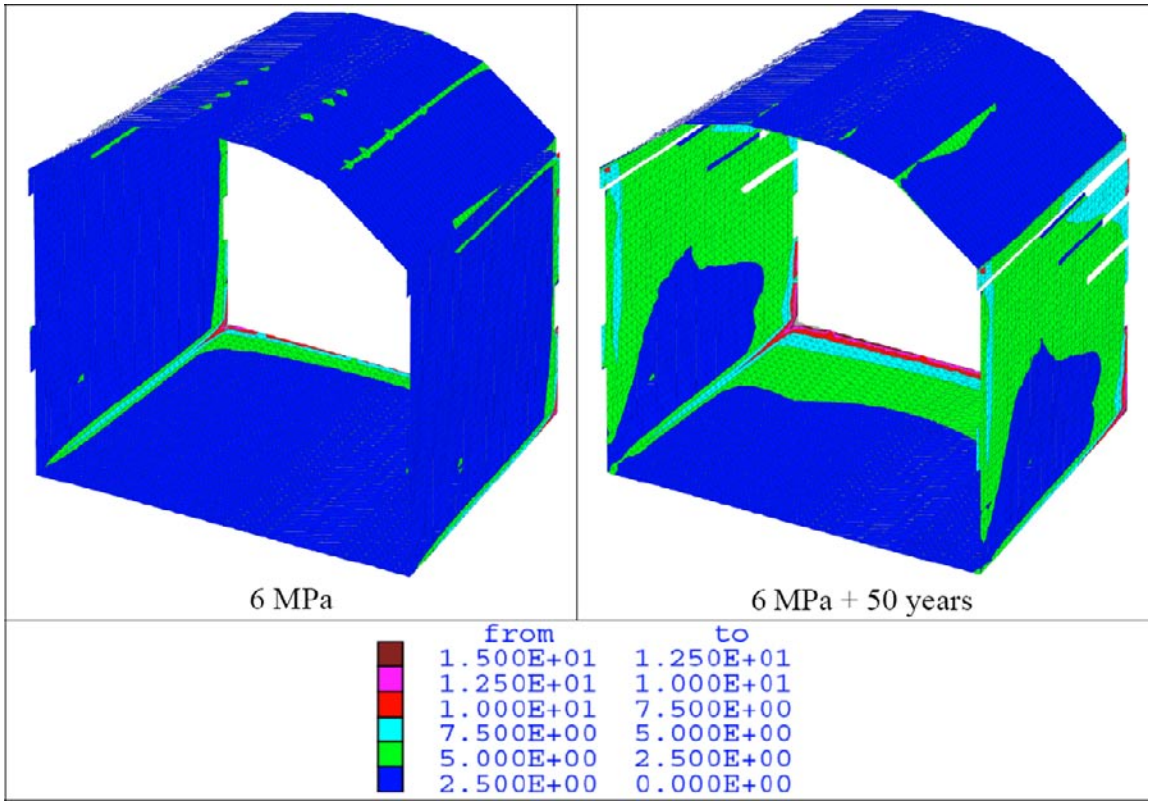

Figure 5-18. *Contour plot of interface shear stress at 6 MPa load (left) and at 6 MPa load + 50 years of heating (right).*

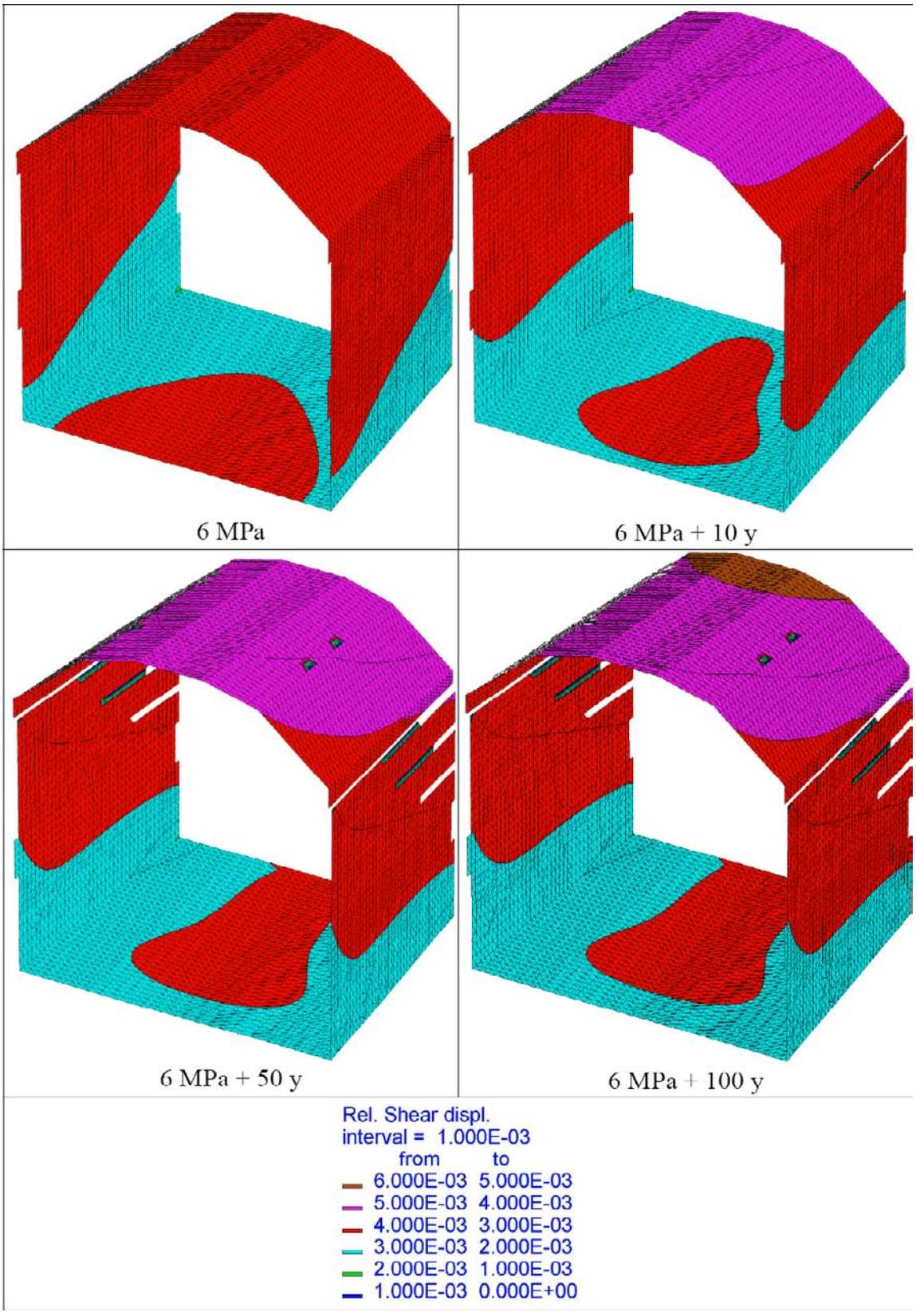

Figure 5-19. *Shear displacement contour plots from four load stages (The transparent areas are due to some anomaly in the 3DEC plotting logic).*

5.2 Importance of constitutive models and pore water pressure

In this section, the sensitivity to the application of different constitutive models for the concrete and for the rock-concrete interface is examined. The results are divided into two sub-sections. The first sub-section presents stresses in the plug and the second sub-section presents rock-concrete interface shear stresses and shear displacements. Two load stages are examined:

- Application of 6 MPa pressure in the backfill.
- Application of 6 MPa pressure in the backfill with the addition of a pore water pressure in the rock-concrete interface (cf. Section 4.3.3). This load stage can be regarded as an accidental case which may correspond to a situation where the bentonite seal in front of the concrete plug has failed.

Results from the following models are presented (cf. Table 4-3):

- 4M_4D_INCL-EL_MO35: Base case model with linear elastic concrete and with a Mohr-Coulomb failure criterion (φ = 35°, cf. Eq. 3) for the interface.
- 4M_4D_INCL-EL_MO45: Model with linear elastic concrete and with a Mohr-Coulomb failure criterion (φ = 45°, cf. Eq. 3) for the interface.
- 4M_4D_INCL-EL_MO50: Model with linear elastic concrete and with a Mohr-Coulomb failure criterion (φ = 50°, c = 2 MPa, cf. Eq. 3) for the interface.
- 4M_4D_INCL-EL_FIP: Model with linear elastic concrete and with a failure criterion according to CEB-FIP MODEL CODE (cf. Eq. 4) for the interface.
- 4M_4D_INCL-PL_FIP: Model with 2 MPa tensile strength in the concrete and with a failure criterion according to CEB-FIP MODEL CODE (cf. Eq. 4) for the interface.

5.2.1 Stresses in the plug

The stresses were evaluated along the same scan-lines as in Section 5.1.2 above, but for readability, the scan-lines are shown here again in Figure 5-20.

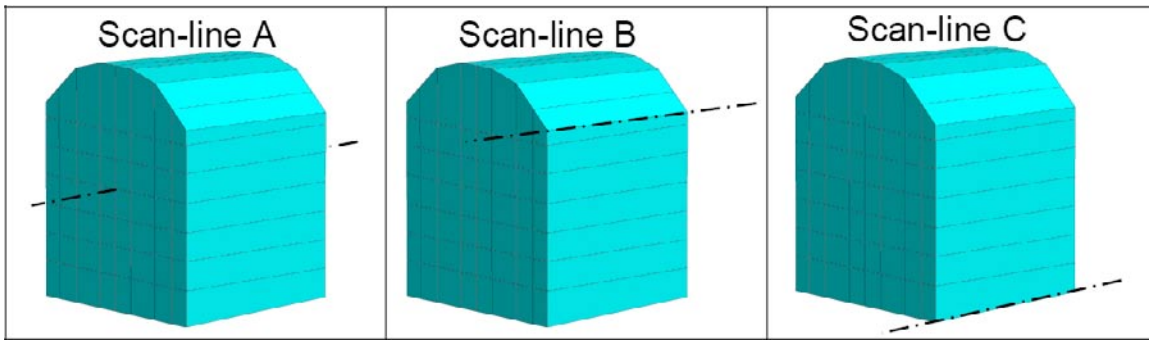

Figure 5-20. *Scan-lines for evaluation of stresses.*

The major and minor principal stresses along scan-line A, B and C are presented in Figure 5-21, Figure 5-22 and Figure 5-23, respectively. The following can be observed:

- *Comparing 4M_4D_INCL-EL_MO35 and 4M_4D_INCL-EL_FIP at 6 MPa load:* The interface model has only importance for the major principal stresses close to the perimeter of the plug. Along scan-line A, there is effectively no difference in the major principal stress. Along scan-lines B and C the FIP model causes significant reduction of the compressive stress close to the plug end compared to the base case. At scan-line B, the reduction is about 7 MPa (43%) (Figure 5-22, left) and at line C it is about 25 MPa (83%) (Figure 5-23, left). This is coupled to the smaller shear displacements when applying the FIP model. Smaller axial displacement gives less lateral compression of the plug.
- *Comparing 4M_4D_INCL-EL_MO35 and 4M_4D_INCL-EL_MO50 at 6 MPa load:* The interface model has only importance for the major principal stresses close to the perimeter of the plug. Along scan-line A, there is effectively no difference in the major principal stress. At the plug end along scan-line B, there is a 50% compressive stress increase when increasing the friction angle from 35° to 50° (Figure 5-22, left). Besides this, changing the friction angle gives only minor variations of the major principal stresses.
- *Comparing 4M_4D_INCL-EL_MO35, 4M_4D_INCL-EL_MO50 and 4M_4D_INCL-EL_FIP at 6 MPa load:* The 4M_4D_INCL-EL_MO50 and 4M_4D_INCL-EL_FIP models, which in general have higher interface strengths than the base case model 4M_4D_INCL-EL_MO35, give in general higher tensile stresses (right images). This gives higher stress anisotropy in these models. The highest tensile stresses amount at 3–4 MPa.
- *Influence of pore water pressure in the rock-concrete interface (Comparing 6 MPa and 6 MPa + pp4 for the base case):* The application of pore water pressure decreases the interface strength and causes larger shear displacements along the interface (see Section 5.2.2 below), which in turn gives a state of higher compression in the plug. The maximum compressive stress in 4M_4D_INCL-EL_MO35 increases from about 30 MPa to about 45 MPa (50%) when the pore water pressure is applied (Figure 5-23, left). The tensile stresses are significantly reduced.
- *Influence of having 2 MPa tensile strength (Comparing 4M_4D_INCL-EL_FIP and 4M_4D_INCL-PL_FIP):* Tensile failure at the plug end causes the stresses to become zero around the tunnel axis indicating cracking of the concrete at this location (Figure 5-21). Along scan-line B and C, the tensile stresses are also reduced due to tensile failure. Along scan-line A, some compressive stress reductions are observed (Figure 5-21, left) and along scan-line C, the compressive stresses remain unchanged (Figure 5-23, left). Along scan-line B, the compressive stresses are increase by about 50% on average (Figure 5-22, left).

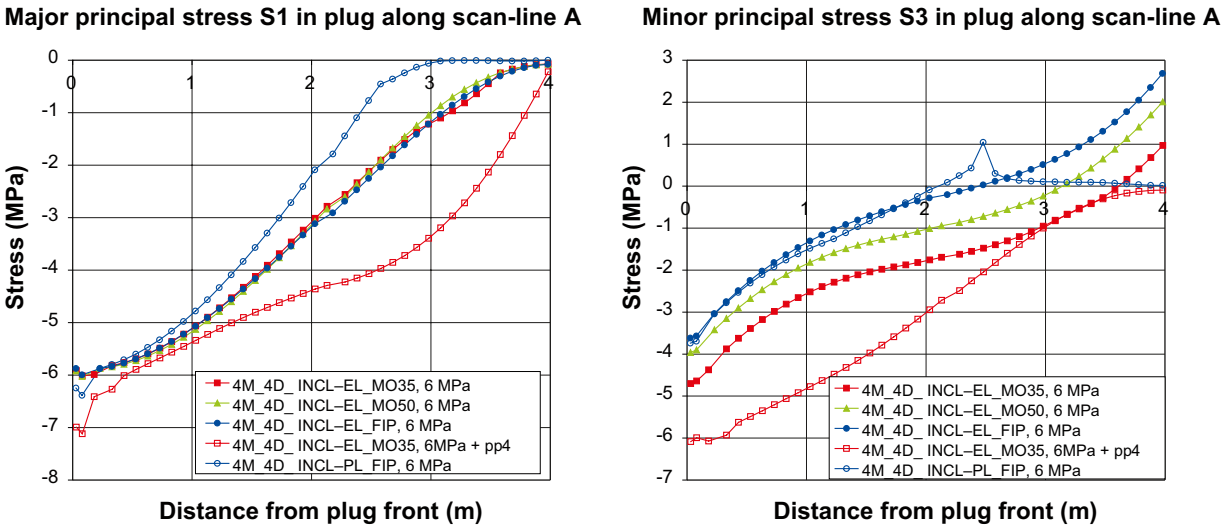

Figure 5-21. *Major (left) and minor (right) principal stresses along scan-line A (cf. Figure 5-20) at 6 MPa backfill pressure. The effects of applying different interface models, 2 MPa concrete tensile strength and pore water pressure in the interface are shown. Compressive stresses are negative. The plug front faces the backfilled deposition tunnel.*

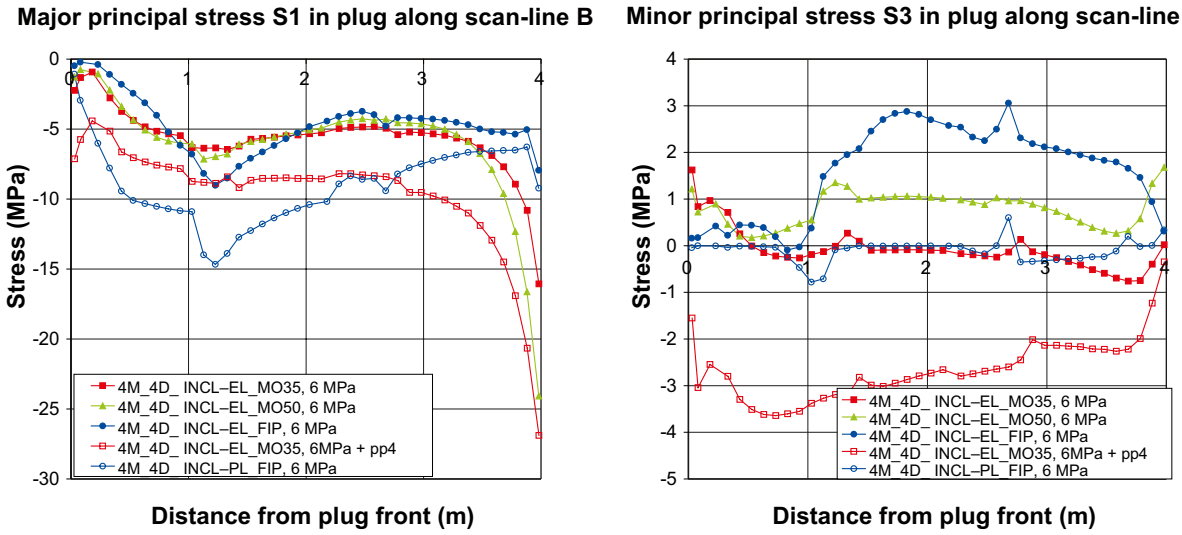

Figure 5-22. *Major (left) and minor (right) principal stresses along scan-line B (cf. Figure 5-20) at 6 MPa backfill pressure. The effects of applying different interface models, 2 MPa concrete tensile strength and pore water pressure in the interface are shown. Compressive stresses are negative. The plug front faces the backfilled deposition tunnel.*

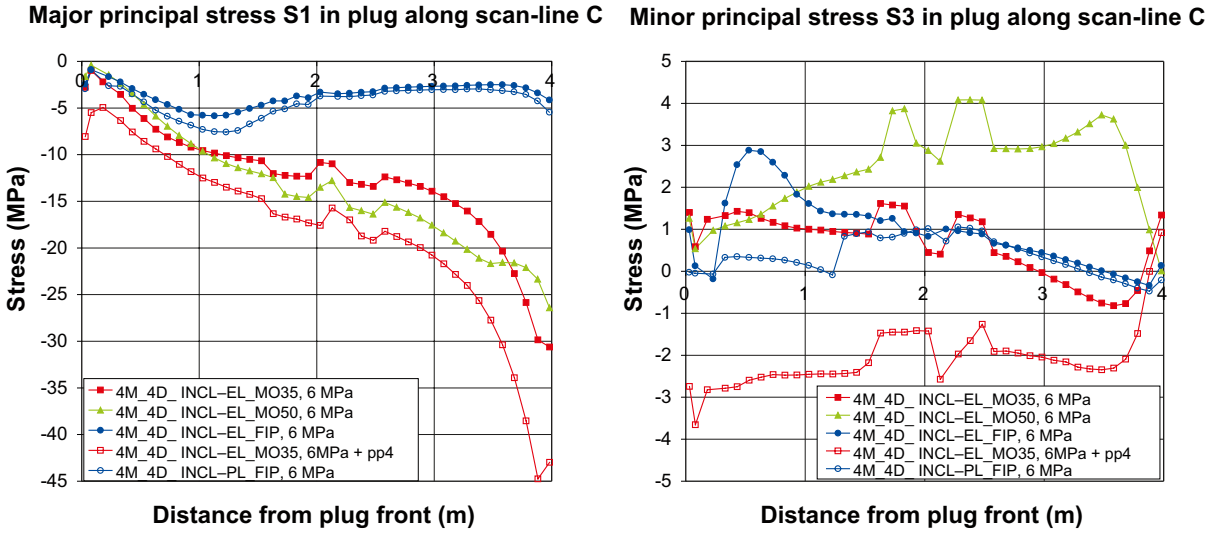

Figure 5-23. *Major (left) and minor (right) principal stresses along scan-line C (cf. Figure 5-20) at 6 MPa backfill pressure. The effects of applying different interface models, 2 MPa concrete tensile strength and pore water pressure in interface are shown. Compressive stresses are negative. The plug front faces the backfilled deposition tunnel.*

5.2.2 Rock-concrete interface shear stress and shear displacements

The shear stresses were evaluated along the same scan-lines as in Section 5.1.3 above, but for readability, the scan-lines are shown here again (Figure 5-24).

The interface shear stresses along the scan-lines indicated in Figure 5-24 are shown in Figure 5-25, Figure 5-26 and Figure 5-27. The following observations can be made:

- *Comparing 4M_4D_INCL-EL_MO35, 4M_4D_INCL-EL_MO45 and 4M_4D_INCL-EL_MO50 at 6 MPa load:* A lower friction angle gives a more even distribution of the shear load along the plug and less stress concentrations at the plug end. The maximum shear stress when applying 35° friction angle is about 5 MPa whereas the maximum stress for the 50°-case is about 12 MPa (Figure 5-25).
- *Comparing Mohr-Coulomb models with FIP model:* The FIP model gives very little shear load along the first meter of the plug. Further, there are no stress concentrations at the plug end similar to what the Mohr-Coulomb model gives. The stress is more concentrated to the mid-region of the plug.
- *Influence of pore water pressure:* The pore water pressure has its maximum at the plug front and then tapers off linearly to zero at the plug end. This pressure distribution results in a redistribution of shear load towards the plug end. The stress concentrations at the end of the plug that arises when applying the Mohr-Coulomb model becomes more pronounced when the pore water pressure is applied. When using the FIP model, the pore water pressure results in loss of shear stress along at least half of the plug length. This gives significant stress increase at the plug end. The large impact of pore pressure when using the FIP model is due to the very high sensitivity to small normal stress changes in this model at low normal stress levels (Figure 4-7); a normal effective stress of 0.5 MPa gives a shear strength of 3 MPa, i.e. more than 8 times the strength of the Mohr-Coulomb model ($\varphi = 35°$) at the same effective normal stress. When these results are interpreted, it shall be remembered that the pore water pressure is high at the plug front and thus gives a very conservative load case.

Figure 5-28 shows shear displacement vector plots from two models: The base case model 4M_4D_INCL-EL_MO35 (top) and the 4M_4D_INCL-EL_FIP model (bottom). To the left, only the 6 MPa load is applied and to the right, the effect of the pore water pressure is added. With 6 MPa load only, the 4M_4D_INCL-EL_FIP model gives significantly smaller displacements than does the 4M_4D_INCL-EL_MO35 model. The maximum displacement is about 0.6 mm when applying the FIP interface model, but it is more than 5 times larger when using the Mohr-Coulomb model.

The difference between the models also becomes clear when the pore water pressure is applied. The maximum shear displacement in the 4M_4D_INCL-EL_FIP model increases from 0.6 mm to 3.9 (more than six times). The corresponding increase for the 4M_4D_INCL-EL_MO35 model is from 3.5 mm to 7 mm (two times). The high sensitivity of the FIP model to pore pressure is in line with the shear stress results shown in Figure 5-25 – Figure 5-27 above.

Figure 5-29 shows a shear displacement vector plot for the 4M_4D_INCL-PL_FIP model, i.e. the model with the concrete tensile strength limited to 2 MPa. When the plot is compared with the corresponding plot for the elastic 4M_4D_INCL-EL_FIP model (Figure 5-28, lower left) it becomes clear that the limited tensile strength only has a small influence on the results. The maximum shear displacement in 4M_4D_INCL-PL_FIP is about 0.1 mm (16%) larger than in 4M_4D_INCL-EL_FIP.

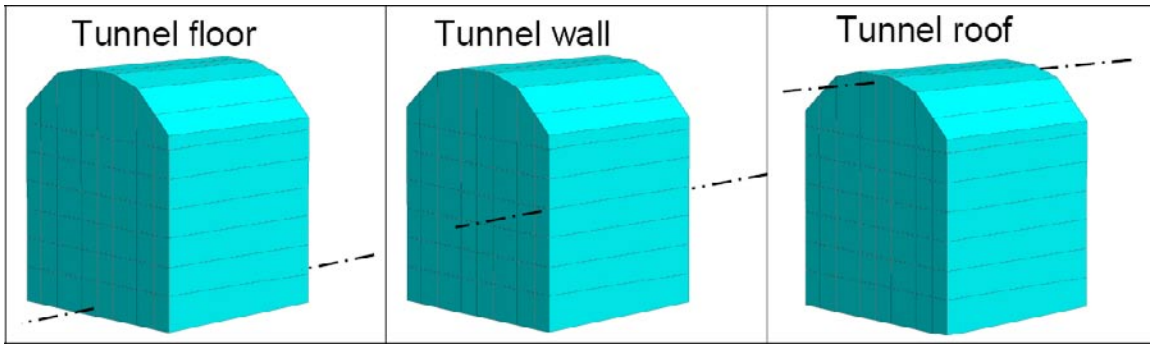

Figure 5-24. *Scan-lines for evaluation of interface shear stresses.*

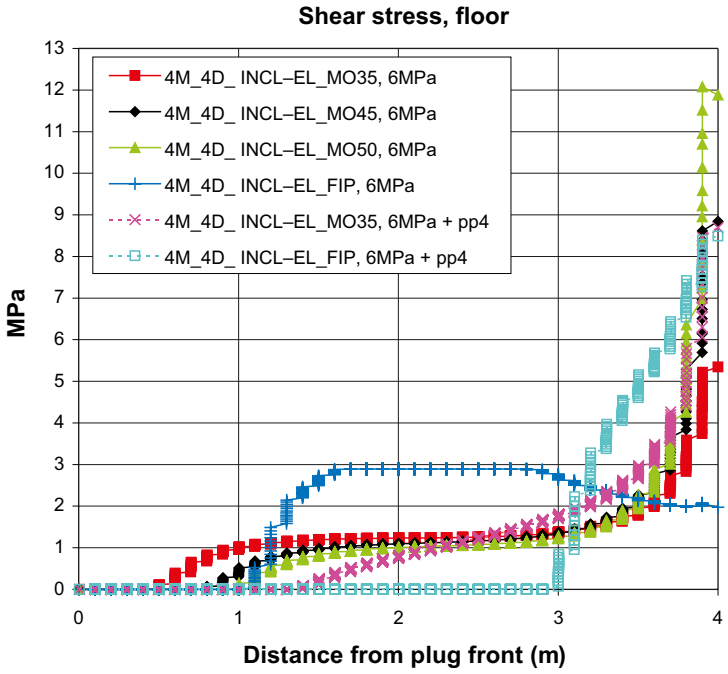

Figure 5-25. *Shear stress in rock-concrete interface along the floor scan-line (cf. Figure 5-24). The effect of different interface models and pore water pressure is shown.*

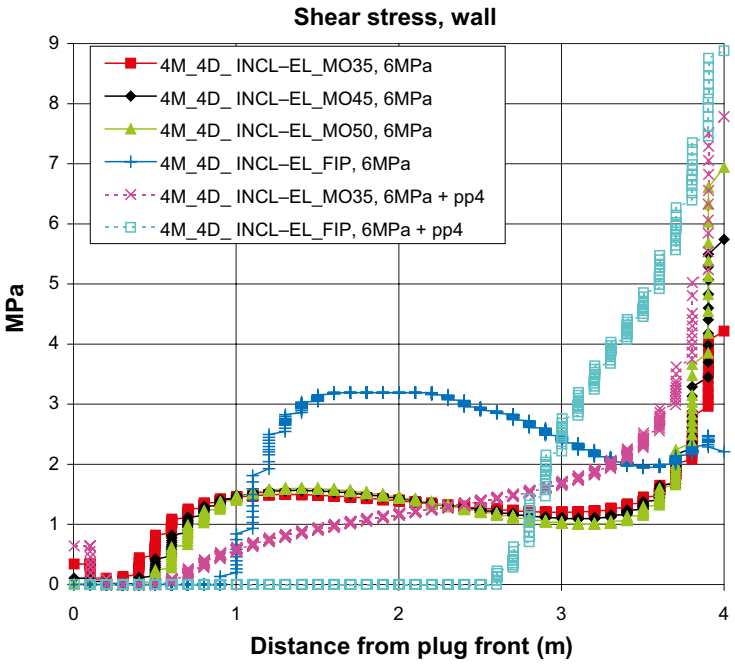

Figure 5-26. *Shear stress in rock-concrete interface along the wall scan-line (cf. Figure 5-24). The effect of different interface models and pore water pressure is shown.*

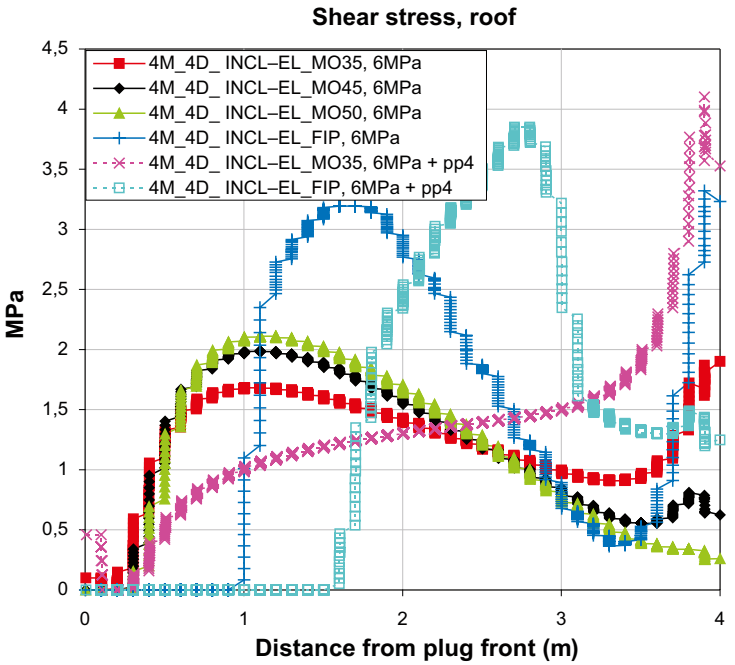

Figure 5-27. *Shear stress in rock-concrete interface along the roof scan-line (cf. Figure 5-24). The effect of different interface models and pore water pressure is shown.*

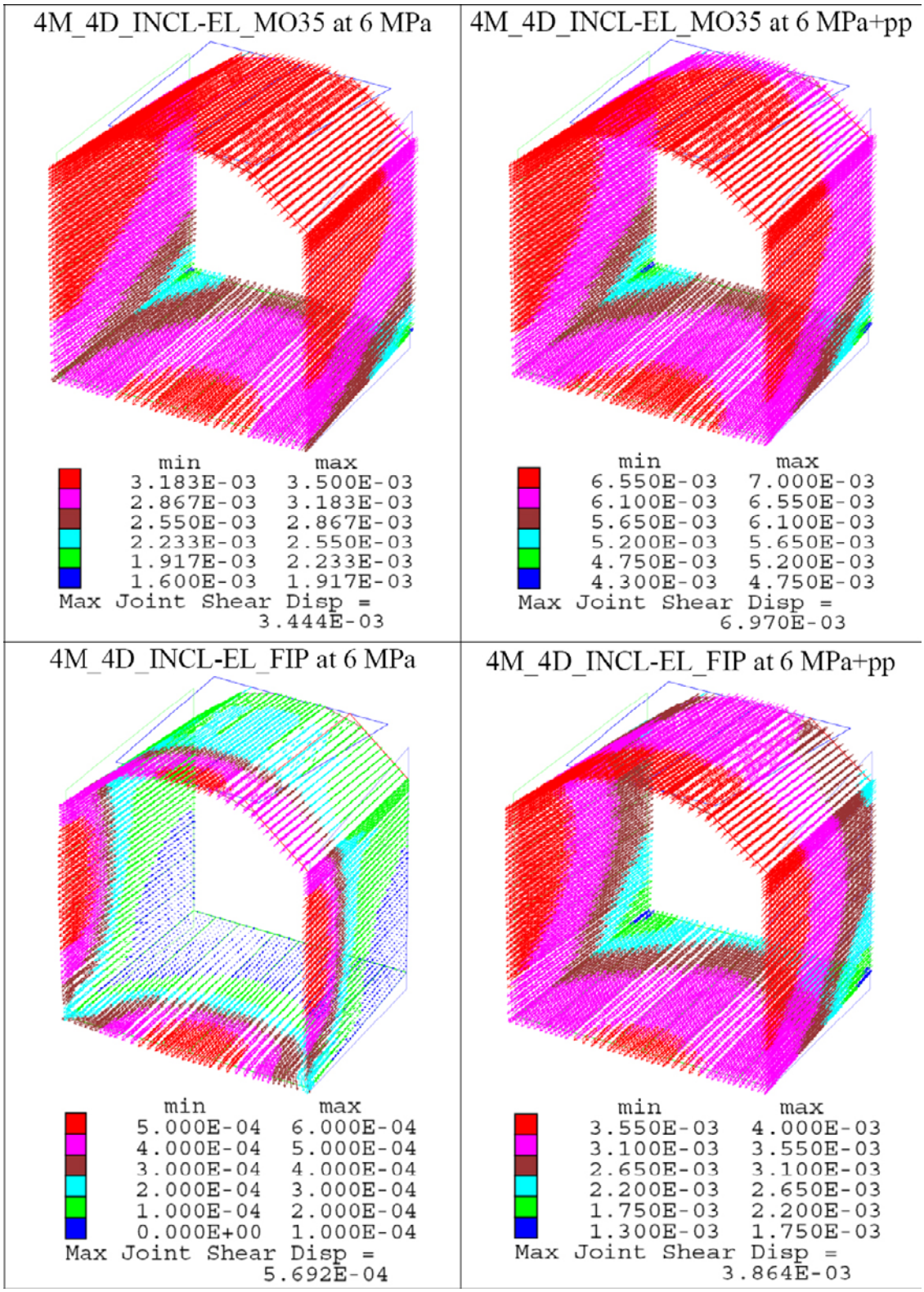

Figure 5-28. *Shear displacement vector plots. Top: 4M_4D_INCL-EL_MO35 (base case). Bottom: 4M_4D_INCL-EL_FIP. The 6 MPa load stage is shown to the left and to the right, the effect of pore water pressure is added.*

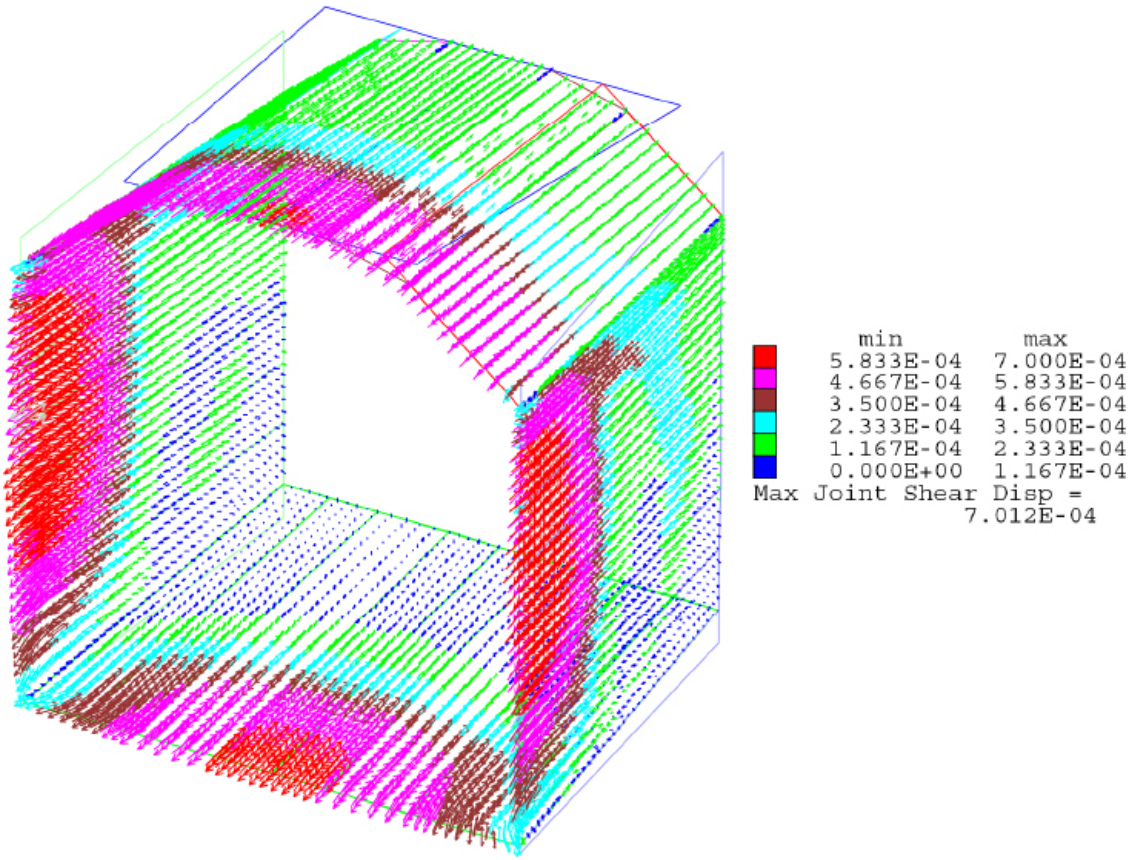

Figure 5-29. *Shear displacement vector plot at 6 MPa load for the 4M_4D_INCL-PL_FIP model. The maximum displacement is 0.1 mm larger than in the 4M_4D_INCL-EL_FIP model (Figure 5-28, lower left).*

5.3 Importance of plug length and look-out angle

In this section, the importance of the plug length and the look-out angle is examined. The first subsection compares results from the 4M_2D_FL-EL_MO45 and 8M_2D_FL-EL_MO45 models, i.e. models with different plug lengths. In the second section, the 4M_2D_INCL-EL_FIP and 4M_4D_INCL-EL_FIP models with different look-out angles are compared. All results in this section were captured at 6 MPa backfill pressure.

5.3.1 Importance of plug length

In Figure 5-30, the major principal (left) and the minor principal stresses (right) along scan-lines A, B and C (cf. Figure 5-20) are shown. The following can be observed:

- The stresses along scan-line B and C in the 8 m-plug are distributed along the entire plug length. This gives smaller compressive stresses in the first part (0–4 m) of the plug compared to the corresponding stresses in the 4 m-plug. The compressive stress at scan-line C at 2 m distance from plug front in the 8 m-model is about 50% of the corresponding stress in the 4 m-model (left).
- The stress concentrations at the plug end are smaller in the 8 m-model than in the 4 m-model. The maximum compressive stress at the end in the 8 m-model is about 10 MPa whereas it is about 4 times larger in the 4 m-model (left).
- In the right diagram it can be observed that also the tensile stresses are reduced when the plug length is increased. At scan-line A at the plug end, the tensile stress in the 4 m-model is about 100% larger than in the 8 m-model. However, it is still below 2 MPa and thus within reasonable bounds.

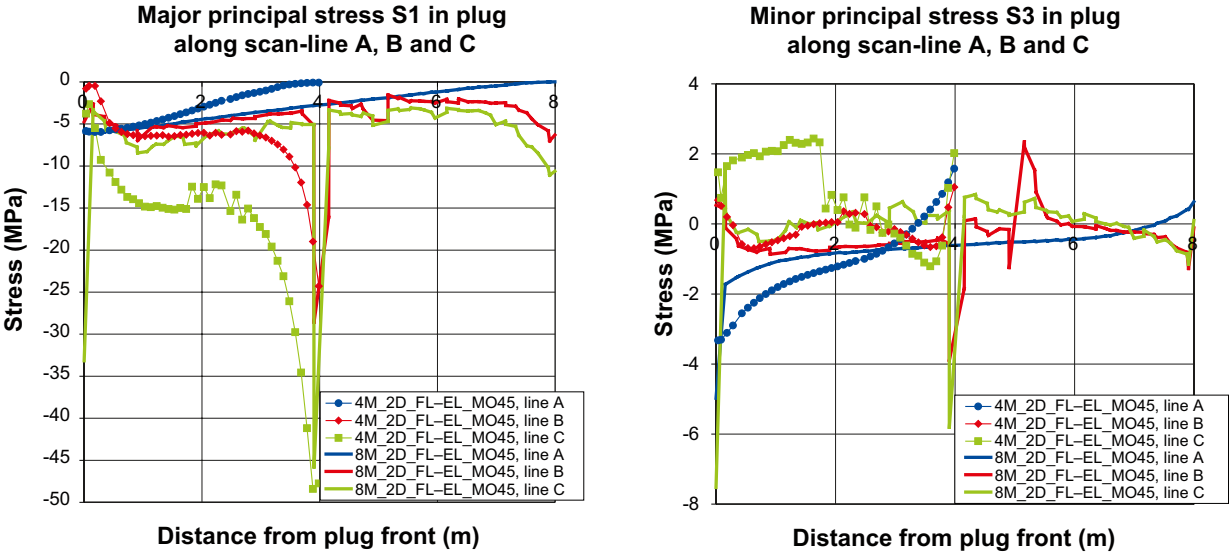

Figure 5-30. *Major (left) and minor (right) principal stresses along scan-line A, B and C (cf. Figure 5-20) at 6 MPa backfill pressure. The influence of plug length is shown. Compressive stresses are negative. The plug front faces the backfilled deposition tunnel.*

The interface shear stresses along three scan-lines (cf. Figure 5-24) for the 4 m-and the 8 m-models are shown in Figure 5-31. Just like the stresses inside the plug shown above, the interface shear stresses are distributed along the entire plug length and thus become less concentrated in the 8 m-model. The 8 m-model shear stress along the wall scan-line at the plug end is about one third of the corresponding value in the 4 m-model.

In Figure 5-32, interface shear displacement vector plots for the 4 m- and the 8 m-models are shown. It can be concluded that the maximum shear displacement in the 4 m-model is about two times that of the 8 m-model. However, the displacement distribution patterns are similar in the models.

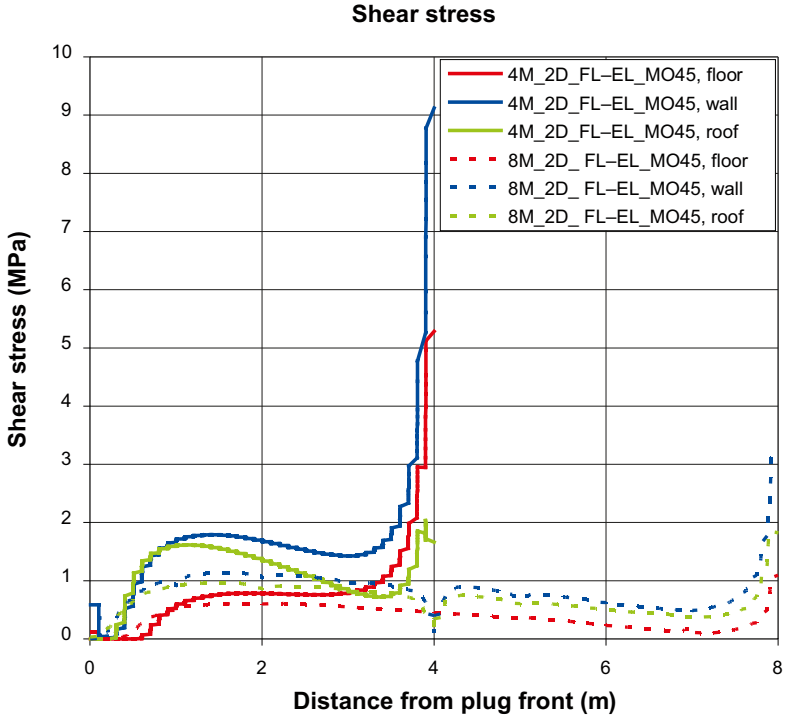

Figure 5-31. *Shear stress in rock-concrete interface along three different scan-lines (cf. Figure 5-24) at 6 MPa backfill pressure. The effect of different plug lengths is shown. The discontinuity in the curves for the 8 m model is due to the notch between the two rounds.*

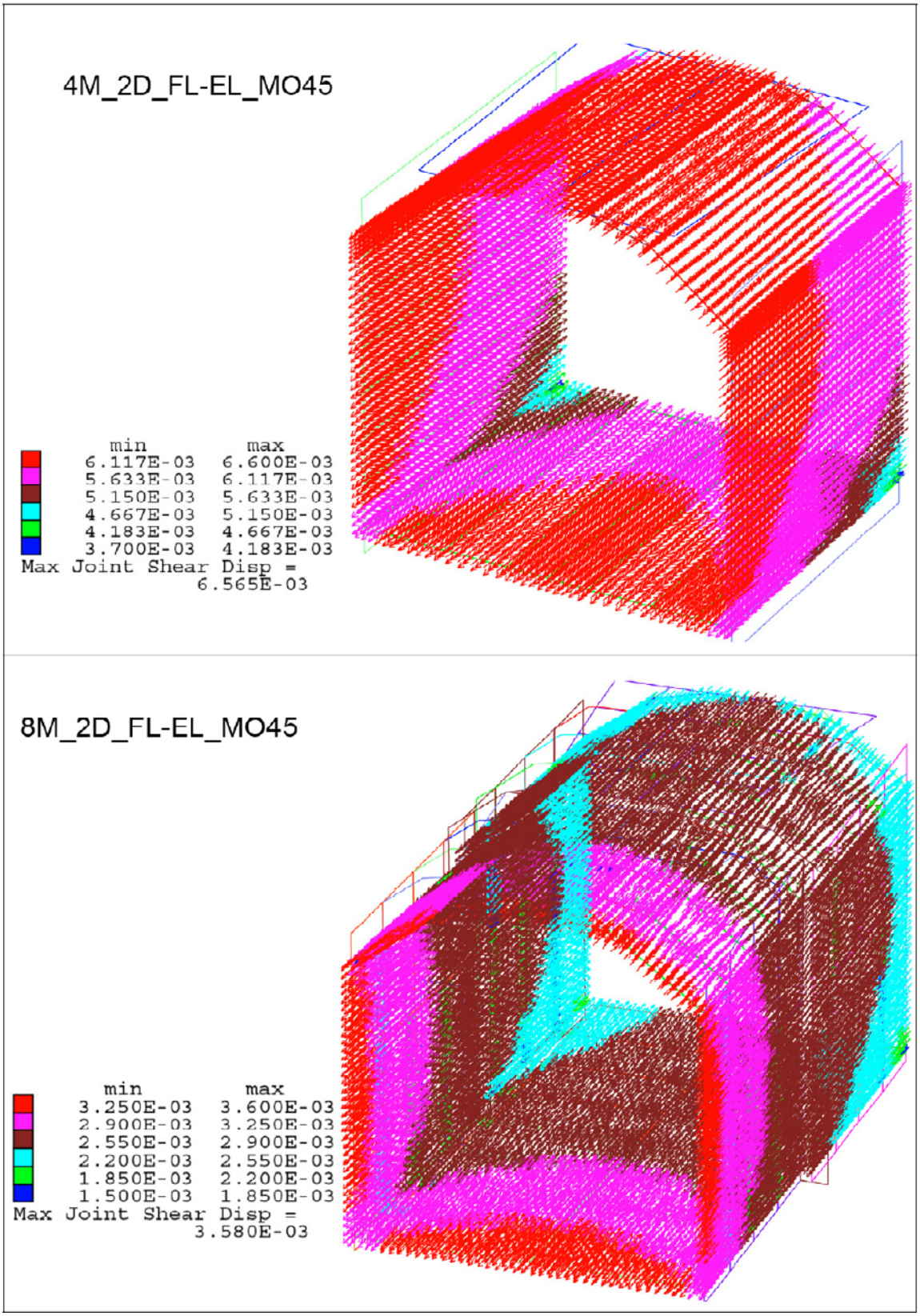

Figure 5-32. *Shear displacement vector plots for 4M_2D_FL-EL_MO45 (top) and 8M_2D_FL-EL_MO45 (bottom) at 6 MPa backfill pressure.*

5.3.2 Importance of look-out angle

In Figure 5-33, the major principal (left) and the minor principal stresses (right) along scan-lines A, B and C (cf. Figure 5-20) are shown for the 4M_2D_INCL-EL_FIP and 4M_4D_INCL-EL_FIP models. The following can be observed:

- The stresses along the tunnel axis are similar in the models.
- The compressive stresses along the edges (scan-lines B and C) are increased when the look-out angle is decreased (left). The increase is due to the larger shear displacements in the 2°-model, which results in a higher lateral compression of the plug. The maximum increase is about 35% in scan-line B and 100% in scan-line C. The shift of look-out angle also gives redistribution of stresses. In the 4°-model, the largest compression is found along scan-line B, but in the 2°-model, it is found along scan-line C.
- No large changes take place in the minor principal stresses as the look-out angle is changed (right). However, just like for the major principal stresses there are some redistributions. When the angle is reduced, the tensile stresses along scan-line B are reduced along about 2/3 of the length, but along scan-line C, the stresses are increased.

The interface shear stresses are shown in Figure 5-34. The reduction of look-out angle results in a redistribution of shear stresses towards the end of the plug. In the roof, the shear stress at the plug end increases by about 70% when the look-out angle is reduced. The corresponding stress increase at the floor is about 50%. The stress redistribution is a result of the larger shear displacements (see below).

Figure 5-35 shows rock-concrete interface shear displacement vector plots for the 2°-model (top) and for the 4°-model (bottom). The maximum displacement is about 60% larger in the 2°-model than in the 4°-model. However, the displacement distribution patterns are similar in the models.

5.4 Rock stresses

Figure 5-36 shows the rock stresses in a vertical plane along the deposition tunnel axis at four load stages: 6 MPa pressure and 6 MPa pressure with the additions of thermal loads after 10, 50 and 100 years, respectively. The tensor symbols scale with the projection of the principal stresses onto the viewing plane and are colored according to the major principal stress. It can be observed that the thermal load has large importance for the stress development. At the beginning of the load history, at 6 MPa load only, the largest stress is about 100 MPa. The heat load increases the stress levels so that the maximum stress is found after 100 years and exceeds 130 MPa. The highest stress levels are found in the main tunnel roof and around the plug front. Stress levels of this magnitude may produce spalling at non-confined surfaces.

From the plots in Figure 5-36, it can also be concluded that the in situ stresses are the main contributors to the high stress levels. The magnitudes of the stresses around the openings depend on the in situ stress levels and on the in situ stress orientations relative to the tunnels. The in situ stresses applied here were taken from the stress model in the Forsmark site descriptive model (SDM) version 1.2 /SKB 2005/ applied at 400 m depth. The major principal stress was oriented along the deposition tunnel. These assumptions may not be in accordance with the conditions at the location where the plug is installed. Therefore, it is interesting to study the stress contributions from the loading only. In Figure 5-37 and Figure 5-38, the same type of plots as in Figure 5-36 are shown, but only the stress contributions from the loading are shown. Figure 5-37 shows stresses along a vertical plane along the deposition tunnel axis. Figure 5-38 shows stresses in a plane that is perpendicular to the deposition tunnel axis and located 0.1 m from the plug end. The following can be observed:

- The 6 MPa load alone yield stress additions that amount at about 15 MPa at a maximum. These stresses are located in the tunnel floor around the plug end (upper left).
- After 100 years, the thermal load has increased the stresses such that the stress additions now amount at about 40 MPa in the deposition tunnel floor around the plug end and in the main tunnel roof (lower right).

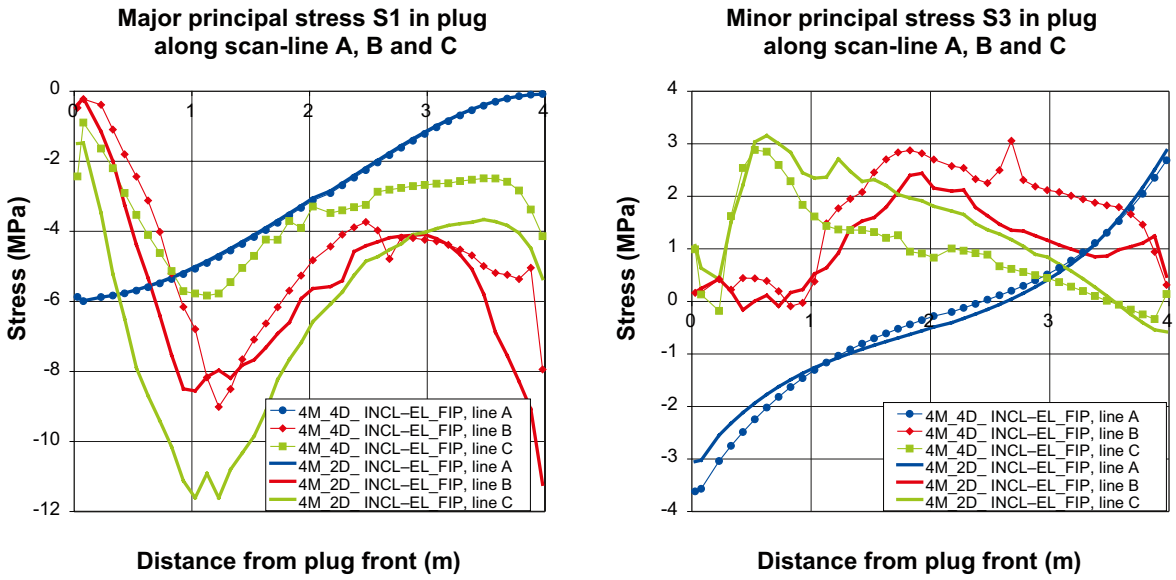

Figure 5-33. *Major (left) and minor (right) principal stresses along scan-line A, B and C (cf. Figure 5-20) at 6 MPa backfill pressure. The importance of look-out angle is shown. Compressive stresses are negative. The plug front faces the backfilled deposition tunnel.*

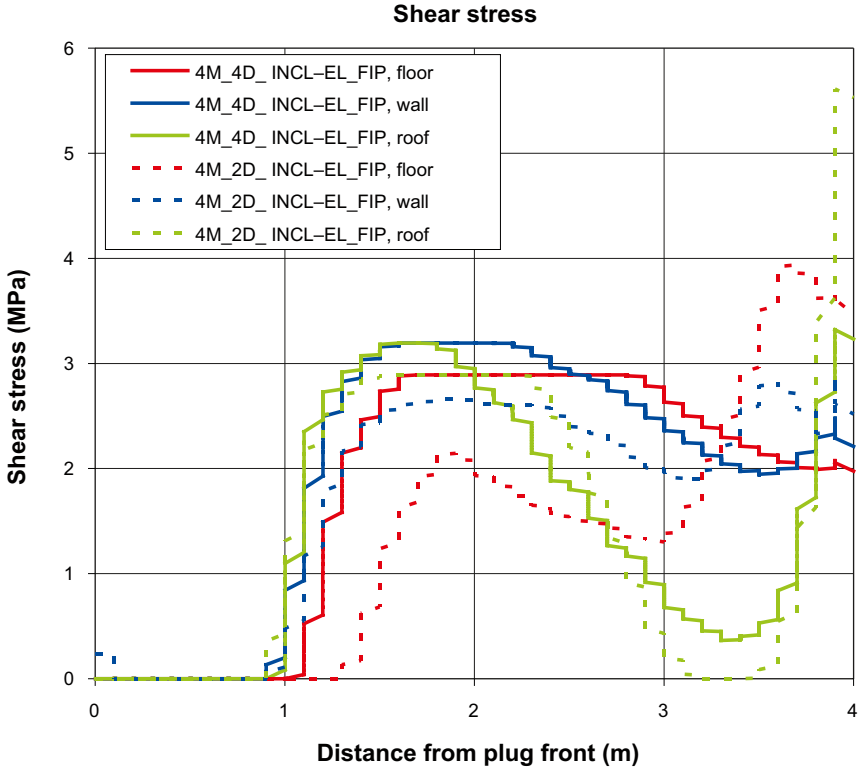

Figure 5-34. *Shear stress in rock-concrete interface along three different scan-lines (cf. Figure 5-24) at 6 MPa backfill pressure. The importance of look-out angle is shown.*

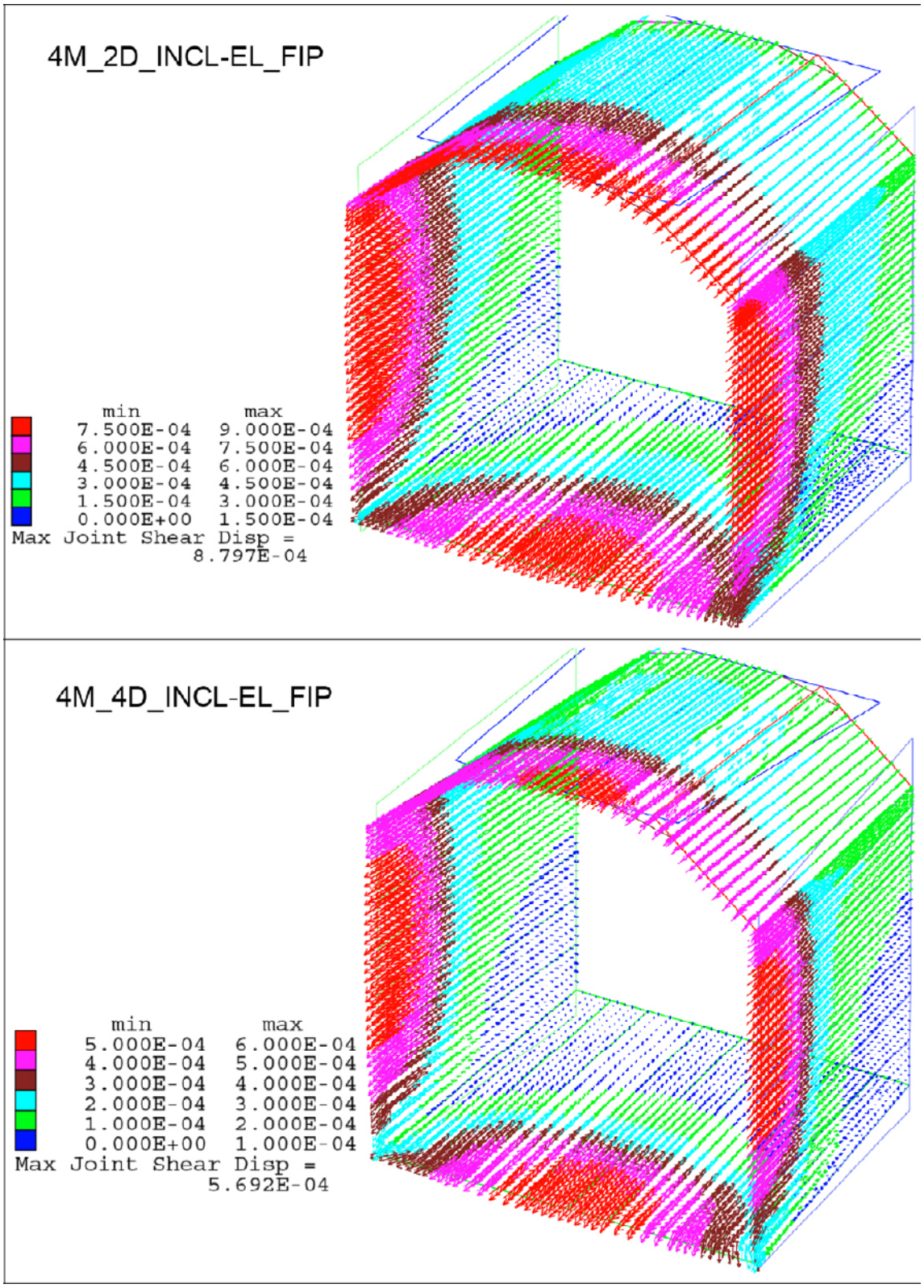

Figure 5-35. *Shear displacement vector plots for 4M_2D_INCL-EL_FIP (top) and 4M_4D_INCL-EL_FIP (bottom) at 6 MPa backfill pressure.*

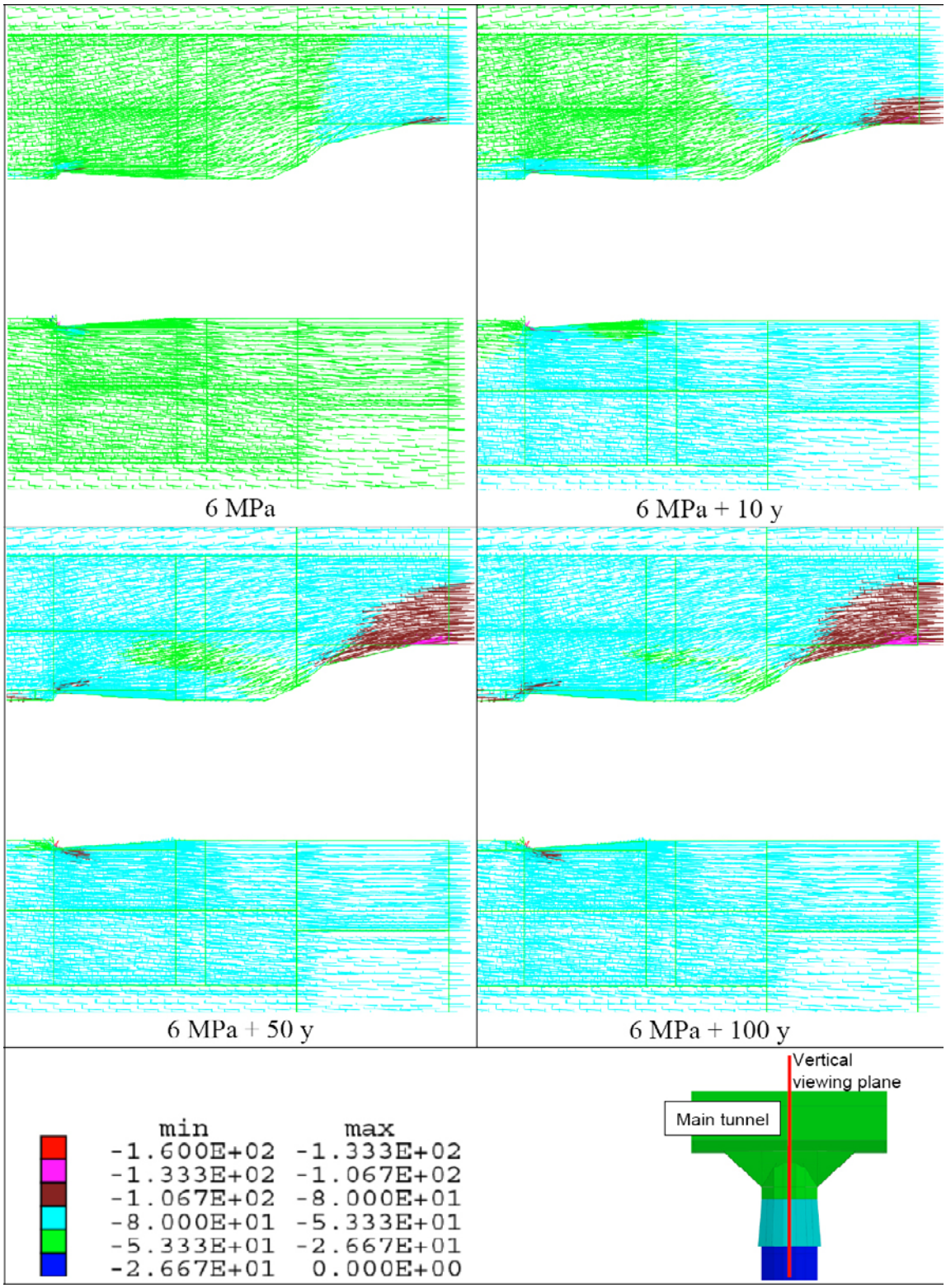

Figure 5-36. *Stress plots from four load stages in a vertical section along the deposition tunnel axis (lower right). The plots show the total stresses in the rock. The tensor symbols scale with the projection of the principal stresses onto the viewing plane and are colored according to the major principal stress.*

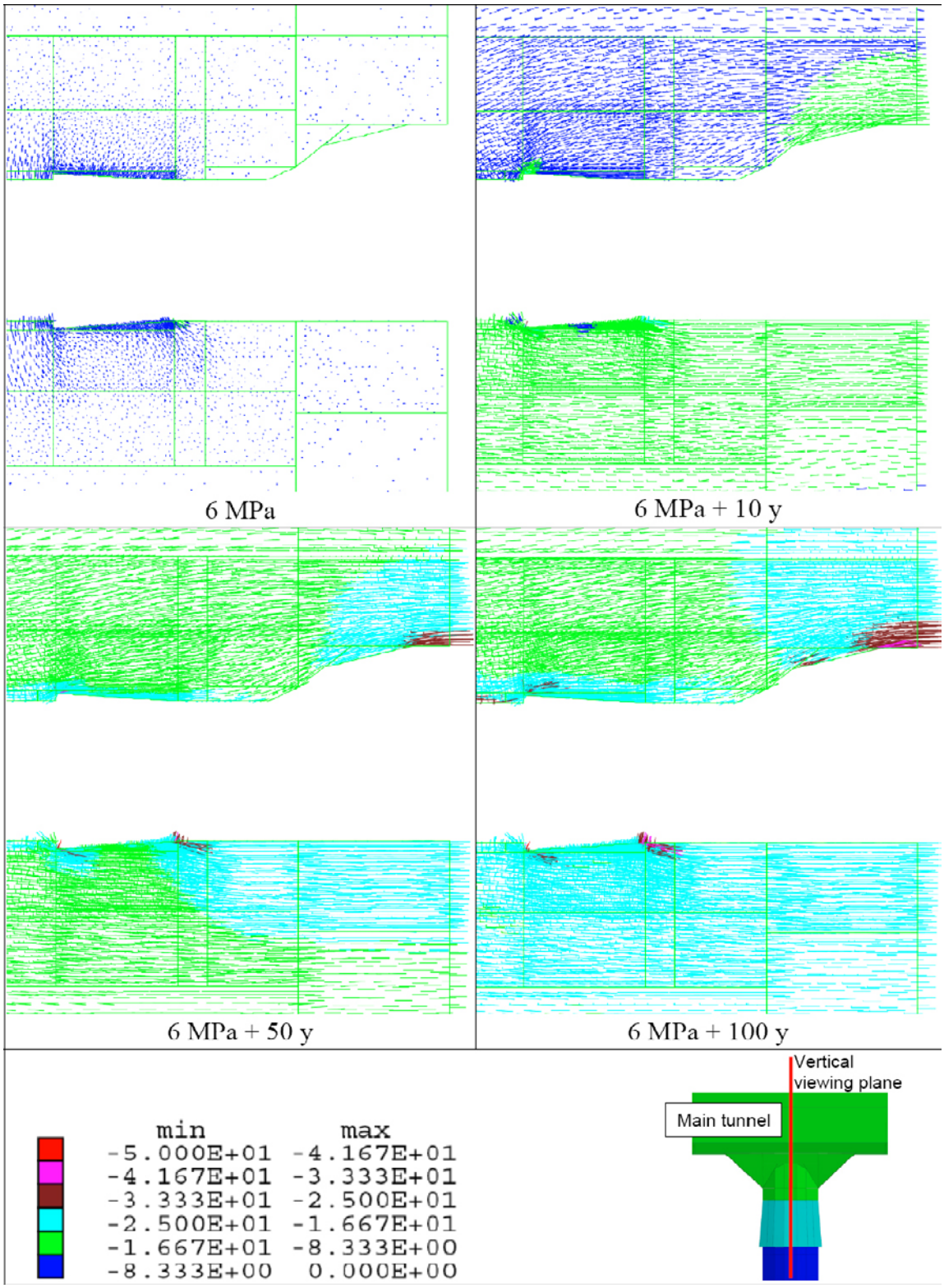

Figure 5-37. *Stress plots from four load stages in a vertical section along the deposition tunnel axis (lower right). The plots show the stress additions in the rock. The tensor symbols scale with the projection of the principal stresses onto the viewing plane and are colored according to the major principal stress.*

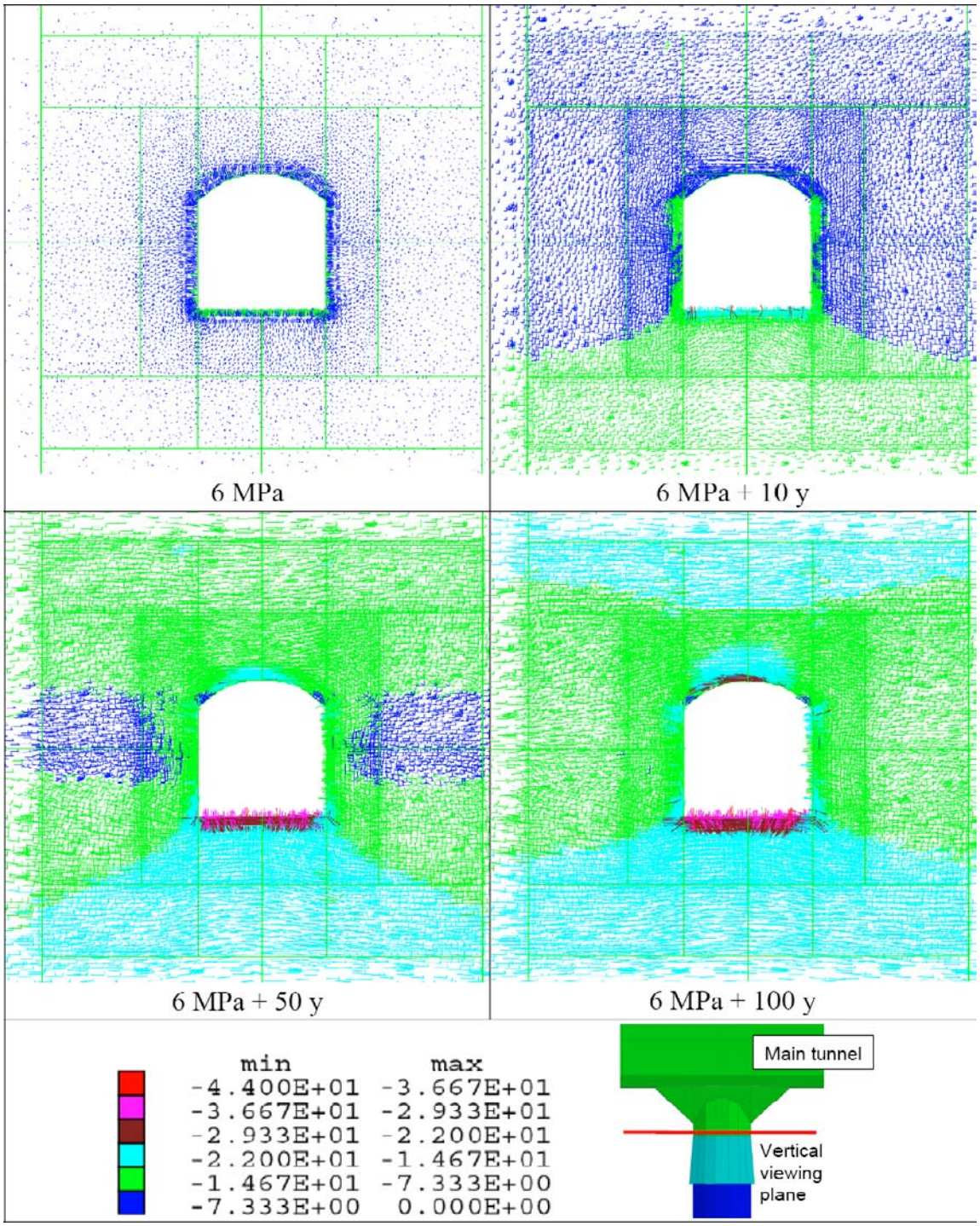

Figure 5-38. *Stress plots from four load stages in a vertical section perpendicular to the deposition tunnel axis (lower right). The plots show the stress additions in the rock. The tensor symbols scale with the projection of the principal stresses onto the viewing plane and are colored according to the major principal stress.*

6 Conclusions and discussion

In order to assess the applicability of the tapered plug concept for plugging of the deposition tunnels in a deep repository for spent nuclear fuel, numerical simulations have been carried out by use of *3DEC*. A 3D-model including a portion of a deposition tunnel and its intersection with a main tunnel was analyzed. In the deposition tunnel, a tapered concrete plug was installed and subjected to the combined load from the swelling of the backfill material and from pore water pressure inside the deposition tunnel. The heat load from the decaying fuel was also taken into account in the model. As an accidental case, the effect of having a high pore water pressure in the rock-concrete interface was analyzed. Site investigation data was used for the rock material and generic parameter values were used for the concrete. A generic repository layout was assumed as a basis for the thermal model. The effects of changing the following parameters were evaluated: concrete material model, rock-concrete interface failure criterion, plug length, look-out angle. The results are summarized and discussed in the following sections.

6.1 Stresses and displacements in the plug

6.1.1 Base case model results

The maximum temperature increase in the plug is found after 100 years and is about 24°C. This temperature increase is in agreement with estimates of the temperature development in the repository by /Ageskog and Jansson 1999/. The heating of the plug is non-even. There is a temperature gradient in the horizontal direction due to the open main tunnel with no heat sources. There is also a temperature gradient in the vertical direction due to the location of the canisters below the tunnel floor. The gradients are largest at the beginning of the heating and become reduced after longer times. At the time when the model was set up, the details of the real repository layout were not known. Thus, the temperature calculations were based on a generic repository layout. Changes in the layout may also change the maximum temperature in the plug. One layout detail that is important for the temperature evolution is the distance between the nearest canister and the plug front. Here it was arbitrarily set to be equal to one canister distance, i.e. 6 m. An increase of this distance would result in a decrease of the temperatures in the plug.

The following can be concluded regarding the stresses in the plug:

- The stresses along the wall-floor and wall-roof edges are in general higher than in the center of the plug due to stress concentrations along the edges. The highest stresses are found at the end of the plug close to the walls and the floor. Without heating, the maximum compressive stress amounts locally at about 50 MPa but is about 20 MPa on average at these locations. The thermal load gives significant increase of the compressive stresses. After 100 years of heating, the peak stress and the average stress along the edges at the plug end have been increased by about 20 MPa and 10 MPa, respectively. The high impact of the heating is due to the high degree of confinement in the plug. It is locked against movement into the deposition tunnel and is thus forced to move toward the main tunnel. Due to its cone-shape it is wedged up when it expands in the axial direction. The wedge effect alone is difficult to quantify since it is dependent on the rock-concrete interface properties. However, the combination of the wedge effect and the lateral expansions of the plug yield high thermal stress additions.
- The maximum tensile stresses amount at 2 MPa at 6 MPa load. The thermal load tends to reduce the tensile stresses around the tunnel axis at the end of the plug and increase them along the edges. After 100 years, the maximum tensile stress amounts at about 4 MPa close to the plug end.
- The thermal stresses cause stress redistributions and rotation of the stress tensors. The directions of the stress tensors clearly indicate how a major part of the roof looses shear stress due to the heating. The compressive stresses increase more in the lower parts than in the upper part of the plug. This is due to that the vertical expansion of the plug is limited by the friction forces along the walls, which increase due to horizontal expansions. The arc-shaped roof also strongly contributes to the lower stress levels in the uppermost parts.

The following can be concluded regarding the shear stresses and shear displacements in the rock-concrete interface. The highest shear stresses amounts at 10–15 MPa and are found at the end of the plug. As the thermal load is applied, stress redistributions take place. At the floor and at the walls, the shear stresses are increased at most locations. This increase is accompanied by loss of shear stress in the roof along about half of the plug length or more. This stress loss is due to the arched roof and the friction along the walls.

The loss of shear stress in the roof is accompanied by an increase of the maximum shear displacement. The maximum shear displacement is located in the roof and is about 3.5 mm at 6 MPa load and about 5 mm after 100 years of heating. The displacements are well below the 10 mm criterion that was established in Section 3.2.2.

The results indicate that an arch-shaped roof is unfavorable compared to a roof with a geometry similar to that of the floor. A non-arched roof or a more circular tunnel section at the plug position may give a more even stress distribution in the plug.

6.1.2 Importance of rock-concrete interface model and pore water pressure

The following can be concluded regarding the stresses in the plug:

- Applying different failure criterions for the rock-concrete interface may significantly change the stress levels along the circumference of the plug. The FIP interface model yields much less interface shear displacements and thus less lateral compression of the plug. The FIP model gives 80–90% reduction of the maximum compressive stress compared to the base case. Increasing the friction angle in the Mohr-Coulomb model from 35° to 50° may give compressive stress increase of about 50%.
- Higher interface strength gives in general higher tensile stresses. Applying the FIP interface model or the use of a higher friction angle than in the base case may increase the maximum tensile stress by up to 100% at some locations.
- The application of pore water pressure decreases the interface strength and causes larger shear displacements along the interface, which in turn gives a state of higher compression in the plug. The maximum compressive stress increase may be of the order of 50% when the pore water pressure is applied. Consequently, the tensile stresses are also significantly reduced.

Regarding interface shear stresses and shear displacements it can be concluded that the relatively high shear strength at low normal stress levels in the FIP model yields small displacements and less stress concentrations than the Mohr-Coulomb model does. The Mohr-Coulomb model (base case) gives more than 5 times larger displacements (3.5 mm) than the FIP model does (0.6 mm).

The application of pore water pressure in the rock-concrete interface gives significant increase of the shear displacements. When using the Mohr-Coulomb interface model (base case), the pore pressure yielded an increase of the maximum displacement of about 100%. When the FIP interface model was used the increase was more than 600%. However, the maximum displacements were still small. In the base case model they were about 7 mm and with the FIP model, they amounted at about 3.9 mm. It shall also be pointed out that the assumption made here regarding the pore pressure is very conservative and should be regarded as a bounding case due to the following:

- The water pressure at the plug front was assumed to be 4 MPa, which is of the order of the hydrostatic pressure at repository depth. However, according to recent hydraulic calculations for the Forsmark site the water pressure inside the backfilled parts of the repository will be about 3 MPa at a maximum due to drainage of the rock caused by the excavations /Svensson 2008/.
- The water pressure at the plug front was held constant, which implies a high water supply from the deposition tunnel.
- The effect of the pore pressure was applied over the entire interface. In a real situation, a leakage is much more likely to take place along discrete channels and will then not have this large impact on the shear strengths in the interface.

6.1.3 Importance of a limited tensile strength in the concrete

The application of a limited tensile strength in the concrete has limited importance for the stresses. Tensile failures at some locations results in stress redistributions. At some locations the compressive stresses are increased by about 50%, but at other locations, they stay effectively unchanged. Tensile stresses at the plug end that exceed the tensile strength become reduced and loads are redistributed into the plug. This indicates that there may be some cracking at the plug end at high loads.

The shear displacements are almost unaffected by the limited tensile strength. The maximum displacement is about 0.7 mm, which is 0.1 mm more than in the corresponding elastic model. This comparison was done with models where the FIP interface model was applied. There may be some difference in the results if some other interface model is used.

6.1.4 Importance of plug length

The stresses in the plug are reduced when the plug length is increased. The loads are distributed along a longer distance and the stress concentrations at the plug end become smaller when a longer plug is used. The maximum compressive stress at the plug end in the 4 m-model is about 4 times larger than in the 8 m-model.

The increase of the plug length also has significant influence of the interface shear stresses and shear displacements. The maximum shear displacement in the 4 m-model is about twice that of the 8 m-model. Correspondingly, the shear stress concentrations at the plug end are reduced by about 50–60% on average when the plug length is doubled.

6.1.5 Importance of look-out angle

A reduction of the look-out angle from 2° to 4° has only minor importance for the stresses in the plug. The stress distribution remains effectively unchanged but some compressive stress increase can be observed along the circumference of the plug due to the larger shear displacements in the 2°-model. At some locations, the compressive stress increases up to about 80%, but at most locations, the increase is less.

The reduction of look-out angle results in increased shear displacements and corresponding increase of the shear stresses at the plug end. The shear displacements and shear stresses increase by about 50–60% when the look-out angle is reduced. It shall be noted that this comparison was done with models where the FIP interface model was applied. There may be some difference in the results if some other interface model is used.

6.1.6 Comparison with acceptance criteria

The base case results indicate that the maximum stresses at some locations in the plug (in particular close to the plug end) clearly will exceed the acceptance criteria (cf. Section 3.2.2). Without heating, the maximum compressive stress amounts locally at about 50 MPa and at about 70 MPa after 100 years of heating. The maximum tensile stress after 100 years was about 4 MPa. The corresponding average compressive stresses amounted at about 20 MPa and 30 MPa, respectively. According to the criteria, the maximum accepted stresses are 30 MPa and 1.5 MPa in compression and tension, respectively. However, adjustments of the plug geometry (in particular the length) have the potential to give significant reductions of the stress levels. In addition, the results indicate that the stress levels may vary depending on the interface behavior. The base case model has relatively low interface shear strength and the compressive stress levels were significantly reduced when the FIP interface model, which has higher shear strength, was applied. Thus, it can be concluded that the compressive stresses can efficiently be reduced by choice of advantageous plug geometry and if a good bond in the rock-concrete interface can be achieved.

The tensile stresses in the base case model exceeded the acceptance criteria at some locations. However, it was indicated in one model that local tensile failures have a very limited importance for the plug behavior. It has also been shown that the tensile stresses can be reduced by adjustment of the plug geometry.

It shall be noted that no effects of confinement were accounted for when the stresses were compared with the acceptance criteria. At most locations, the concrete is confined to some degree. The effect of this is difficult to quantify exactly, but results from triaxial tests indicate a significant increase in strength due to confinement. For instance, in triaxial tests by /Sfer et al. 2002/, a concrete with an unconfined compression strength of about 33 MPa exhibited a strength increase of about 30% at 1.5 MPa confinement stress. At 4.5 MPa confinement stress, the strength was increased by about 50%. Strong influence of confinement is also reported in Betonghandboken /Svensk Byggtjänst 1990/, which indicates a strength increase of 20% in biaxial compression and yet more in triaxial compression. The material at the outer end of the plug has one free surface and the load state at these locations may be regarded as biaxial. Thus, it should be possible to count in an increase of the maximum accepted compressive stress of 20% close to the plug end where the compressive stresses are as largest. At locations inside the plug where the degree of confinement is higher, yet larger strengths can be expected.

6.2 Rock stresses

The stress additions due to the pressure load alone amount at about 15 MPa, and with the addition of the heat load, the stress additions increase to about 40 MPa. If the total effect of the loads and the in situ stresses is taken into account, the stresses may exceed the spalling limit of the rock at some locations. However, the stress magnitudes and their locations are dependent on both the magnitudes and the orientations of the in situ stresses. In addition, the repository layout (specifically the distance to the nearest canister) has importance for the contribution from the thermal load.

6.3 Items for further work

The models used in the present study were to a large extent based on generic assumptions. If the tapered plug concept will be taken into further consideration, some items should be subject to further study in order to develop better models of the plug. Here is a list of items that could be addressed (or considered) in further work.

- The results indicate that the constitutive model applied for the rock-concrete interface may have significant importance for the model behavior. There are uncertainties about the relevance of the interface models that were used here (Mohr-Coulomb, FIP model). In order to evaluate the relevance of the models (or develop a new), a more detailed study of the interface behavior is suggested. A 2D-model could be used for such a study. The study should result in a best estimate of the interface behavior, which then could be applied in a 3D-model of the plug.
- A concept for manufacturing low-pH concrete has been developed at CBI /Vogt et al. 2008/. A complete set of data from that study was not at hand when this study was carried out. Thus, the models used here were analyzed using data for ordinary concrete. For further studies, the data for low-pH concrete should be used.
- In the present study an unlimited compressive strength was applied for the concrete. This resulted in high compressive stresses locally. In order to examine how stresses will be redistributed by local failure in compression, a non-linear constitutive model that includes a limited compressive strength could be used in future modeling work. Numerical models with this feature should also be able to indicate the risk for progressive failure and collapse.
- The modeling results indicate that the heat load has a significant importance for the stress evolution in the plug. Thus, when developing new models, it is essential that the thermal model (repository layout, thermal properties etc) is as relevant as possible. The distance between the closest canister and the plug is of particular importance.
- In the present study, two look-out angles were tried but the plug was always symmetric. In further studies, the effect of having a non-symmetric plug (due to e.g. larger over break at one side) should be studied.

- Further modeling work should consider the effect of having rock fractures at the location of the plug. Since the state of stress has importance for the behavior of fractures (and for the resulting stresses around the openings), the best in situ stress model available should be used, both in terms of stress magnitudes and in terms of stress orientation with respect to the tunnels. The sensitivity to variations in stress orientation and stress magnitudes should be tested. If it is possible, site specific stress data should be used.
- Due to very conservative assumptions for the water pressure load on the plug, it is recommended for future studies to also include results from site specific hydrogeological modeling of the actual ground water hydrostatic pressures in the vicinity of the plug structures. At present this type of calculations indicates an applied water pressure that is about 25% lower than what was assumed in the present study /Svensson 2008/.

In Chapter 2, a tentative design for a tapered plug system was presented. If it is decided that the tapered plug concept shall be developed further, it is likely that there will be revisions of the design during the course of the work. Figure 6-1 shows a proposal for how the plug system in Figure 2-1 may be revised. The bentonite blocks, the pre-fabricated concrete beams and the layer with filter material has been omitted in order to reduce the complexity of the system and thereby reduce time and costs for the installation. It is assumed that the last row of backfill blocks together with a pre-fabricated steel plate can serve as concrete casting mould. The proposed design is based on the assumption that the concrete plug in it self can be made water tight enough that it prevents backfill material from being eroded and transported out from the deposition tunnel.

In order to test the technique for the installation of a tapered plug, to assess its performance and to obtain data for comparison with numerical models, a full scale field test should be carried out.

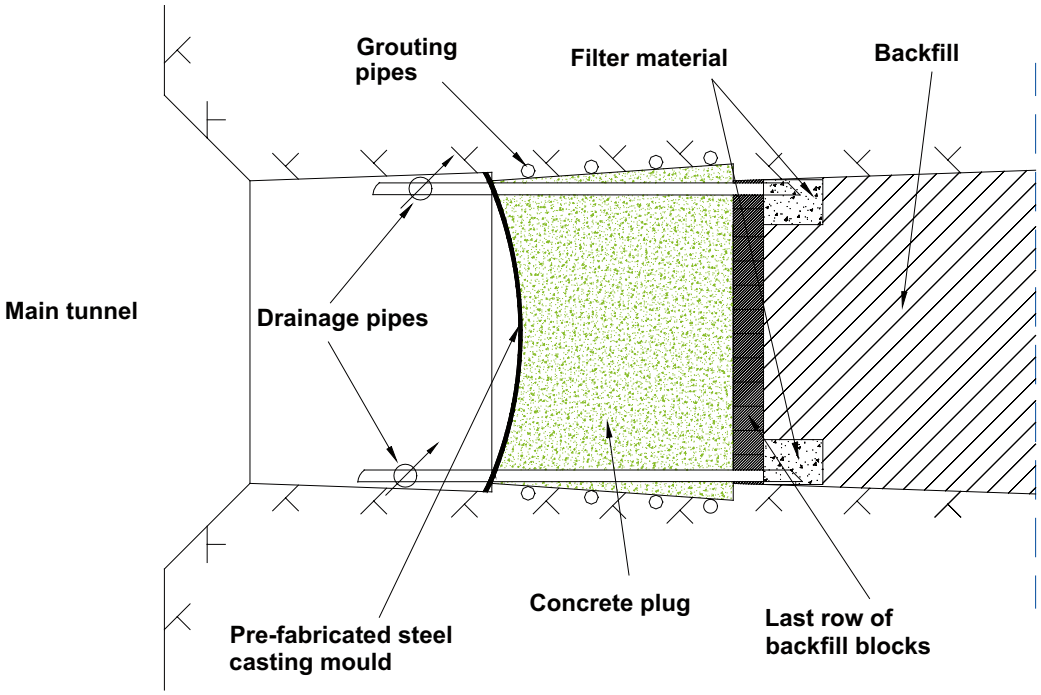

Figure 6-1. *Schematic sketch of tentative design of tapered plug system without bentonite blocks in front of the concrete plug.*

6.4 Concluding remarks

The present study has been carried out in order to assess the applicability of the tapered plug concept for plugging of deposition tunnels in a repository for spent nuclear fuel. The models were based on data that was regarded as the most relevant available. The following concluding remarks can be made:

- The displacements in the plug will be within acceptable ranges but the stresses may locally be high enough that they exceed the acceptance criterion applied here. However, the results indicate that the stresses can be kept within acceptable ranges by choice of advantageous plug geometry and by having a good rock-concrete bond. In addition, it is also assumed that the confinement of the concrete will allow for higher stresses than indicated by the acceptance criterion. Thus, it can be concluded that, with choice of an appropriate design, the tapered plug concept seems to be an applicable concept for plugging of deposition tunnels. This should however be confirmed by a full-scale field test.
- The results show that the plug length has a significant importance for the stresses in the plug. In order to ensure a robust construction, the plug should be at least 4 m long.
- The stress additions in the rock due to the pressure loads are within reasonable bounds. However, the thermal load yields significant stress additions and may, when added to the in situ stresses, locally exceed the spalling limit of the rock.
- The modeling technique that has been developed is available for further work and can be developed to take into account the improvements listed in Section 6.3 above.

7 References

Ageskog L, Jansson P, 1999. Heat propagation in and around the deep repository. Thermal calculations applied to three hypothetical sites: Aberg, Beberg and Ceberg. SKB TR-99-02. Svensk Kärnbränslehantering AB.

Boverket, 2004. Boverkets handbok om betongkonstruktioner BBK 04. ISBN 91-7147-816-7. Boverket.

Bodén A, Lundin J, 2007. SFR KONTROLLPROGRAM Bergkontroll. Bergkontrollgruppens årsrapport 2006. Huvudrapport. Vattenfall Power Consultant AB, report no 2448900-001, 2007-03-05.

CEB, 1993. CEB-FIP MODEL CODE 1990. Comité Euro-International du Béton, Lausanne, Switzerland.

Fälth B, Hökmark H, 2006. Mechanical and thermo-mechanical discrete near-field analyses based on preliminary data from the Forsmark, Simpevarp and Laxemar sites. SKB R-06-89. Svensk Kärnbränslehantering AB.

Glamheden R, Fredriksson A, Persson L, Röshoff K, Karlsson J, Bohlin H, Lindberg U, Hakami H, Hakami E, Johansson M, 2007. Site descriptive modeling. Forsmark stage 2.2. Rock mechanics. SKB R-07-31. Svensk Kärnbränslehantering AB.

Gunnarsson D, Börgesson L, Hökmark H, Johannesson L-E, Sandén T, 2001. Report on the installation of the Backfill and Plug Test. SKB-ÄHRL IPR-01-17.

Hökmark H, Fälth B, 2003. Thermal dimensioning of the deep repository. SKB TR-03-09. Svensk Kärnbränslehantering AB.

Itasca, 2003. *3DEC* – 3-Dimensional Distinct Element Code, User's Guide. Itasca Consulting Group, Inc., Minneapolis, USA.

Itasca, 2005. *FLAC* – Fast Lagrangian Analysis of Continua, User's Guide. Itasca Consulting Group, Inc., Minneapolis, USA.

Johansson F, 2005. Stability Analyses of Large Structures Founded on Rock – An Introductory Study. Licenciate Thesis. School of Architecture and the Built Environment, Royal Institute of Technology, Stockholm, Sweden.

Sfer D, Carol I, Gettu R, Etse G, 2002. Study of the Behavior of Concrete under Triaxial Compression. Journal of Engineering Mechanics, Vol 128, pp 156–163.

SKB, 2005. Preliminary site description. Forsmark area – version 1.2. SKB R-05-18. Svensk Kärnbränslehantering AB.

SKB, 2006a. Slutförvar för använt kärnbränsle. Preliminär anläggningsbeskrivning – layout D. SKB R-06-33. Svensk Kärnbränslehantering AB.

SKB, 2006b. Data report for the safety assessment SR-Can. SKB TR-06-25. Svensk Kärnbränslehantering AB.

SKB, 2007. RD&D Programme 2007. Programme for research, development and demonstration of methods for the management and disposal of nuclear waste. SKB TR-07-12. Svensk Kärnbränslehantering AB.

SKB, 2008a. Design, production and initial state of the backfill and plug in deposition tunnels for the safety assessment SR-Site. In prep. Svensk Kärnbränslehantering AB.

SKB, 2008b. Forsmark. Site Engineering Report. Guidelines for Underground Design Step D2. SKB R-08-83. Svensk Kärnbränslehantering AB.

Slunga R, 1991. The Baltic Shield earthquakes. Tectonophysics 189:323-331. Elsevier Science Publishers B.V., Amsterdam.

Svensk Byggtjänst, 1990. Betonghandboken utgåva 2. Svensk Byggtjänst AB. Stockholm.

Svensson U, 2008. PFM 2.2 –Hydro modeling of open repository Forsmark, 2nd model – Inflow distributions for three grouting alternatives and three stages of the repository. In prep. Svensk Kärnbränslehantering AB.

Vogt C, Lagerblad B, Wallin K, Baldy F, 2008. Low pH self compacting concrete for deposition tunnel plugs. SKB R-09-07. Svensk Kärnbränslehantering AB.